Drive implementation of a permanent magnet synchronous motor

A dissertation presented to

The School of Electrical, Electronic and Computer Engineering

North-West University

In partial fulfilment of the requirements for the degree

Magister Ingeneriae

in Electrical and Electronic Engineering

by

Andries de Klerk

Supervisor: Prof. G. van Schoor
Co-Supervisor: Prof. S.R Holm
Assistant supervisor: Mr. A.C Niemann

December 2007

Potchefstroom Campus

"Trust in the Lord forever, for the Lord, the Lord, is the Rock eternal."
Isaiah 26:4

SUMMARY

The North-West University has been focussing on the development and implementation of active magnetic bearings (AMBs) as well as the modelling and control of the AMBs. Recently the need for a high speed flywheel system arose and research has shown that permanent magnet synchronous machines (PMSMs) are an effective solution for high speed applications. The university decided to combine the AMB and PMSM technology to develop a high speed flywheel system with a magnetically suspended rotor.

The aim of this project is to develop a 3-phase ac drive that will control the speed of the PMSM. The power amplifier consists of power electronics for the voltage generation as well as protection systems to ensure safe operation of the power amplifier. A control algorithm was developed to control the speed of the PMSM. A flyback converter will provide power for the small signal electronics.

The design process includes the derivation of a mathematical model that describes the behaviour of the PMSM. From the model a control algorithm is designed that will ensure synchronization between the stator magnetic field and the magnetic field of the permanent magnets. The control algorithm is a constant V/f algorithm that controls the flux in the motor. From start-up to half speed constant torque control is implemented and from half speed to rated speed constant power control is implemented. The control algorithm is realised with a dSPACE® real-time development tool.

The power amplifier is designed to operate from a 310 V dc supply. The amplifier delivers adequate power to the PMSM to enable the motor to achieve a speed of 30 000 rpm and deliver 2 kW of power with a maximum torque of 0.6 Nm. The switching devices of the power amplifier operate at a switching frequency of 50 kHz and can withstand 25 A current. The drive comprises various protection systems. The thermal protection ensures that the temperature of the heat sink does not increase above safe operating levels for the power electronic devices. The short circuit protection protects the switching devices from a short in the phases of the PMSM. An external enable let the user decide when the switching devices should be turned on and protects the devices from switching on together during system initialization. An ac filter is implemented between the output of the power amplifier and the input of the motor. The filter greatly reduces the current ripple and minimizes the effect of electromagnetic interference (EMI).

The simulated results showed good correlation to the experimental results. The power amplifier performed according to the design specifications and the control algorithm proved to be sufficient for the application. The project is concluded and any unforeseen phenomena are discussed. Recommendations are made based on the experimental results to improve the performance of the drive in the future.

The knowledge acquired on PMSM drives will be useful for future development and will ensure technological advancement in the research group.

OPSOMMING

Die Noordwes Universiteit fokus vir 'n geruime tyd op die ontwikkeling en implementering van aktiewe magnetiese laers (AML) asook die modellering en beheer van die AML. Die behoefte vir 'n hoë spoed vliegwielstelsel het onlangs onstaan en navorsing het getoon dat die permanente magneet sinkrone masjien (PMSM) 'n effektiewe oplossing is vir hoë spoed toepassings. Die universiteit het besluit om die AML tegnologie te kombineer met dié van die PMSM om 'n hoë spoed vliegwielstelsel met magneties gesuspendeerde rotor te ontwikkel.

Die doel van die projek is om 'n 3-fase wisselrigter te ontwikkel wat die spoed van die PMSM sal beheer. Die wisselrigter bestaan uit drywingselektronika wat die spanning genereer asook bekermingstelsels wat verseker dat die kragversterker veilig bedryf word. 'n Beheeralgoritme moet ook ontwikkel word wat die spoed van die PMSM sal beheer. 'n "Flyback" omsetter sal krag voorsien aan die kleinseinelektronika.

Die ontwerpproses behels die afleiding van 'n wiskundige model wat die gedrag van die PMSM beskryf. Vanuit die wiskundige model is 'n beheeralgoritme ontwerp wat die sinkronisasie tussen die magneetveld van die stator en die magneetveld van die permanente magnete bewerkstellig. Die beheeralgoritme is 'n konstante V/f algoritime wat die vloed in die motor beheer. Konstante wringkragbeheer word uitgeoefen vanaf stilstand tot halfspoed waarna konstante drywingsbeheer toegepas word tot volspoed. Die beheeralgoritme word gerealiseer met 'n dSPACE® intydse ontwikkelingstelsel.

Die kragversterker is ontwerp om te opereer vanaf 'n 310 V gelykstroom toevoer. Die versterker lewer genoeg krag aan die PMSM sodat die motor 'n spoed van 30 000 opm kan haal en 2 kW drywing kan lewer teen 'n maksimum wringkrag van 0.6 Nm. Die skakelelemente van die kragversterker skakel teen 'n frekwensie van 50 kHz en kan 25 A stroom hanteer. Daar is ook 'n verskeidenheid beskermingstelsels op die kragversterker. Die termiese beskerming verhoed dat die hitteput se temperatuur onveilige vlakke bereik vir die skakelelemente. Die kortsluitbeskerming beskerm die komponente van moontlike kortsluitings in die fases van die motor. 'n Eksterne skakelmagtiging stel die gebruiker in staat om die skakelelemente veilig aan te skakel en te beskerm teen gelyktydige aanskakeling tydens inisiëring van die stelsel. 'n Wisselstroom filter word tussen die uitset van die kragversterker en die inset van die motor geplaas. Die filter verminder die stroom rimpel en minimeer die effek van elektromagnetiese steurings (EMS).

Daar is goeie korrelasie tussen die gesimuleerde resultate en die gemete resultate. Die kragversterker funksioneer wel volgens die ontwerpspesifikasies en die beheeralgoritme het ook na verwagting presteer. Die projek word saamgevat en enige onvoorsiene gedrag word bespreek. Aanbevelings word gemaak oor hoe die projek verder verbeter kan word in die toekoms.

Die kennis wat ontwikkel is oor PMSM aandrywing sal nuttig wees vir toekomstige tegnologiese groei in die navorsingsgroep.

ACKNOWLEDGEMENTS

I would like to firstly thank M-Tech Industrial and THRIP for funding this research and granting me the opportunity to further my studies.

I would like to acknowledge my supervisors Proff. George van Schoor and S.R Holm and Mr. Andre Niemann for their support and guidance throughout this project.

I would also like to acknowledge the following people, in no particular order, for their contributions during the course of this project:

- Ms. A. Holm for the fundamental support in implementing the V/f control algorithm.
- Mr. E.O Ranft for his support and advice
- My fiancé, Hester Viljoen, for her love, support and understanding.
- My family for their love and loyalty.
- My friends, Arnold, Stefan, Jan and Jacques.

TABLE OF CONTENTS

NOMENCLATURE

LIST OF FIGURES

LIST OF TABLES

LIST OF ABBREVIATIONS

ac	Alternating current
AMB	Active Magnetic Bearing
back-EMF	Back Electro Magnetic Force
d-axis	Direct axis
dc	Direct current
EMI	Electromagnetic Interference
GTO	Gate-turn-off transistor
IGBT	Insulated-gate bipolar transistor
MMF	Magneto Motive Force
PA	Power Amplifier
PCB	Printed Circuit Board
PMSM	Permanent Magnet Synchronous Motor
PWM	Pulse Width Modulation
q-axis	Quadrature axis
rms	Root mean square
rpm	Revolutions per minute

LIST OF SYMBOLS

c_{Fe}	iron loss coefficient
c_{str}	stray loss coefficient
$F_{s\alpha\beta}$	mmf
i_{abc}	phase current
I_d	stator current in d-axis
I_q	stator current in q-axis
I_{md}	magnetizing current in d-axis
I_{mq}	magnetizing current in q-axis
I_s^*	command current
$i_{s\alpha\beta}$	stator current in $\alpha\beta$-axis
L_m	per phase motor winding inductance
λ_m	rotor permanent magnet flux
$L_{s\sigma}$	stator inductance
M	mutual inductance
Ω_r	angular electrical rotor speed
P_{Fe}	iron core losses
P_{str}	stray losses
$\Re$	reluctance
r_{abc}	winding resistance
R_m	per phase motor winding resistance
R_s	stator resistance
T_e	electromagnetic torque
θ	rotor angle
V_s^*	command voltage
V_{sd}	stator voltage in d-axis

V_{sq}	stator voltage in q-axis
ω	angular speed
ω_s^*	command speed
X_m	magnetizing reluctance
$\Phi_{\alpha\beta}$	total flux in PMSM

1 Chapter

Introduction

This chapter gives some background on the permanent magnet synchronous machine and alternating current speed drives for these motors. The problem statement is given after which the issues to be addressed and methodology are discussed. The chapter is concluded with an overview of the document.

1.1 Background

The North-West University has been focussing on the development and implementation of AMBs as well as the modelling and control of AMBs. Recently the need for a high speed flywheel system emerged and research has shown that the permanent magnet synchronous machine (PMSM) is an effective solution for high speed applications. The research group has decided to combine the AMB and PMSM technology to develop a high speed flywheel system with a magnetically suspended rotor.

The flywheel will have to reach speeds of up to 30 000 rpm and it must be able to maintain this speed for a considerable amount of time. A drive must be developed that will control the speed of the PMSM effectively. This section will discuss the PMSM as well as possible drives that will be used to control the speed of the motor.

1.1.1 Permanent magnet synchronous motor

The stator of the PMSM is a three phase stator similar to the induction machine. The rotor of the PMSM has surface-mounted permanent magnets whereas the rotor of the induction machine has no magnets on the rotor. This means that the PMSM air gap magnetic field is produced by the permanent magnets which make it much easier to design a more efficient motor. Some of the key features of a PMSM include:

- Reduced construction complexity

- High reliability at very high speeds (no brushes)
- High efficiency
- Less torque ripple

Figure 1-1 shows the rotor-stator configuration of a PMSM. The outer casing is the stator core and the inner circle is the rotor core. The space between the stator- and rotor core is the air gap.

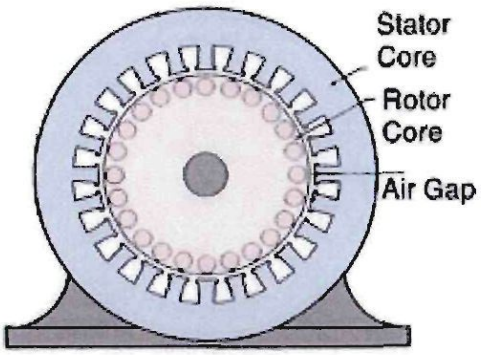

Figure 1-1 PMSM rotor-stator configuration [1]

The PMSM is not a self-starting machine like an induction machine, thus an ac supply cannot be used to start the motor. If the stator terminals are connected to an ac supply, the motor will start to vibrate in stead of starting up. To achieve synchronization, some kind of speed control method must be implemented. One speed control method is the sensorless voltage-frequency control method. The other is scalar control which is more commonly used in the industry [1].

1.2 Problem statement

This project entails the drive implementation of a permanent magnet synchronous motor that will start the motor, control the speed of the motor from start-up to full speed and the drive will also be able to stop the motor. The drive will be powered from a 310 V dc power supply and must be able to deliver currents of up to 25 A. It must deliver 2 kW of power to the motor and the motor must achieve a maximum speed of 30 000 rpm. The torque of the motor will be constant up to half speed and at half speed the motor will deliver maximum power. From half speed to full speed the torque of the motor will decrease whilst the output power of the motor will be kept constant.

1.3 Issues to be addressed and methodology

The following issues must be addressed for the development of the PMSM drive.

- Literature study – PMSM modelling, control and drives
- Drive specification
- Drive modelling
- PMSM control
- Drive implementation and integration
- Drive evaluation

1.3.1 Literature study – PMSM modelling, control and drives

The most important part of any project is the literature study. First a literature survey must be done to acquire enough resources that might be used to gather enough information on PMSM and motor drives. The system modelling can commence once the literature study has been completed.

1.3.2 Drive specifications

Every part of the project must be built to certain specifications. The most important specifications which will determine the performance of the drive is given in table 1-1:

Table 1-1 PMSM drive specifications

Specifications	Value	Specified by / calculated
Max. motor speed	30 000 rpm	Motor designer
Operating current	25 A (max)	Motor designer
Operating voltage	310 V dc	Motor designer
Variable supply output frequency	1 Hz - 500 Hz	Motor designer
Motor drive switching frequency	50 kHz	Project manager
Maximum torque	0.6 Nm	Motor designer
Motor start-up time	± 513 s	Calculated / simulated
Motor stopping time	± 300 s	Calculated / simulated

1.3.3 Drive modelling

The different aspects that need to be considered for this project are the permanent magnet synchronous motor model, the motor drive and most probably some kind of over speed protection. Each of the abovementioned will be taken into account.

PMSM model

A model for the PMSM must be derived from fundamentals. This model must include the inductance, resistance and possible reactance. It must also include equations regarding the calculation of the coupled magnetic fields, the torque and speed of the motor, the position of the rotor as well as the current in each phase of the motor.

The model will be simulated with the use of SIMULINK®. Figure 1-2 shows a simulation block diagram layout.

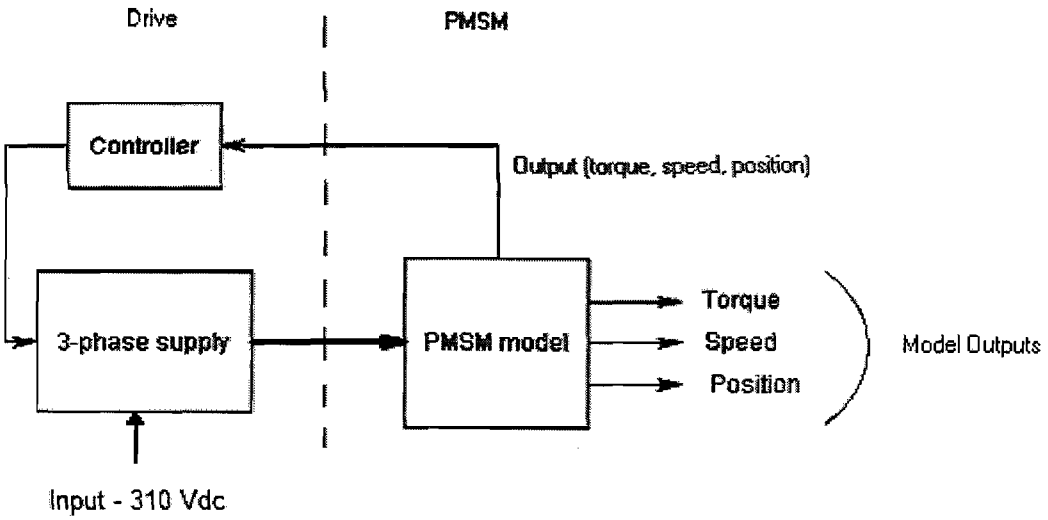

Figure 1-2 Block diagram of PMSM simulation

The input-output of the PMSM is discussed in terms of figure 1-2. A 3-phase drive will generate a 3-phase voltage that will serve as input to the PMSM. Torque, speed or position will be used as feedback to a controller depending on the type of control that will be implemented. The controller, drive and PMSM form a closed loop speed drive.

Motor drive

The motor drive will consist of the power electronics as well as the controller that will be used to start, control the speed and stop the motor. The block diagram of the motor drive can be seen in figure 1-3.

A direct current (dc) supply will supply the power amplifier (PA) with a dc voltage. The power electronics on the PA will generate a 3-phase voltage supply for the PMSM. The output of the controller will be used to vary the 3-phase supply of the PA to successfully control the speed of the motor.

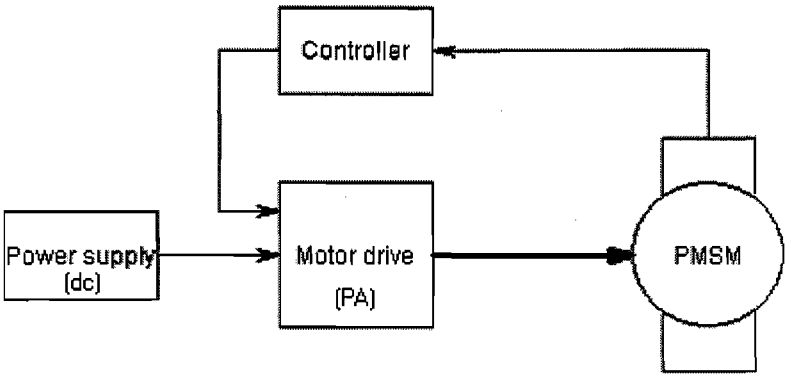

Figure 1-3 Block diagram of motor drive

PMSM scalar control

The PMSM scalar control is a voltage-frequency (V/f) control method that will be used to control the PMSM speed. The current in two of the phases of the motor will be measured and used to calculate a voltage reference value. This value will increase over time to ensure that the motor speed increases gradually in order to establish synchronism.
To ensure that the PMSM does not lose synchronism, a stabilizing loop is incorporated. This loop is an oscillating sine wave that will counter the oscillating effect of the torque and it will stabilize the speed of the PMSM as well.

The PMSM scalar control will be simulated with SIMULINK® and the final control algorithm will be implemented in dSPACE® (a real time software based development tool).

1.3.4 Drive implementation and integration

The implementation stage will include the design and manufacturing of the drive. After the printed circuit board (PCB) of the drive has been manufactured, the hardware (electrical components) must be placed or populated on the manufactured PCB. The PMSM scalar control then needs to be programmed in dSPACE®. After completion of each individual component of the drive system, the components will be integrated to form the PMSM drive.

PMSM model

In the implementation phase the PMSM model will be replaced with the actual PMSM. The PMSM is designed in the McTronX research group.

Motor drive

The motor drive will be designed in ORCAD®. The design will include a power supply, the 3-phase inverter (with protection circuitry), an analogue circuit for signal conditioning and an LC filter on the output of the inverter.
The power supply must be able to rectify 220 V AC to 310 V DC. The 3-phase inverter will be switched with PWM signals to generate the necessary voltage to operate the motor. The protection circuitry will include the thermal protection, optical isolation for the PWM signals as well as short circuit protection. The LC filter will reduce the current ripple and filter the high voltage PWM signals, dramatically reducing the emission of electric fields.
The circuit design in ORCAD LAYOUT will be used to create a PCB of the drive.

PMSM scalar control

The PMSM scalar control will be simulated in SIMULINK® and the simulation will include the V/f control method as well as the stabilizing loop. The speed will be evaluated against the reference speed. The torque of the motor will be measured including the current in each phase of the motor. Then the working simulation will be programmed to dSPACE®.

Over speed protection

Protection is very important in any electrical or mechanical system. There will be various protection mechanisms for the motor as well as for the drive, but the most important one is the over speed protection. Failure at high speeds will cause a disaster. The over speed protection block diagram can be seen in figure 1-4.

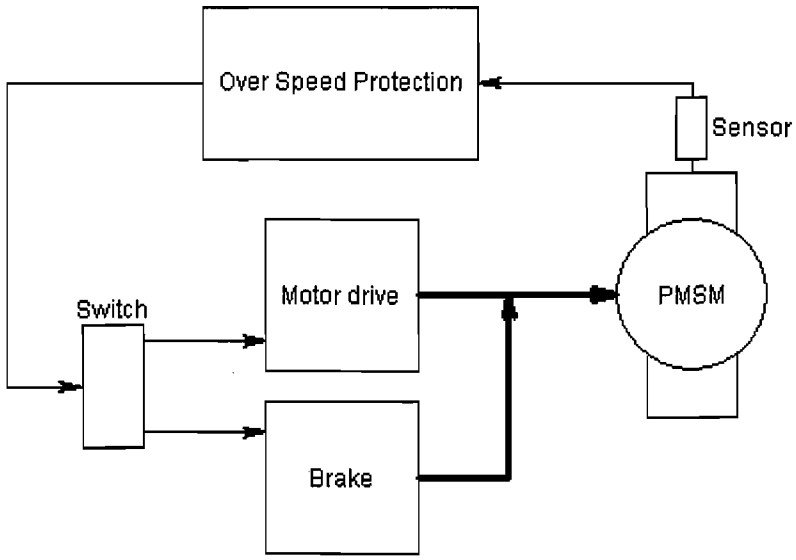

Figure 1-4 Block diagram of over speed protection

While the motor runs, the speed will be measured by some sort of speed sensor. This signal will be fed into a controller where it will be conditioned into useful data. The controller will switch a relay or contactor that will control the input to the motor. This means that either the motor drive that supplies the power to the motor or the braking resistor that will stop the motor will be connected to the motor.

To ensure that the developer of the system can't be held liable for any damage caused by over speed failure, the whole over speed system will be off-the-shelf as an off-the-shelf product is certified and has passed all the quality and safety checks. An in-house developed system on the other hand might not meet all the safety requirements of a certified product.

Drive integration

When every individual process has been modelled and implemented, the system must then be integrated. Each section however, must work individually before integration commences. Any uncertainties must be eliminated before integration because an error in the system might be futile. The complete block diagram of the system layout can be seen in figure 1-5.

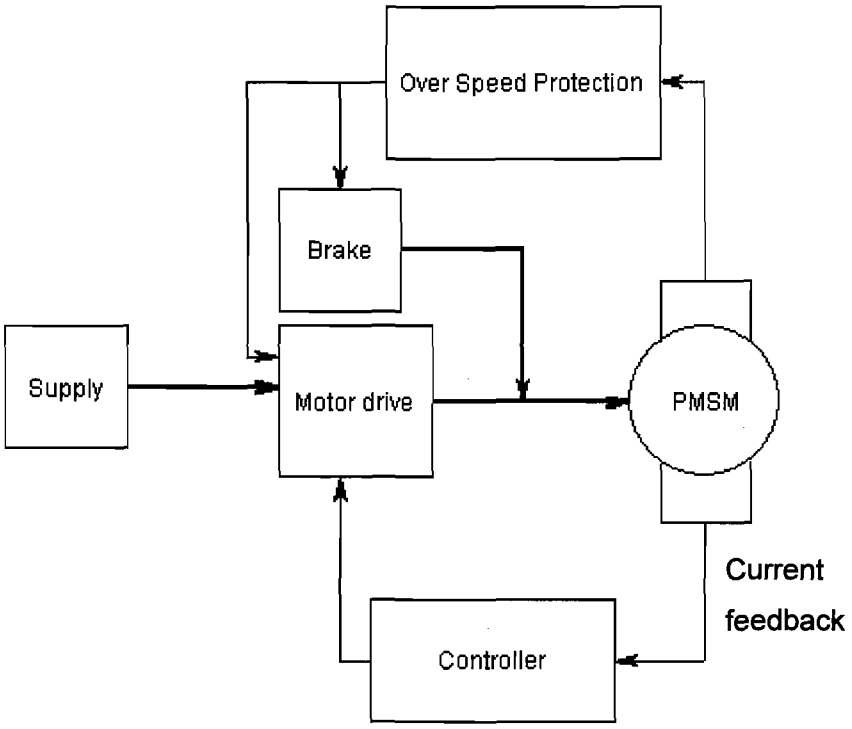

Figure 1-5 Block diagram of system layout

The power supply must be connected to the motor drive. This will supply the drive with a dc-supply that will be converted into a 3-phase voltage for input to the PMSM. There are two measuring points on the motor: one is for the over speed protection and the other for the controller. The controller will be connected to the motor drive to control the speed whereas the over speed protection will be connected to the motor drive as well as a brake.

This closed loop system should be able control the speed of the PMSM from start-up to full speed and back to stand still effectively.

1.3.5 Drive evaluation

Various tests will be done on the system to determine its reliability and usability. The switching signals of the inverters will be measured as well as the output voltage and current of the inverter. The speed of the motor and the frequency of the supply will be measured and compared to ensure that the motor starts properly and to guarantee that the motor is operated in synchronism. All of the abovementioned measurements will be done to ensure that the system performs to specification.

This will determine whether or not the project is a success or a failure. The data of the evaluated system must correspond with the simulations and any deviation from the specified system will result in performance limitations.

1.4 Overview of the dissertation

Chapter 2 contains a literature study of the design and features of the PMSM as well as literature on the ac drive that is used to control the speed of the PMSM.

The PMSM model and controller design is discussed is Chapter 3. The mathematical model of the PMSM is derived and is then used to design a control algorithm that will effectively control the speed of the PMSM. The control algorithm is discussed in detail as well as the results obtained from simulation of the controller.

Chapter 4 gives an overview of the design of the ac drive and the ac filter. The drive is used to generate a three phase voltage that acts as the supply to the motor. The drive design includes the inverter-, inverter gate driver-, optical isolation-, thermal protection-, over current protection- and short circuit protection design. The filter is designed to reduce the current ripple on the supply to the motor and to minimize the effects of electro magnetic interference (EMI).

The complete system is evaluated in Chapter 5. Measurements of the output voltages and currents of the drive are evaluated before and after filter implementation. The pulse width modulated (PWM) signals on the switches of the inverter are also shown.

In the final chapter, Chapter 6, the discrepancies between the actual results and simulated results are discussed and recommendations are made for improvements on the drive.

Chapter 1 gave background on the PMSM. The problem statement, the issues that need to be addressed as well as the methodology were discussed in detail. The chapter was concluded with an overview of the remainder of the report. Chapter 2 will contain literature regarding the PMSM, various control schemes for the PMSM as well as background on the six switch 3-phase inverter.

2
Chapter
Literature Study

Chapter 2 contains a detailed literature study on PMSMs. The study starts with an introduction to PMSMs discussing the dq-transformation and the modelling of the PMSM. The losses and electrical limits are also discussed as well as various control schemes and drives for the PMSM.

2.1 Permanent magnet synchronous motor

For a long time dc motor drives were the most popular for speed and position applications [2]. These drives are popular because of the low cost of implementation of the converter and because of ease of control. DC motors pose the following drawbacks [3]:

- not very robust
- lack of overload capacity
- lower torque than ac motors
- high maintenance on brushes and commutator .

When looking at the dc motor's drawbacks, it is no surprise that ac motors are gaining market share [4]. AC motors has been used for some time now and have proven itself a worthy competitor of the dc motor. When permanent magnets were introduced to the rotor of the ac motor, the permanent magnet synchronous machine (PMSM) was born. The PMSM has advantages like the fact that it is no longer necessary to supply the stator of the motor with a magnetizing current to obtain a constant air gap flux. The stator current is used to produce torque [5]. PMSM's are mostly used in high performance applications like aerospace actuators, machine tool spindles, robotics, centrifugal compressors and pumps, microturbine starter/generating units [4, 6]. The PMSM is fast developing and the popularity of these machines will keep increasing due to the availability of the low-cost high-energy permanent magnet [7].

Some of the other advantages of PMSMs are [6]:

- the PMSM is lightweight
- very small in size
- high power to mass ratio
- high power to volume ratio
- high efficiency to reduce heat generation in the rotor.

2.1.1 D-Q transformation

The transformation of a three phase system to a rotating two phase system is done because the torque and the flux of the motor can then be controlled individually. Figure 2-1 shows what the direct axis and quadrature axis is.

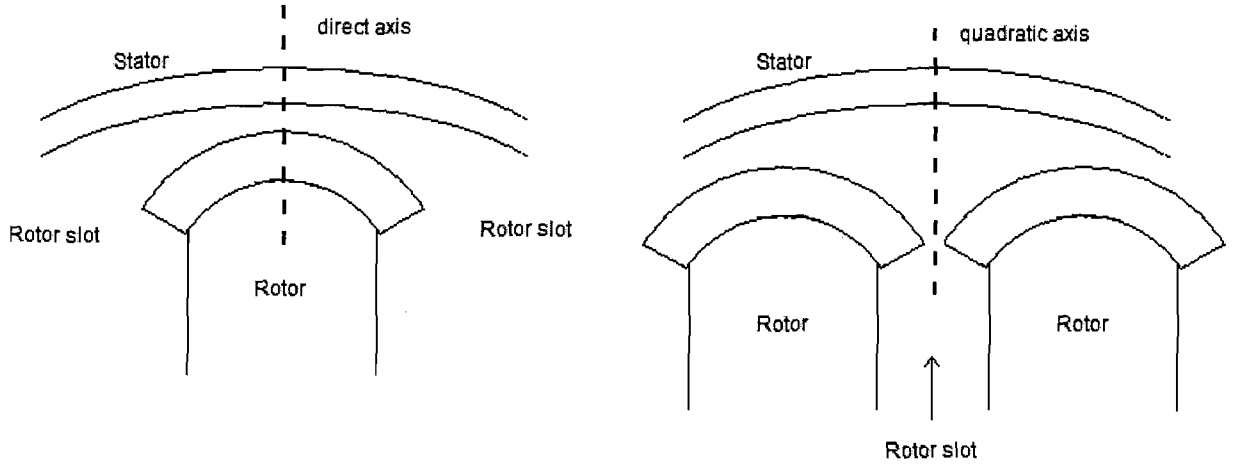

Figure 2-1 Direct- and quadrature axis representation

In the figure can be seen that the direct axis is represented as the part where the rotor is the closest to the stator and the quadrature axis is represented by the part where the rotor is the furthest away from the stator.

To derive a *dq*-axis estimation model of a motor, the following must be assumed:

- the winding flux linkage is sinusoidal, and
- the working flux distribution is sinusoidal.

Two types of effects must be ignored when deriving the *dq*-axis model. The first is the magnet surface, the effects of slotting and the shape of the rotor iron [8]. The other effect relates to the nonlinear magnetizing effects of the iron core material. These include the effects of the unequal

mutual inductances and the saturation [8]. These effects are ignored because the d-q-axis model of the PMSM is already accurate enough.

2.1.2 Physical modelling of PMSM [8]

This section discusses the physical modelling of the surface PMSM. The torque, voltage and motion of the surface PMSM are discussed in terms of the machine's inertia. In (2.1) the motion ($J.\frac{d\omega}{dt}$) is:

$$J.\frac{d\omega}{dt} = T_m - B_\omega - T_L \quad and \quad \frac{d\theta}{dt} = \omega \tag{2.1}$$

where T_m is the output torque, T_L is the load torque, p is the number of pole pairs, J the inertia, B is the friction factor, ω is the angular speed and θ the rotor angle. The inductance matrix is given in (2-2):

$$L_{abc}(\theta) = \begin{bmatrix} L_{aa}(\theta) & L_{ab}(\theta) & L_{ac}(\theta) \\ L_{ba}(\theta) & L_{bb}(\theta) & L_{bc}(\theta) \\ L_{ca}(\theta) & L_{cb}(\theta) & L_{cc}(\theta) \end{bmatrix} \tag{2.2}$$

The winding inductance is a function of the current position and the rotor position. This is because the nonlinear magnetization properties are in the iron core. The inductance matrix, cogging torque and the flux linkage contributed by the permanent magnets are all dependant on the rotor position.

2.1.3 PMSM losses [9]

Like any system ever created, the PMSM also has losses. The most significant losses of the PMSM are the following:

- copper losses,
- iron losses,
- stray losses,
- mechanical losses,
- harmonic losses.

Copper losses –the losses in the stator windings due to the load current that flows through the winding.

$$P_{Cu} = r_s I_s^2 \tag{2.3}$$

where P_{Cu} is the is the copper losses, r_s is the stator resistance and I_s is the stator current.

Iron losses – losses in the iron of the PMSM is caused by the eddy currents and the hysteresis.

$$\begin{aligned} P_{Fe} &= c_{Fe}\omega_e{}^{\beta}\phi_m{}^2 \\ &= c_{Fe}\omega_e{}^{\beta}X_m{}^2 I_m{}^2 \end{aligned} \tag{2.4}$$

where P_{Fe} is the iron losses, c_{Fe} is the iron loss coefficient, ω_e is the supply frequency and ϕ_m is the air gap flux. $\beta = 1.5 \approx 1.6$

Stray losses – these are the losses that can be seen on the copper and the iron of the machine.

$$P_{str} = c_{str}\omega_e{}^2 I_s{}^2 \tag{2.5}$$

where P_{str} is the stay losses and c_{str} is the stray loss coefficient.

Mechanical losses – these losses are proportional to the square of the speed of the motor and are caused by the friction in the motor as well as winding losses in the stator.

$$P_m = c_m\omega_e{}^2 \tag{2.6}$$

where P_m is the mechanical losses and cm is the mechanical loss coefficient.

Harmonic losses – nonsinusoidal stator voltages cause these types of losses. This loss also has an effect on the copper losses and iron losses. For example the stator copper losses will increase when there are harmonic currents present and the iron losses will increase with the presence of harmonic voltages.

2.1.4 Electrical limits [12]

The two electrical limits of the PMSM are the voltage and the current. These limits are imposed by the motor itself and the maximum dc bus voltage of the inverter. Equations (2.7) and (2.8) describe these constraints

$$\begin{aligned} I_s &= \sqrt{I_d^{\,2} + I_q^{\,2}} \\ &\leq I_{s\max} \end{aligned} \tag{2.7}$$

where I_s is the rated current and I_d and I_q are the d-axis and q-axis current respectively.

$$\begin{aligned} U_s &= \sqrt{U_d^{\,2} + U_q^{\,2}} \\ &\leq U_{s\max} \end{aligned} \tag{2.8}$$

where U_s is the dc bus voltage of the inverter and U_d and U_q are the voltages in the d-axis and q-axis respectively. When neglecting the ohmic drops of the PMSM and assuming that the equations of the PMSM are in the steady state, then the following equations are valid:

$$U_d = -\Omega_r L_q I_q \tag{2.9}$$

$$U_q = \Omega_r L_d I_d + \Omega_r \lambda_m \tag{2.10}$$

where λ_m is the permanent magnet flux linkage and Ω_r is the angular electrical rotor speed. Figure 2.2 represents the electrical limits in the form of a graph.

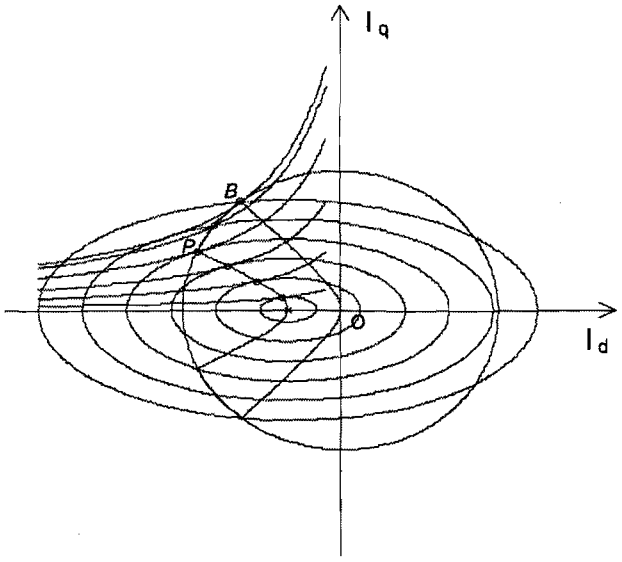

Figure 2-2 Voltage and current limits of the PMSM

In figure 2-2 the voltage limits are represented by the ellipses and the current limits by the circle while the electromagnetic torque is signified by the hyperbolic curves. The field weakening limits are represented by the line between point P and B. The line between point B and the origin indicates the maximum torque per ampere limit.

2.2 PMSM model

When working with super-high speed drives, sensorless position control is required for the following reasons [13]:

- difficulty to install and maintain mechanical shaft position sensor,
- reduces the cost of conventional sensors,
- improves reliability.

Two types of sensorless speed control are usually used when working at super-high speeds. The one is open-loop control where there is no rotor feedback and this is sufficient for speeds up to 100 000 rpm. The second is vector control which is a closed loop control scheme [6]. The open-loop scheme has a few drawbacks however. The performance of a PMSM operating at super-high speeds depends on the motor parameters and the load conditions. There is also a phenomenon called power swing that will result in the motor losing synchronization that can cause total system failure. These effects can be overcome with the use of closed-loop control.

Three of the most common sensorless speed control schemes are:

- constant V/f mode,
- vector control,
- hybrid voltage-vector mode

These three control schemes are discussed in the next section.

2.2.1 PMSM mathematical model

The PMSM must be transformed to the *dq*-reference frame as discussed in section 2.1.1. To transform the PMSM from the stationary 3-phase reference frame to a rotating 2-phase reference frame, the following steps must be completed:

- The Clarke-transformation ($C_{\alpha\beta 0,abc}$) transforms a 3-phase to a 2-phase reference frame
- The rotation matrix ($C_{rot}(-p\theta)$) transforms from the stationary reference frame to the rotating reference frame.

The combination of the abovementioned is called the Park-transformation ($C_{park}(p\theta) = C_{\alpha\beta 0,abc}C_{rot}(-p\theta)$) that transforms from the stationary 3-phase to the rotating 2-phase. The transformation axis is shown in figure 2-3.

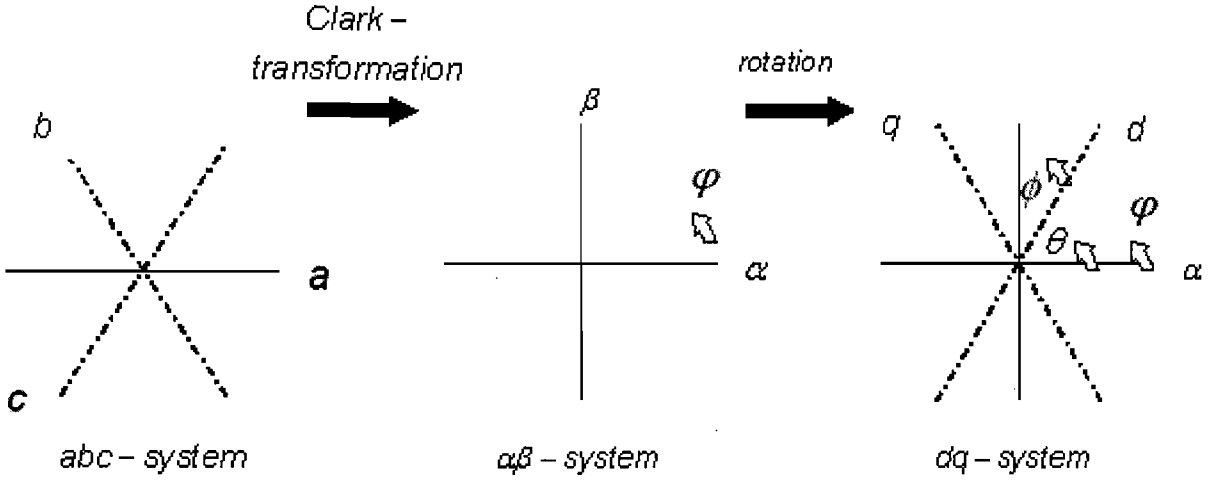

Figure 2-3 Park-transformation [15]

The stator equations for the PMSM are given by [15]:

$$U_{s\alpha\beta} = R_s i_{s\alpha\beta} + \frac{d\lambda_{s\alpha\beta}}{dt} \tag{2.11}$$

$$F_{s\alpha\beta} = \sqrt{\frac{3}{2}} N_s i_{s\alpha\beta} \tag{2.12}$$

$$\lambda_{s\alpha\beta} = L_{s\sigma} i_{s\alpha\beta} + \lambda_{sm\alpha\beta} \tag{2.13}$$

$$\lambda_{sm\alpha\beta} = \sqrt{\frac{3}{2}} N_s \Phi_{\alpha\beta} \tag{2.14}$$

where $\Phi_{\alpha\beta}$ is the total flux of the PMSM, R_s the stator resistance, $i_{s\alpha\beta}$ the stator current, $L_{s\sigma}$ the stator inductance and $F_{s\alpha\beta}$ the magneto motive force (mmf) of the stator. Since the rotor of the PMSM is salient, the mmf and the flux lie in two different quadrants, also called the *dq*-axis. The mmf and the flux are related in the following manner:

$$\Phi_d = \frac{F_{s,d}}{\Re_d} \tag{2.15}$$

and

$$\Phi_q = \frac{F_{s,q}}{\Re_q} \tag{2.16}$$

$\Re_d$ and $\Re_q$ are the reluctances related to the d and q-axis respectively. If the rotor had a cylindrical shape, $\Re_d$ would be equal to $\Re_q$.

The flux can be written in vector form as [15]

$$\Phi_{dq} = \begin{pmatrix} \Phi_d \\ \Phi_q \end{pmatrix} = \begin{pmatrix} \frac{1}{\Re_d} & 0 \\ 0 & \frac{1}{\Re_q} \end{pmatrix} \begin{pmatrix} F_{s,d} \\ F_{s,q} \end{pmatrix} \tag{2.17}$$

Equations (2.11) – (2.14) are in the $\alpha\beta$ - reference frame and needs to be transformed into the dq - reference frame. To accomplish this, the above mentioned equations are multiplied by the rotation matrix, $C_{rot}(p\theta)$ given by (2.18)

$$C_{rot}(p\theta) = \begin{pmatrix} \cos p\theta & -\sin p\theta \\ \sin p\theta & \cos p\theta \end{pmatrix} \tag{2.18}$$

where p is the number of pole pairs and θ is the angle between the d-axis and the α-axis. Equations (2.11) – (2.14) now become [15]

$$U_{sdq} = R_s i_{sdq} + C_{rot}(-p\theta)\frac{d}{dt}(C_{rot}(p\theta)\lambda_{sdq}) \tag{2.19}$$

$$F_{sdq} = \sqrt{\frac{3}{2}} N_s i_{sdq} \tag{2.20}$$

$$\lambda_{sdq} = L_{s\sigma} i_{sdq} + \lambda_{smdq} \tag{2.21}$$

$$\lambda_{smdq} = \sqrt{\frac{3}{2}} N_s \Phi_{dq} \tag{2.22}$$

Solving the second part of (2.19) yields

$$\begin{aligned} C_{rot}(-p\theta)\frac{d}{dt}(C_{rot}(p\theta)\lambda_{sdq}) &= C_{rot}(-p\theta)\frac{dC_{rot}(p\theta)}{dt}\frac{d(p\theta)}{dt}\lambda_{sdq} \\ &\quad + C_{rot}(-p\theta)C_{rot}(p\theta)\frac{d\lambda_{sdq}}{dt} \\ &= p\omega_m \begin{pmatrix} 0 & -1 \\ 1 & 0 \end{pmatrix}\lambda_{sdq} + \frac{d\lambda_{sdq}}{dt} \end{aligned} \tag{2.23}$$

$\omega_m = \frac{d\theta}{dt}$ which is the change of angle of the rotor over time also referred to as the motor speed.

The equations for the stator are now in the *dq*-reference frame:

$$U_{sdq} = R_s i_{sdq} + p\omega_m \begin{pmatrix} 0 & -1 \\ 1 & 0 \end{pmatrix}\lambda_{sdq} + \frac{d\lambda_{sdq}}{dt} \tag{2.24}$$

$$F_{sdq} = \sqrt{\frac{3}{2}} N_s i_{sdq} \tag{2.25}$$

$$\lambda_{sdq} = L_{s\sigma} i_{sdq} + \lambda_{smdq} \tag{2.26}$$

$$\lambda_{smdq} = \sqrt{\frac{3}{2}} N_s \Phi_{dq} \tag{2.27}$$

The main field inductance is given by

$$L_{dm} \equiv \frac{\frac{3}{2}N_s^2}{\Re_d} \tag{2.28}$$

and

$$L_{qm} \equiv \frac{\frac{3}{2}N_s^2}{\Re_q} \tag{2.39}$$

By writing U_{sdq} in vector form, U_d and U_s are obtained in the dq-reference frame:

$$U_d = R_s i_d - p\omega_m \lambda_q + \frac{d\lambda_d}{dt} \tag{2.30}$$

$$U_q = R_s i_q + p\omega_m \lambda_d + \frac{d\lambda_q}{dt} \tag{2.31}$$

$$\lambda_d = L_{s\sigma} i_d + L_{dm} i_d \tag{2.32}$$

$$\lambda_q = L_{s\sigma} i_q + L_{qm} i_q \tag{2.33}$$

The synchronous inductances are given by

$$L_d \equiv L_{dm} + L_{s\sigma} \tag{2.34}$$

and

$$L_q \equiv L_{qm} + L_{s\sigma} \tag{2.35}$$

(2.30) – (2.33) is then simplified to:

$$U_d = R_s i_d - p\omega_m \lambda_q + \frac{d\lambda_d}{dt} \tag{2.36}$$

$$U_q = R_s i_q + p\omega_m \lambda_d + \frac{d\lambda_q}{dt} \tag{2.37}$$

$$\lambda_d = L_d i_d \tag{2.38}$$

$$\lambda_q = L_q i_q \tag{2.39}$$

Since a PMSM with no damper winding is used in this application, an equation for the field winding is added

$$U_f = R_f i_f + \frac{d\lambda_f}{dt} \tag{2.40}$$

The field winding does not exist in the PMSM. The field windings are used to model the flux due to the magnets. Since the rotor field winding lies in the d-axis, it couples only with the d-axis winding. The flux linkage for the q-axis remains unchanged:

$$\begin{aligned} \lambda_q &= L_{s\sigma} i_q + \lambda_{qm} \\ &= L_{s\sigma} i_q + L_{qm} i_q \\ &= L_q i_q \end{aligned} \tag{2.41}$$

Since there are two coupled coils on the d-axis, the flux linkage equations now become

$$\begin{aligned} \lambda_d &= L_{s\sigma} i_d + \lambda_{dm} \\ &= L_{s\sigma} i_d + L_{dm} i_d + M_{sf} i_f \\ &= L_d i_d + M_{sf} i_f \\ \lambda_f &= M_{sf} i_d + L_f i_f \end{aligned} \tag{2.42}$$

where M is the mutual inductance. Equation (2.42) needs to be written in a form where the air-gap flux is central. In order to achieve this, the field inductance (L_f) is split into two parts

$$L_f = L_{fm} + L_{fr} \tag{2.43}$$

where L_{fm} is the motor field inductance and L_{fr} is the rotor field inductance. By choosing L_{fm} to be ideally coupled to L_{dm}, $\left(\frac{M_{sf}^2}{L_{dm} L_f} = 1\right)$ (2.42) becomes

$$\begin{aligned}\lambda_f &= L_{fr} i_f + \lambda_{fm} \\ &= L_{fr} i_f + M_{sf} i_d + L_{fm} i_f\end{aligned} \tag{2.44}$$

The torque of the PMSM is given by

$$T_e = p(-i_d \lambda_q + i_q \lambda_q) \tag{2.45}$$

2.3 PMSM control schemes

Three of the most common control schemes will de discussed, namely:

- Constant V/f mode
- Vector control
- Hybrid voltage-vector mode

2.3.1 Constant V/f mode [6]

For the V/f control scheme, a reference speed curve is generated and the V/f ratio is specified depending on the type of load that is used. The abovementioned is used to generate a command voltage (V_s^*) and a command speed (ω_s^*). A block diagram of the V/f control scheme is given in figure 2-4.

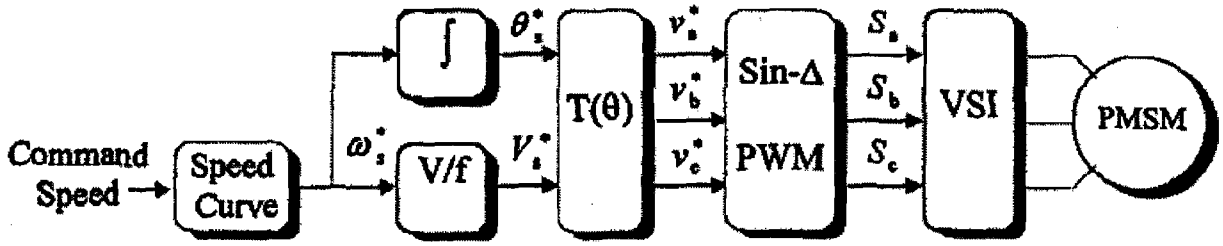

Figure 2-4 V/f control scheme block diagram [6]

The command speed is integrated over time to obtain the angle of the rotor. The command speed is also used as input to the V/f control to obtain the command voltage. Equations (2.46) and (2.47) show how the reference stator voltages are obtained with the use of V_s^* and ω_s^*.

$$\theta_s^* = \int_0^t \omega_s^*(\tau) d\tau \tag{2.46}$$

$$\upsilon_a^* = V_s^* \sin\theta_s^* \tag{2.47}$$

To obtain υ_b^* and υ_c^*, 120 ^{0} is added and subtracted from (2.47) respectively. The PWM signals (S_a, S_b, S_c) that will be applied to the gate of the switching devices is derived in the $\mathrm{Sin}-\Delta$ comparison by using the command voltages υ_{abc}^*. The most important thing to remember when developing a V/f control scheme, is that the reference speed curve must be chosen carefully and correctly. The incorrect choice of the reference speed curve will prevent or "destroy" synchronism between the rotor and the stator. The reference speed curve in figure 2-5 is used as baseline when determining the reference speed curve for this system.

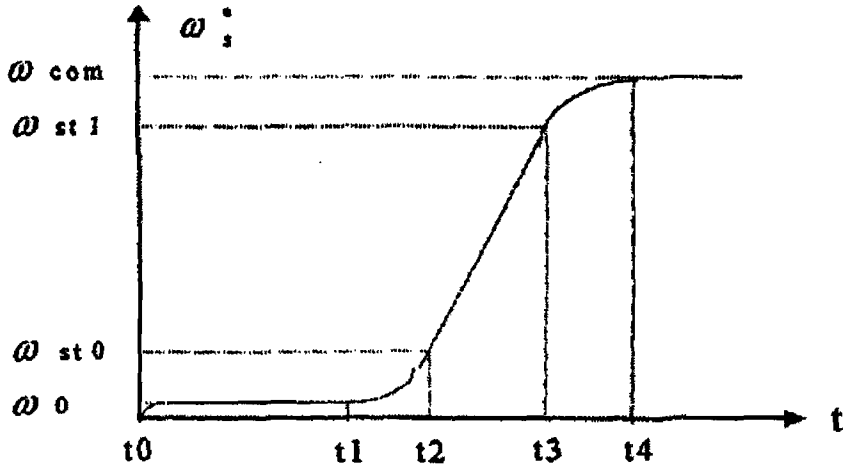

Figure 2-5 Reference speed curve [6]

The interval (t0 – t1) is the starting interval. In order to start the motor, a short interval of constant frequency is needed to overcome the rotor inertia at standstill. The next interval (t2 – t3) is the acceleration interval. If the acceleration rate is too high, over current and possible instability may occur. The slope of the acceleration curve is determined from trail and error iterations. Intervals (t1 – t2) and (t3 – t4) are the transition intervals from start-up to accelerate and accelerate to constant speed respectively. The transitions must be as smooth as possible. If these curves are too sharp, the results will cause over current and loss of synchronism.

A voltage boost is also required at start-up for V/f control. The voltage boost graph can be seen in figure 2-6.

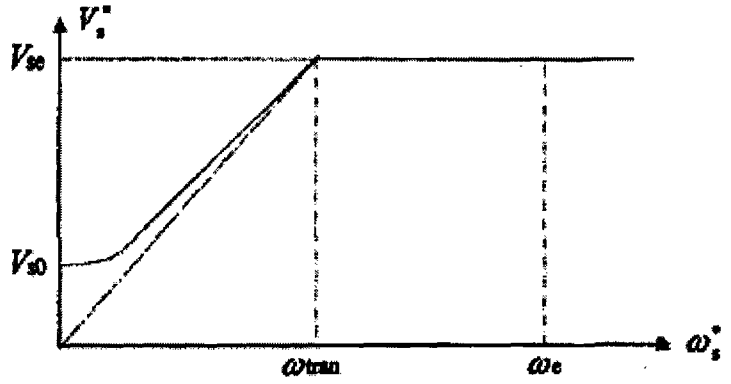

Figure 2-6 Voltage boost [6]

In figure 2-6, V_{sc}^* is the rated voltage, V_{s0}^* the boost voltage at zero speed and ω_e the rated speed. The curve is only for a specific PMSM. When the load increases, the boost voltage must also increase.

The V/f control scheme is thus very sensitive to the slope of the reference speed curve. The wrong curve can cause the PMSM to never reach synchronism or lose synchronism very quickly.

2.3.2 *Vector control [6]*

Vector control is also a good way to control the speed of the motor. With vector control, the starting current of a PMSM can be significantly reduced with the use of a current feedback loop. Figure 2-7 shows the vector control scheme.

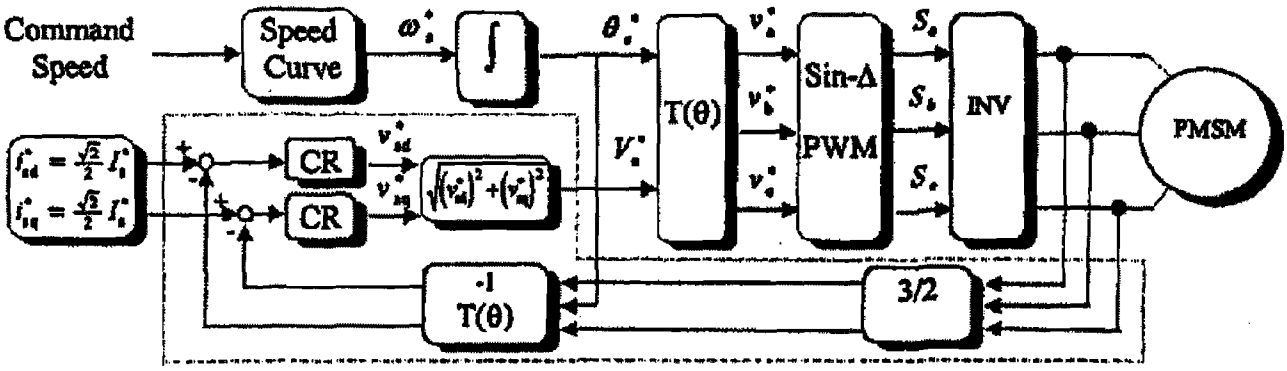

Figure 2-7 Vector control scheme [6]

Vector control is almost the same as V/f control. The difference is that a current regulator (inside the dashed line) is used to calculate the command voltage. The control method also

needs current sensors to close the feedback loop. Depending on the inertia and the load of the system, the command current (I_s^*) must be chosen empirical. Only 10 % of the current is needed to start the PMSM and to accelerate to the desired speed. The vector control is better than the V/f control because:

- vector control remains stable even when PMSM lose synchronism, and
- easier to start the motor from standstill.

Vector control also has its limits. It is more difficult to run a PMSM at very high speeds because of the back-EMF [6]. The higher the speed the bigger the effect of the back-EMF.

2.3.3 *Hybrid voltage-vector mode [6]*

The hybrid voltage-vector control is, as the name says, a combination of the V/f mode and the vector control schemes. By combining these control schemes a control mode is developed that is very easy to implement but also very stable. The hybrid mode control scheme is shown in figure 2-8.

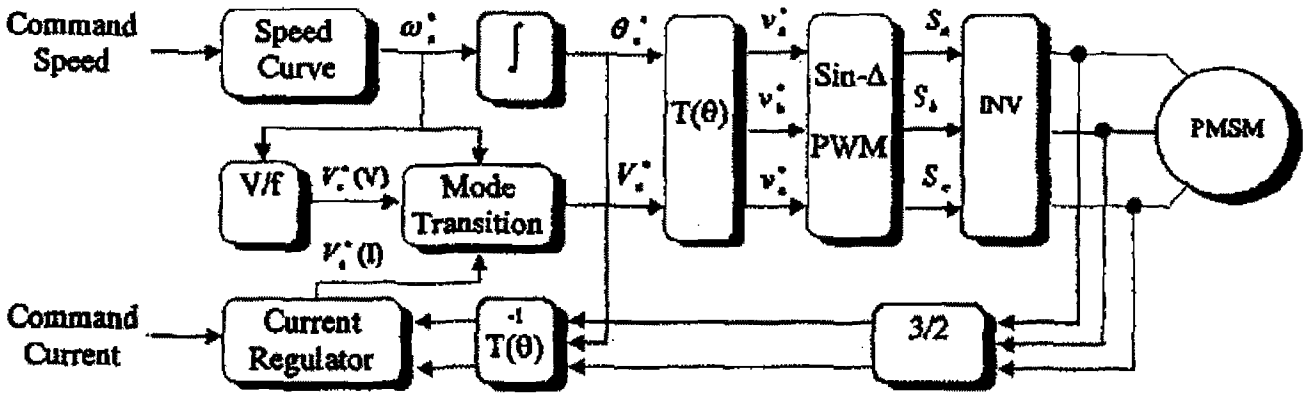

Figure 2-8 Hybrid voltage-vector control [6]

This control scheme also needs a reference speed curve like the V/f control, the difference however is that the vector control starts the PMSM and then starts to accelerate to a predetermined speed. Beyond this value the control will switch over from vector control to V/f mode and the motor will continue to accelerate until the maximum speed is reached. The transition is made by the "Mode Transition" block in figure 2-8. Figure 2-9 shows the reference speed curve for the hybrid mode.

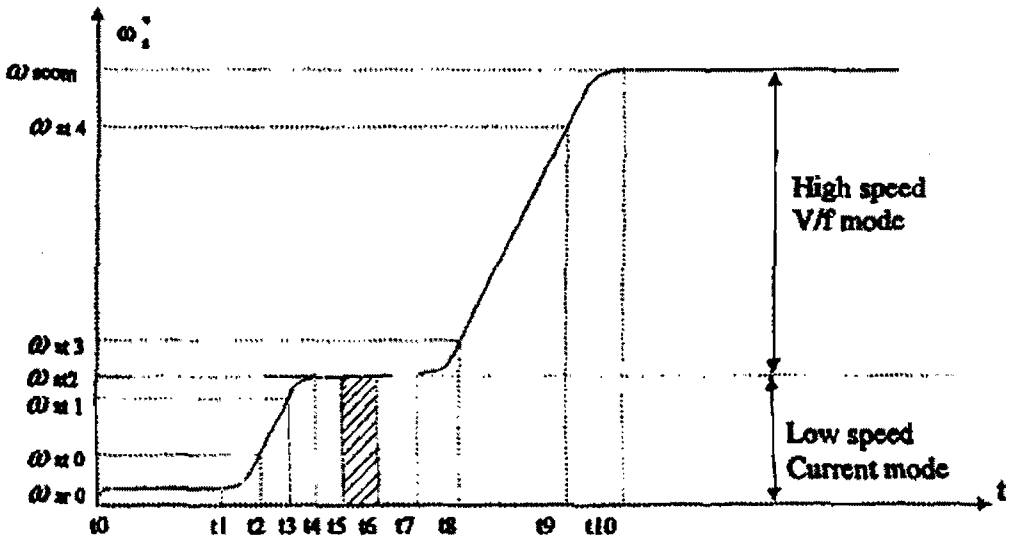

Figure 2-9 Reference speed curve for hybrid mode [6]

The transition modes must be as smooth as possible, because sharp transitions may cause over current. The hybrid mode performs excellent at PMSM start-up with a low starting current and smooth acceleration to full speed. This method is however still very dependant on the slope of the reference speed curve as well as the ratio of V/f.

2.4 PMSM drives [14]

AC inverters are placed in two categories. The one is current-source inverters (CSI) and the other is voltage-source inverters (VSI) [1]. IGBTs or GTOs are most commonly used to build voltage-source inverters. Inverters have the following characteristics:

- can be single phase,
- can be multi phase,
- deliver bipolar current waveforms,
- allow bi-directional power flow.

The most common use of inverters is in drives for ac motors [1]. For this project a voltage-source inverter will be used because it is most commonly used in medium power and high power applications. The main purpose of the inverter is to provide a three phase voltage source. It is important that the frequency, phase and amplitude of the voltage should be controlled. The VSI is shown in figure 2-10.

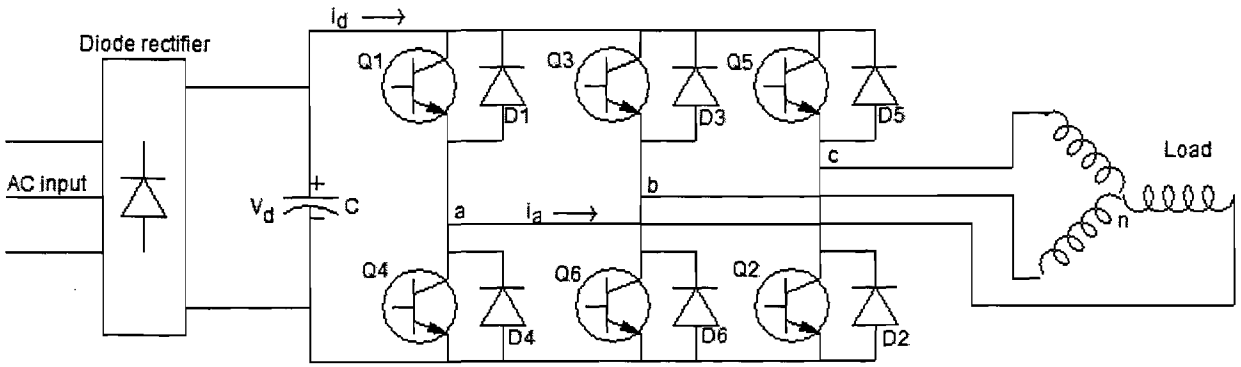

Figure 2-10 3-pase inverter

The inverter consists of a diode rectifier that will rectify the ac input to a dc level. A capacitor is placed across the output of the rectifier to filter or smooth the ripple component that might be on the dc voltage. The dc voltage is applied to the six switch inverter that is connected to the ac motor. To enable the inverter to generate a 3-phase voltage, each half-bridge configuration is mutually phase shifted by $2\pi/3$ rad or 120°. To generate the 3-phase voltage, the switching devices must switch in different states. The switching states of the VSI are given in table 2.1.

Table 2-1 Switch states

Switch states	State number	v_{ab}	v_{bc}	v_{ca}
Q1,Q2 and Q6 are on and Q4,Q5 and Q3 are off	1	v_d	0	$-v_d$
Q2,Q3 and Q1 are on and Q5,Q6 and Q4 are off	2	0	v_d	$-v_d$
Q3,Q4 and Q2 are on and Q6,Q1 and Q5 are off	3	$-v_d$	v_d	0
Q4,Q5 and Q3 are on and Q1,Q2 and Q6 are off	4	$-v_d$	0	v_d
Q5,Q6 and Q4 are on and Q2,Q3 and Q1 are off	5	0	$-v_d$	v_d
Q6,Q1 and Q5 are on and Q3,Q4 and Q2 are off	6	v_d	$-v_d$	0
Q1,Q3 and Q5 are on and Q4,Q6 and Q2 are off	7	0	0	0
Q4,Q6 and Q2 are on and Q1,Q3 and Q5 are off	8	0	0	0

From the table can be seen that for states 7 and 8 the output will be 0 V. The reason for this is that the current will freewheel in this time, through either the upper switches or lower switches. The switching states also ensure that the devices in the same leg do not switch on simultaneously, thus avoiding a short circuit. The carrier signal and modulating signals are shown in figure 2-11.

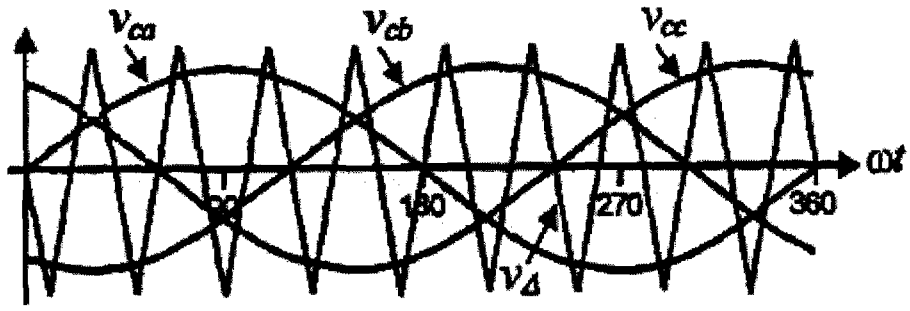

Figure 2-11 Carrier signal and modulating signals [14]

The phases of the PMSM is wye-connected (figure 2-10) which means that the line voltages (v_{ab}, v_{bc}, v_{ca}) must be transformed to obtain the phase voltages (v_{an}, v_{bn}, v_{cn}). The PWM with the ac output voltage is shown in figure 2-12.

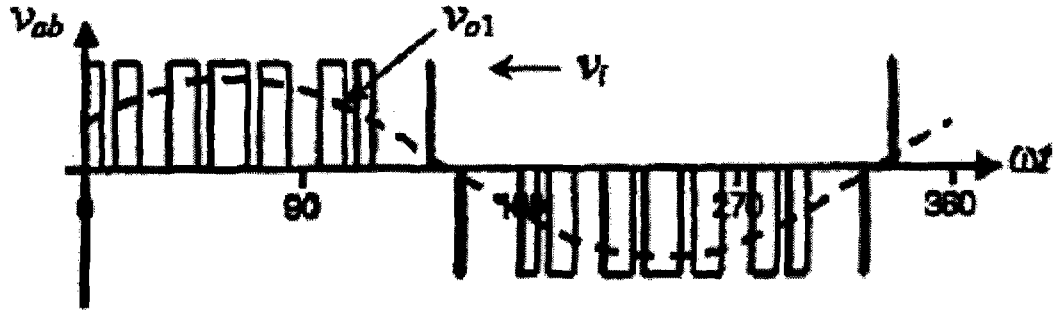

Figure 2-12 AC output voltage

The line voltages can be represented in vector form as:

$$\begin{bmatrix} v_{ab} \\ v_{bc} \\ v_{ca} \end{bmatrix} = \begin{bmatrix} v_{an}-v_{bn} \\ v_{bn}-v_{cn} \\ v_{cn}-v_{an} \end{bmatrix} \tag{2.48}$$

The line voltages can be written as a function of the phase voltages by obtaining the inverse matrix of the phase voltages. This relation, in vector form is given by (2.56)

$$\begin{bmatrix} v_{ab} \\ v_{bc} \\ v_{ca} \end{bmatrix} = \begin{bmatrix} 1 & -1 & 0 \\ 0 & 1 & -1 \\ -1 & 0 & 1 \end{bmatrix} \begin{bmatrix} v_{an} \\ v_{bn} \\ v_{cn} \end{bmatrix} \tag{2.49}$$

This is a singular system which means that the line voltages will add up to zero. This implies that the phase voltages cannot be obtained with the use of the inverse matrix. If the phase voltages add up to zero, then (2.49) can be written as [14]

$$\begin{bmatrix} v_{ab} \\ v_{bc} \\ 0 \end{bmatrix} = \begin{bmatrix} 1 & -1 & 0 \\ 0 & 1 & -1 \\ 1 & 0 & 1 \end{bmatrix} \begin{bmatrix} v_{an} \\ v_{bn} \\ v_{cn} \end{bmatrix} \tag{2.50}$$

Equation (2.50) is not singular, meaning that it can be rewritten as:

$$\begin{aligned} \begin{bmatrix} v_{an} \\ v_{bn} \\ v_{cn} \end{bmatrix} &= \begin{bmatrix} 1 & -1 & 0 \\ 0 & 1 & -1 \\ -1 & 0 & 1 \end{bmatrix}^{-1} \begin{bmatrix} v_{ab} \\ v_{bc} \\ 0 \end{bmatrix} \\ &= \frac{1}{3} \begin{bmatrix} 2 & 1 \\ -1 & 1 \\ -1 & -2 \end{bmatrix} \begin{bmatrix} v_{ab} \\ v_{bc} \end{bmatrix} \end{aligned} \tag{2.51}$$

2.5 Filters

When connecting a 3 phase inverter to a flywheel system, various aspects must be taken into consideration. These are:

- Common mode voltages,
- Differential mode voltages,
- Noise due to switching frequencies.

The effects that the abovementioned have on the system are:

- Deterioration of the motor winding isolation with the potential of line to chassis failure,
- Reduced motor efficiency,
- Increased eddy current and hysteresis losses,
- High leakage current from the motor windings through the flywheel main chassis due to parasitic capacitance,
- EMI on the magnetic bearing flywheel position sensors.

The design of a filter is thus needed to eliminate the aforementioned threats. Common mode and differential mode voltages are explained with the use of figure 2-13.

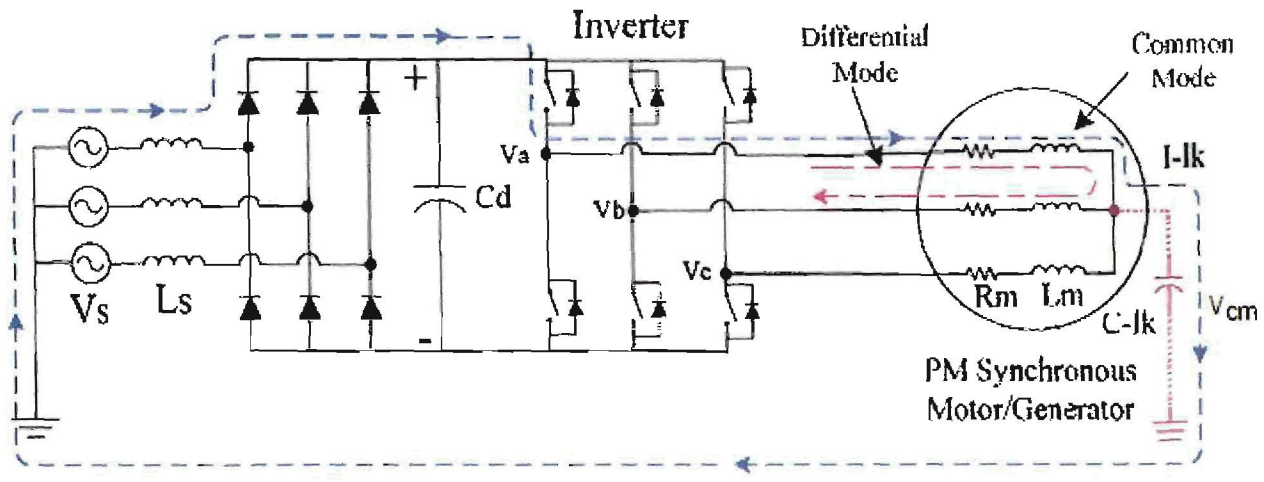

Figure 2-13 Inverter/flywheel connection [21]

From figure 2-13 can be seen that the common mode voltage is across the leakage capacitance (*C-Ik*) that is located between the motor and the housing of the flywheel. Equation (2.52) shows the equations that represent the common mode voltages:

$$\begin{aligned} v_a - v_{cm} &= R_m i_a + L_m \frac{di_a}{dt} \\ v_b - v_{cm} &= R_m i_b + L_m \frac{di_b}{dt} \\ v_c - v_{cm} &= R_m i_c + L_m \frac{di_c}{dt} \end{aligned} \tag{2.52}$$

where v_a, v_b, and v_c are the voltages at the motor terminals with respect to ground and R_m and L_m are the per phase motor winding resistance and inductance respectively. Differential mode voltages are caused by the IGBTs high voltage/short rise time combination. This results in high dv/dt line to line voltages. Both of these phenomena will be greatly reduced with the implementation of a RLC-filter between the power amplifier output and the terminals of the PMSM. The filter will also reduce the current ripple and minimize electromagnetic interference (EMI).

In this chapter the PMSM was discussed in detail. The dq-transformation was explained as was the modelling of the PMSM. The effects of the back-EMF were then discussed and the various losses and electrical limits were argued. Various control schemes such as constant V/f mode, vector control and hybrid voltage-vector mode were mentioned along with the functionality of the 3-phase inverter. The next chapter looks at the design of the PMSM control.

3
Chapter

PMSM control

This chapter deals with the detailed design of the controller. The mathematical model of the PMSM is given and is then used to derive a control algorithm. The simulation of the control algorithm is done in SIMULINK® and discussed as well as the results obtained from the simulation.

3.1 Introduction

The PMSM is a stationary 3-phase system with phases a, b and c. To model the PMSM, the stator of the PMSM must be referenced to the rotor. The transformation is necessary to derive a mathematical model for the PMSM. This section will look at the transformation and mathematical model of the PMSM.

3.2 PMSM SIMULINK® model

To control the speed of the PMSM, a sensorless voltage over frequency (V/f) control method is implemented. This control method was chosen because of its implementation simplicity. The method uses the current in two of the phases of the motor to determine the magnitude to which the voltage should increase to control the speed of the motor. The voltage magnitude is calculated with a series of equations (explained in this section). A reference speed is calculated to keep the V/f ratio constant so that the motor speed will increase in such a way, that the motor speeds up in synchronism. There is also a build in stabilizer. The function of the stabilizer is to ensure that the motor does not fall out of synchronism as the speed increases.

This method is discussed throughout this section as well as the simulation of the control with the PMSM.

The simulation of the V/f speed control and the PMSM can be seen in figure 3-1. The PMSM model can be seen on the right hand side of the figure and the V/f control can be seen on the left. The PMSM represents the mathematical model derived in section 2.2.

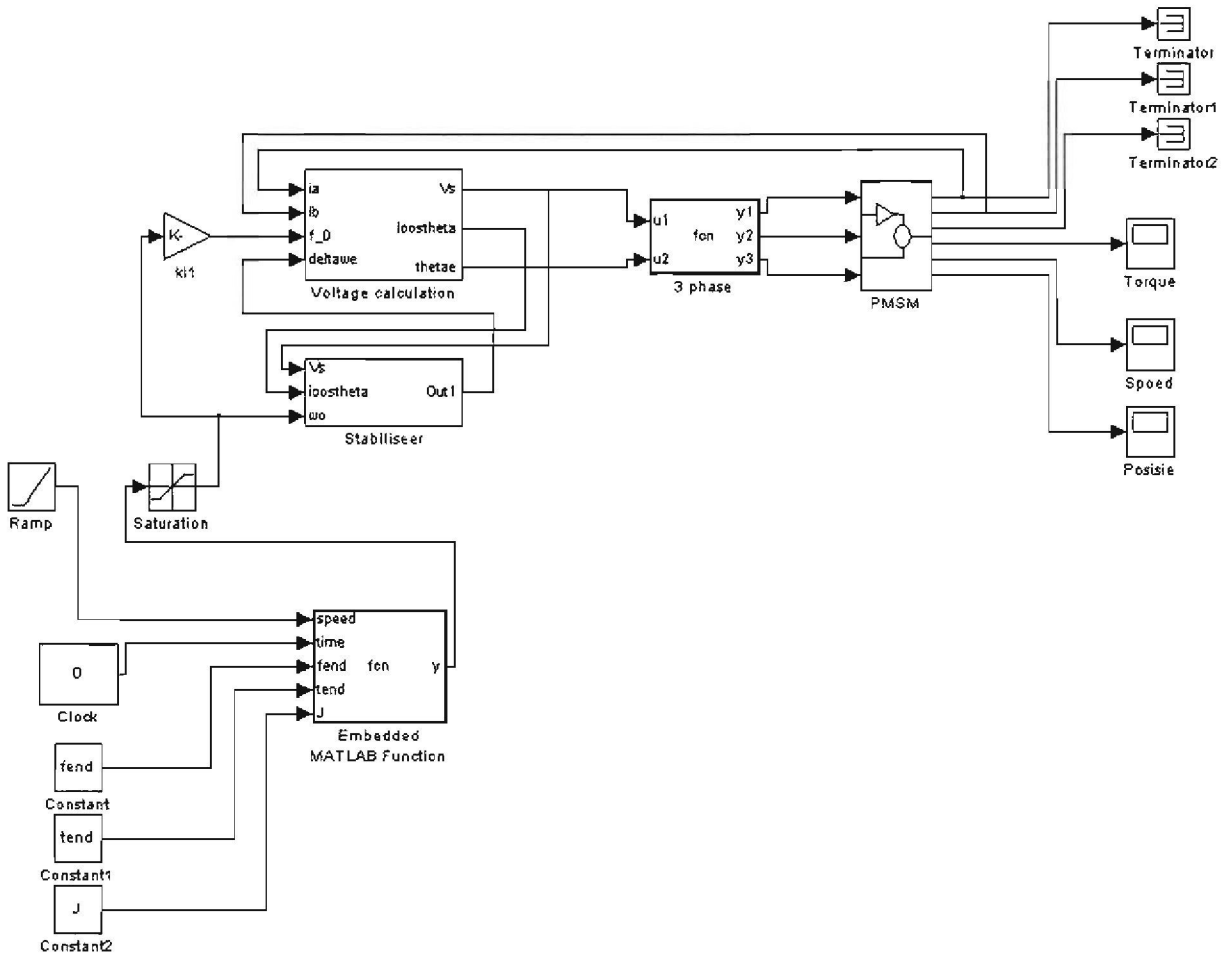

Figure 3-1 PMSM SIMULINK® model

The voltage magnitude is calculated to keep the stator flux linkage in the PMSM constant. When the stator flux linkage is kept constant, the PMSM will deliver constant torque over any frequency range [16]. Figure 3-2 shows the voltage magnitude calculator.

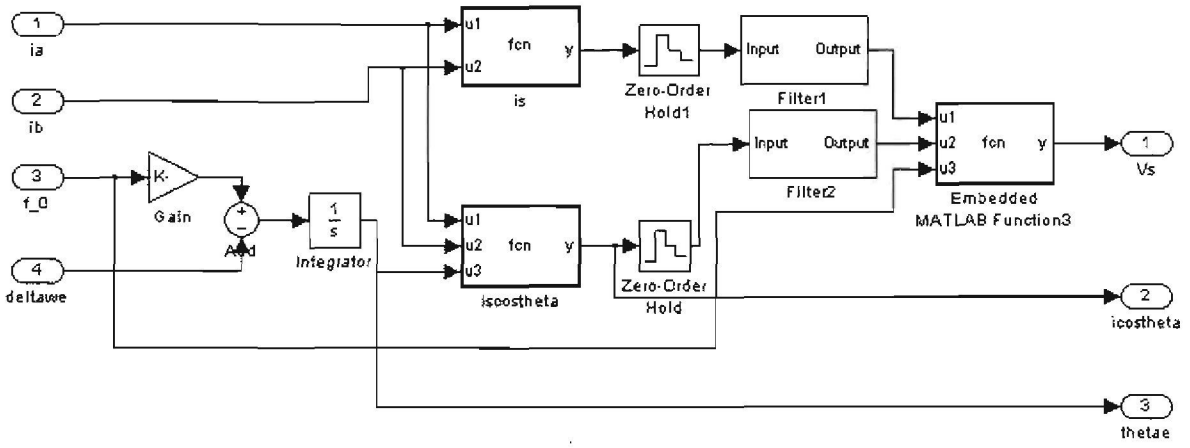

Figure 3-2 Voltage calculator

The variables needed to calculate the magnitude of the voltage are two stator currents (i_{as}, i_{bs}) and the position of the voltage vector in the stationary position (θ_e). The voltage vector is calculated as follows:

The applied frequency to the machine, f_0 is used to calculate the speed of the motor in radians with

$$\omega = 2\pi f_0 \tag{3.1}$$

To obtain the angle or position of the voltage vector (3.2), (3.1) is integrated over time

$$\theta_e = \int \omega \, dt \tag{3.2}$$

It seems like unnecessary calculations as the frequency could have been used as input instead of the integral of the speed, but the voltage that must be supplied to the motor (ie v_a) is calculated as

$$v_a = V_s \sin(\omega t)$$

with V_s the magnitude of the voltage and ω the same as in (3.1). Figure 3-3 shows what happens when the frequency is changed without integrating. The frequency does not change at a zero crossing in time, causing the motor to run out of synchronism for the time period of change.

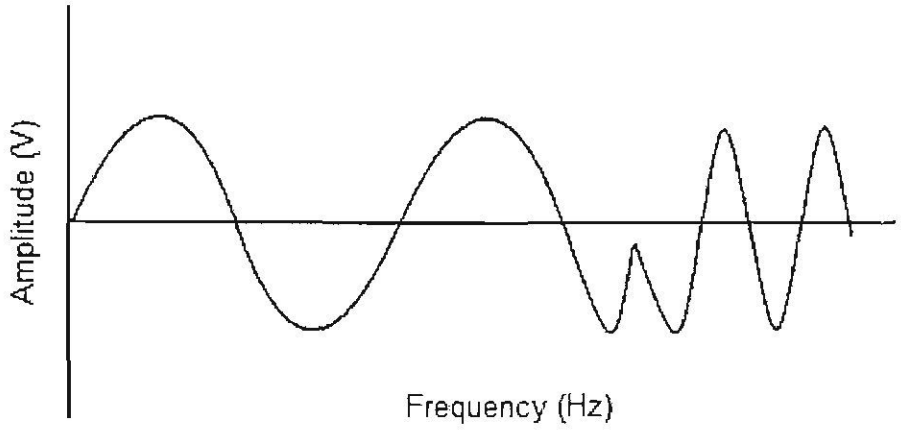

Figure 3-3 Frequency change without integration

When integrating the speed over time, this phenomenon does not appear since an integrator does not allow sudden changes (figure 3-4).

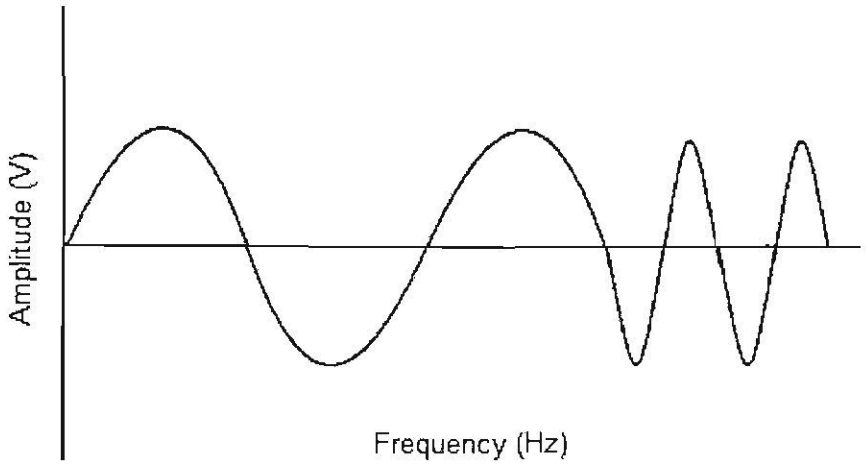

Figure 3-4 Frequency change with integration

Four steps must be followed to determine the voltage command or magnitude of the voltage. The first step is to calculate the instantaneous value of magnitude of the current vector (i_s). This is done by adding the two phase currents

$$\begin{aligned} i_s &= \sqrt{(i_{ds}^s)^2 + (i_{qs}^s)^2} \\ &= \sqrt{\frac{1}{3}(i_{as} + 2i_{bs})^2 + (i_{as})^2} \end{aligned} \tag{3.3}$$

Then the instantaneous value of magnitude of the power-factor angle ($i_s \cos\phi$) can be calculated as

$$i_s \cos\phi = \frac{2}{3}\left[i_{as} \cos\theta_e + i_{bs} \cos(\theta_e - \frac{2\pi}{3}) - (i_{as} + i_{bs}) \cos(\theta_e + \frac{2\pi}{3}) \right] \tag{3.4}$$

(3.3) and (3.4) are both filtered with a low pass filter that has a cut-off frequency of 5 kHz. These values are then combined to obtain the voltage command as

$$V_s = (i_s \cos\phi) r_s + \sqrt{(2\pi f_0 \lambda_m)^2 + (i_s \cos\phi)^2 r_s^2 - i_s^2 r_s^2} \tag{3.5}$$

where λ_m is the rotor permanent magnet flux and r_s is the stator winding resistance per phase. There is enough information available to generate a three phase voltage that will supply the motor. Figure 3-5 shows the voltage generator command block.

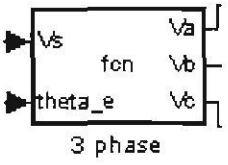

Figure 3-5 Voltage generator command block

Inside this block the three phase voltages are generated as follows:

$$\begin{aligned} \nu_a &= V_s \cos\theta_e \\ \nu_b &= V_s \cos(\theta_e + \frac{2\pi}{3}) \\ \nu_c &= V_s \cos(\theta_e - \frac{2\pi}{3}) \end{aligned} \tag{3.6}$$

with ν_a, ν_b and ν_c the voltage of each phase individually.

The speed of the motor will increase as the voltage increases causing an instability. This instability will increase and cause the motor to fall out off synchronism. Figure 3-6 shows the stable and unstable operating frequencies of a PMSM with no load.

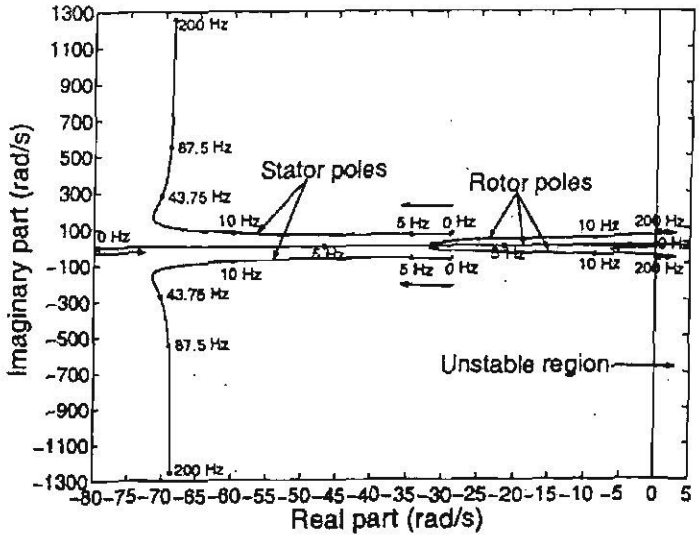

Figure 3-6 Eigenvalue plot under no-load [16]

Figure 3-6 shows two types of machine poles. The poles to the left are the stator poles that represent the fast-acting electrical dynamics in the stator and the rotor poles to the right that signifies the slow electrical dynamics of the machine. Note how the rotor poles migrate to the unstable region of the s-plane after exceeding a certain frequency. Figure 3-7 shows the same plot, but with different load conditions indicating only the rotor poles. Depending on the load, the rotor will enter the unstable region at about 15 Hz.

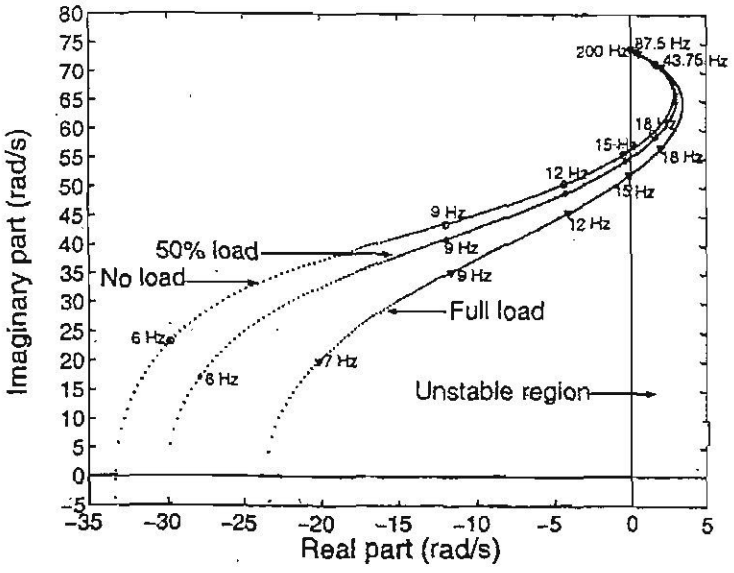

Figure 3-7 Rotor poles for different load conditions [16]

The stabilizer will counter this effect to ensure that the motor does not fall out of synchronism and the stability loop is implemented as shown in figure 3-8.

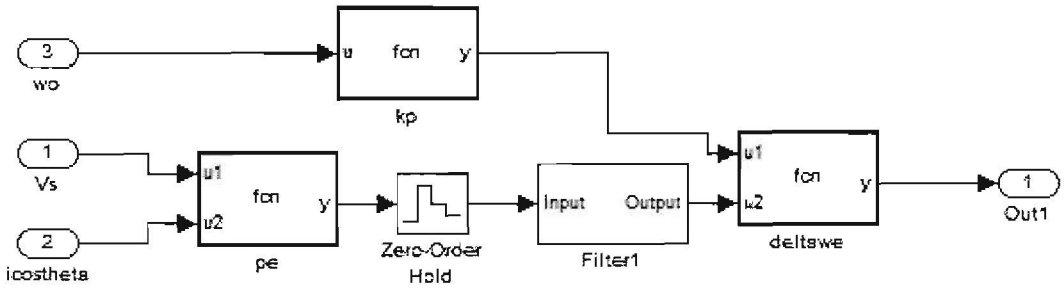

Figure 3-8 Stabilizer

The command voltage magnitude and the instantaneous stator current vector component are used to calculate the input power (p_e)

$$p_e = \frac{3}{2} v_s i_s \cos\phi \tag{3.7}$$

To extract the perturbations in the input power, a first order high-pass filter is used and a gain for the stabilizing loop is calculated. This determines the damping of the stabilizing loop and is given in (3.8) as:

$$k_p = \frac{c_l}{\omega_0}, \ \omega_0 \neq 0 \tag{3.8}$$

with k_p the gain, c_l a gain constant value and ω_0 the speed of the motor. The gain and the filtered input power are multiplied to obtain $\Delta\omega_e$. $\Delta\omega_e$ is the deviation of the frequency modulated signal or reference speed for short. The abovementioned is shown in (3.9)

$$\Delta\omega_e = -k_p(\Delta p_e) \tag{3.9}$$

The output of the stabilizing loop is a sine wave that is 180 ° out of phase with the actual speed. This means that the deviation of the speed will be counter acted by the stabilizer.

3.3 PMSM simulation results

From the simulation of the speed control in section 3.1.2, the following results were obtained. Figure 3-9 shows the output of the voltage command calculator.

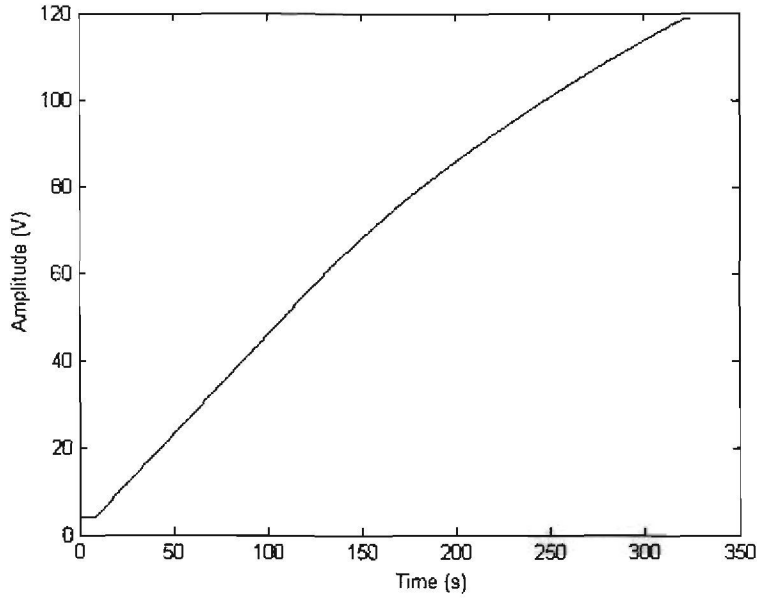

Figure 3-9 Voltage command

Note the constant output for the first few seconds of the simulation. This is to overcome the inertia of the motor in the stationary position and to ensure that the motor is in synchronism. The amplitude will increase until the motor reaches full speed and then remain constant to keep the speed of the motor constant.

The voltage applied to each phase of the motor is shown in figure 3-10.

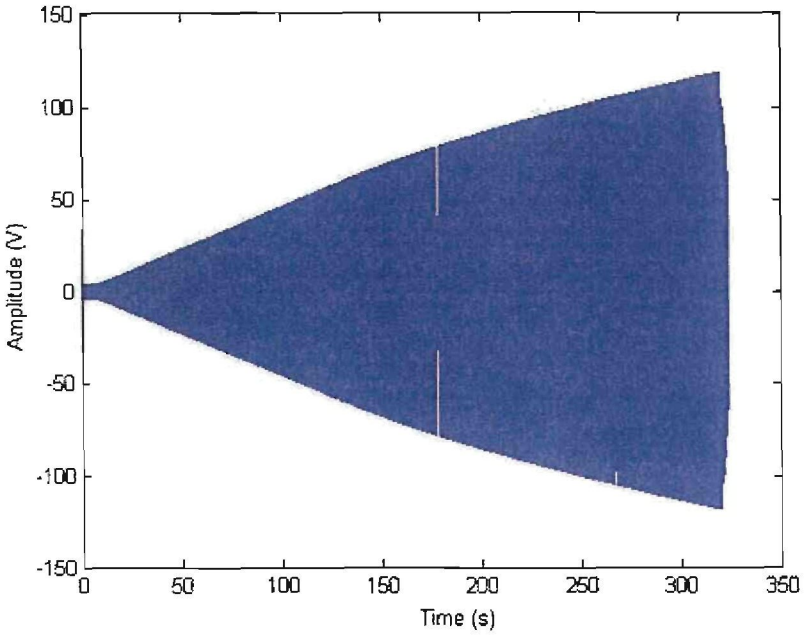

Figure 3-10 Voltage applied to each phase of the motor

From this figure can be seen that the amplitude of the voltage increases over time as it does in figure 3-9. It is clear that the voltage control is working correctly, as this is V/f control, the frequency has to change to keep the V/f ratio constant. The frequency increases over time, but is not visible from figure 3-10 due to the long simulation time. Figure 3-11 shows how the frequency increases. The V/f ratio must be kept constant to ensure that the motor never falls out of synchronism.

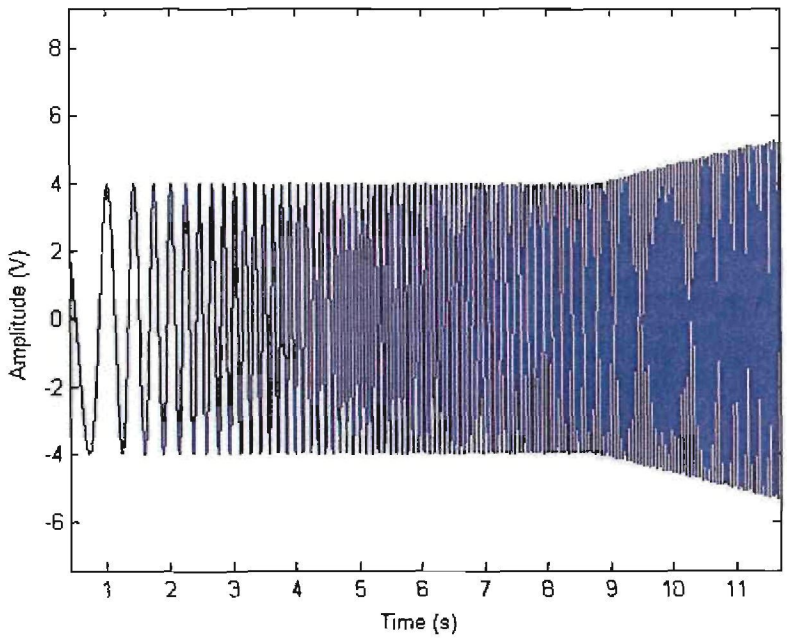

Figure 3-11 Frequency increase over time

Figure 3-12 shows the reference speed and the actual speed of the motor on the same graph.

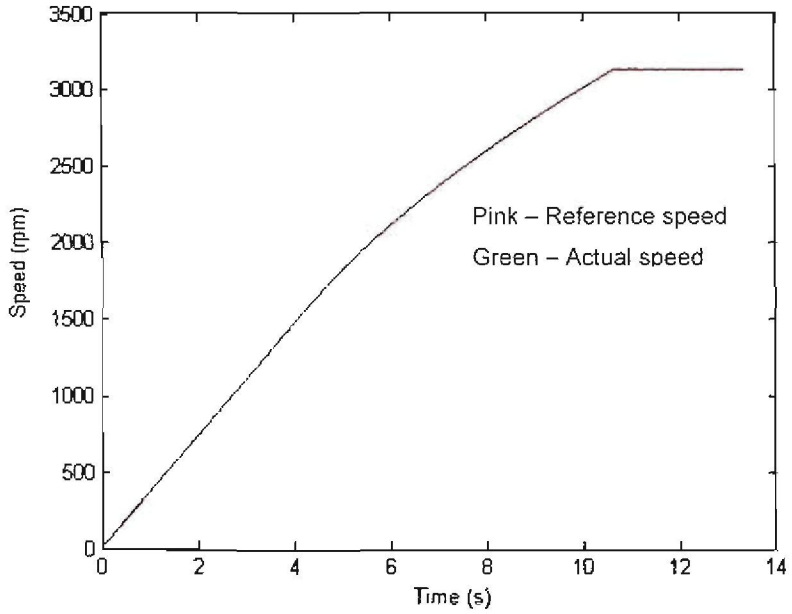

Figure 3-12 Reference speed and actual speed

It looks like only one line, but when zoomed in (figure 3-13); one can see how the actual speed oscillates around the reference speed. These oscillations will decrease and then increase as the rotor moves into the unstable frequency range (previous section).

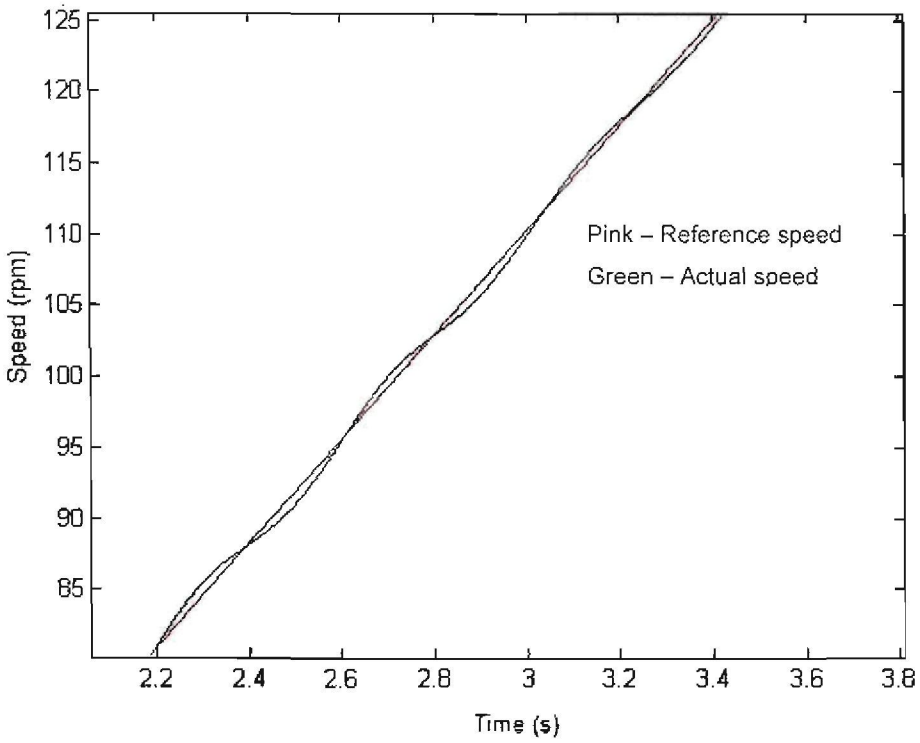

Figure 3-13 Reference speed and actual speed (zoomed in)

The simulation of the V/f speed control for a PMSM appears to be working correctly. The simulation will be used to control the speed of the motor in the final assembly.

Chapter 3 discussed the detailed design of the controller. The mathematical model of the PMSM was given and was used to develop a control algorithm that will control the speed of the motor. A control scheme that suits the application was chosen and discussed and the control along with the model of the PMSM was simulated. The results obtained from the simulation showed that the speed of the PMSM will be controlled and that the motor will speed up in synchronism. In the next chapter the design process of the PMSM drive is explained.

4
Chapter
Drive Design

Chapter 4 contains detailed design discussions on the drive design of the permanent magnet synchronous motor. A detailed specification is followed by designs of the various components of the drive. In conclusion some results obtained from simulations are shown.

4.1 Drive Specification

Power amplifiers (PA) are used to drive a load. In this case the load is a three phase motor. This means that the PA must be designed to generate a three phase voltage. To ensure this, a 3 phase PA must be designed.

Table 4-1 Drive specifications

Specifications	Value
Motor speed	30 000 rpm
Operating current	25 A (max)
Operating voltage	310 V dc
Supply output frequency	500 Hz
Motor drive switching frequency	50 kHz
Maximum torque	0.6 Nm

The specifications for the drive are given in table 4-1. The drive must be operated from a 310 V dc supply and must be able to deliver 2 kW of power to the PMSM at 25 A. The drive switching frequency is 50 kHz and the inverter output frequency at full speed is 500 Hz. The functional block diagram of the drive is given in figure 4-1.

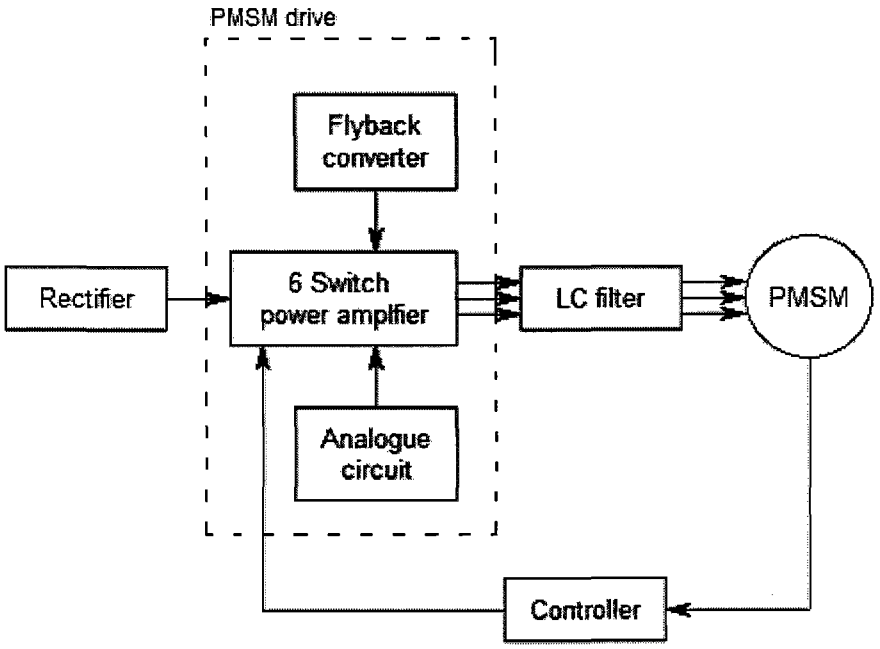

Figure 4-1 Functional block diagram of the drive

The 220 V ac input voltage is rectified by the diode rectifier. A 310 V dc voltage is supplied to the 6 switch power amplifier. On the power amplifier there is a flyback converter that will serve as power supply for the drive electronics. The analogue circuit will mainly be used for signal conditioning of the pick-up coil (coils used for speed sensing) signals. The output of the drive will pass through an LC filter that will filter the PWM voltage. The filter output serves as input to PMSM. The controller in the return path will contain the control algorithm that determines the appropriate PWM signals for the power amplifier to control the speed of the motor.

The next couple of sections will discuss the design of the drive with the following sub-sections:

- Rectifier design
- Flyback converter design
- Power amplifier design
- Analogue circuit design
- LC filter design

4.2 Rectifier design

The rectifier is used to convert the 220 V ac to 310 V dc that is needed to operate the drive. Figure 4-2 shows the diode rectifier layout. The 220 V ac enters from the left and is then rectified to a dc voltage. The capacitor is used to reduce the ripple voltage to a specified level. The transformer is an isolation transformer with a turn ratio of 1:1 and is rated at 2.5 kVA.

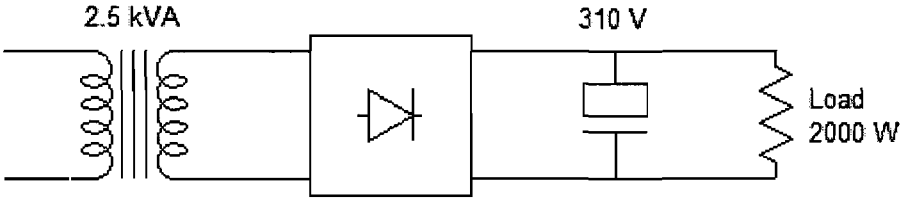

Figure 4-2 Diode rectifier

The average current through the load is calculated as

$$\begin{aligned} I_{average} &= \frac{P_{load}}{V} \\ &= \frac{2000}{310} \\ &= 6.5 \text{ A} \end{aligned} \tag{4.1}$$

The filter capacitor value is calculated with the average current and the change in voltage over time. The input is a 50 Hz sine wave (period of 0.02 s) and the rectified signal is equivalent to a 100 Hz (period of 0.01 s) signal. The maximum ripple voltage is chosen as 5 % of the supply voltage. With the use of (4.2), the value of the capacitor is calculated as

$$\begin{aligned} i &= C\frac{dV}{dt} \\ C &= 6.5\frac{0.01}{0.05x310} \\ &= 4000 \text{ µF} \end{aligned} \tag{4.2}$$

The current calculated in (4.1) is the amount of current that must be delivered by the capacitor for the time that the rectified voltage is below 95 % of the peak. Figure 4-3 shows the rectified voltage as well as the current that flows.

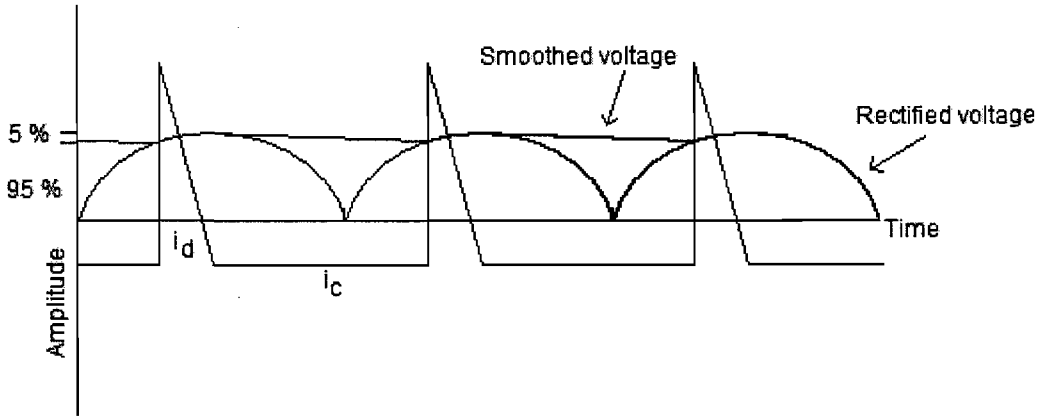

Figure 4-3 Current flow through diode and capacitor

From the figure the peak current that flows for the time that the voltage is above 95% of the peak can be calculated with (4.3) – (4.6). Through (4.3)-(4.4) the total time that the current flows is calculated:

$$\sin(2\pi ft) = 1 \quad t = 5 \text{ ms} \tag{4.3}$$

To determine the time to 95 % of the voltage, set (4.3) equal to 0.95 (frequency is 100 Hz) to obtain the time as

$$\begin{aligned} \sin(2\pi ft) &= 0.95 \\ t &= 3.989 \text{ ms} \end{aligned} \tag{4.4}$$

The time that the capacitor must supply the load current is $5 \text{ ms}+3.989 \text{ ms}=8.989 \text{ ms}$. This means that for $5 \text{ ms}-3.989 \text{ ms}=1.1 \text{ ms}$ the diode will conduct. If the charging current is assumed to be triangular (figure 4-4), then the peak current can be estimated by taking the average current through the capacitor as zero. The peak capacitor current is calculated in (4.5) as

$$\begin{aligned} A_\Delta &= \frac{1}{2} bxh \\ 8.989x6.5 &= \frac{1}{2} 1.1x10^{-3} \cdot h \\ &= 106 \text{ A} \end{aligned} \tag{4.5}$$

The peak current that flows in the 5 ms is calculated (4.6) as

$$I_{total} = 106 + 6.5 = 112.5A \tag{4.6}$$

The average current that flows in the diode is calculated as

$$I_{average} = \frac{0.5x112.5x1x10^{-3}}{20x10^{-3}} = 2.813\ A \tag{4.7}$$

Equation (4.7) is divided by 20 ms because the current peak through the diode will only occur once in a 50 Hz cycle. The rms current is

$$I_{rms} = \frac{1}{\sqrt{3}} x112.5x\sqrt{\frac{1}{20}} = 14.52A \tag{4.8}$$

The diode rectifier specifications are 310 V, 14.52 A. The DB2506 diode rectifier is sufficient. The specifications of the diode are given in table 4-2.

Table 4-2 Diode rectifier specifications

Type	V	I
DB2506	600V	25A

4.3 Flyback-converter design

The flyback converter used in this application is based on a previous design. The original design was adjusted to fulfil the needs for the current project. The flyback converter design will include the coupled inductor design and specifying the correct switching devices and capacitors. A block diagram of the flyback converter is given in figure 4.4.

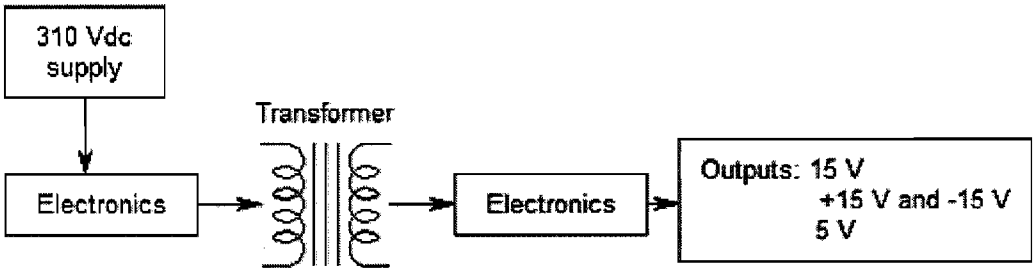

Figure 4-4 Flyback converter block diagram

The supply to the flyback converter is 310 V dc. The transformer is designed with one primary winding and four secondary windings. The flyback converter provides three 15 V outputs and one 5 V output. These outputs will be used as supply to the low voltage circuits on the inverter as follows:

- + 15 V for the PWM drivers,
- ± 15 V for the analogue electronics on the inverter,
- + 5 V for the logic circuits on the inverter.

The specifications in table 4-3 will be used to design the flyback converter.

Table 4-3 Flyback converter specifications

V_{in}	150-350 V
V_{out}	5 V @ 500 mA 15 V @ 200 mA ± 15 V @ 200 mA
V_r (% allowable ripple)	Less than 2 % on all outputs
f_s (switching frequency)	50 kHz
V_d (output voltage drop)	1 V
D_{max} (max duty cycle)	45 %

4.3.1 Coupled inductor design

The following steps will be followed in the design of the coupled inductor of the flyback converter:

- Determine turns ratio of coupled inductor,
- Determine primary inductance,
- Determine the minimum duty cycle,
- Choose coupled inductor core,
- Calculate copper wire thickness,
- Determine window area.

To determine the turns ratio of the main coil, (4.9) is used:

$$\begin{aligned}\frac{V_{out}}{V_{in}} &= n\times\left(\frac{D}{1-D}\right)\\ n &= \frac{D_{\max}\times V_{in\_\min}}{(1-D_{max})(V_o+V_d)}\\ &= \frac{0.45\times 150}{(1-0.45)(5+1)}\\ &= 20.455\end{aligned} \tag{4.9}$$

where V_{out} and V_{in} are the output and input voltages respectively, D_{max} is the maximum duty cycle, and n is the turns ratio of the primary winding and the 5 V secondary winding.

The next step is to determine the required primary inductance. The inductance is calculated with the use of (4.10) – (4.13). The output power is calculated as:

$$\begin{aligned}P &= \sum V_s\times I_s\\ &= V_{o5}\times I_{o5}+3\times V_{o15}\times I_{o15}\\ &= 5\times 0.5+3\times 15\times 0.2\\ &= 11.5\ \text{W}\end{aligned} \tag{4.10}$$

where V_s and I_s are the output voltages and currents respectively. The peak current of the primary, with an efficiency of 70 %, is calculated as:

$$\begin{aligned} I_{pr\_peak} &= \frac{2 \times P}{\eta \times V_{in\_min} \times D_{max}} \\ &= \frac{2 \times 11.5}{0.7 \times 150 \times 0.45} \\ &= 0.487 \text{ A} \end{aligned} \tag{4.11}$$

where I_{pr_peak} is the peak current of the primary, P is the power, η is the efficiency, V_{in_min} is the minimum input voltage and D_{max} is the maximum duty cycle. The peak currents of the 5 V and 15 V secondary coils are approximated as:

$$\begin{aligned} I_{s5\_peak} &= I_{o5} \times 4 & I_{s15\_peak} &= I_{o15} \times 4 \\ &= 0.5 \times 4 & &= 0.2 \times 4 \\ &= 2 \text{ A} & &= 0.8 \text{ A} \end{aligned} \tag{4.12}$$

The required primary inductance can now be calculated with (4.13) as:

$$\begin{aligned} L &= \frac{V_{in\_min} \times D_{max}}{I_{pr\_peak} \times f_s} \\ &= \frac{150 \times 0.45}{0.487 \times 50000} \\ &= 2.772 \text{ mH} \end{aligned} \tag{4.13}$$

where f_s is the switching frequency. The maximum rms currents of the primary and 5 V and 15V secondary coils are calculated in (4.14):

$$\begin{aligned} I_{pr\_rms} &= \frac{I_{pr\_peak}}{\sqrt{6}} & I_{s5\_rms} &= \frac{I_{s5\_peak}}{\sqrt{6}} & I_{s15\_rms} &= \frac{I_{s15\_peak}}{\sqrt{6}} \\ &= \frac{0.487}{\sqrt{6}} & &= \frac{2}{\sqrt{6}} & &= \frac{0.8}{\sqrt{6}} \\ &= 0.198 \text{ A} & &= 0.816 \text{ A} & &= 0.327 \text{ A} \end{aligned} \tag{4.14}$$

Throughout these calculations, the maximum duty cycle was used with the minimum input voltage. To determine the minimum duty cycle with maximum input voltage, (4.15) is used:

$$D_{\min} = \frac{L \times I_{pr\_peak} \times f_s}{V_{in\_max}} = \frac{2.772 \times 10^{-3} \times 0.487 \times 50000}{350} = 0.193 \quad (4.15)$$

The fourth stage in the coupled inductor design, is to choose a core for the coupled inductor, and then to design or calculate the number of primary and secondary windings of the coupled inductor. The core of the coupled inductor was chosen to be an RM8 core with the following specifications:

Table 4-4 Specifications of the RM8 core

l_e – core length	38 mm
μ_r – relative permeability	5870
A_w – window area	30 mm^2
A_e – core area	64 mm^2
l_g – air gap	0.2 mm

With the core type known, the number of primary turns can be calculated from (4.16) as:

$$N_p = \sqrt{L \times \left(\frac{l_e}{\mu_o \times \mu_r \times A_e} + \frac{l_g}{\mu_o \times A_e} \right)} = \sqrt{L \times \left(\frac{38 \times 10^{-3}}{4\pi \times 10^{-7} \times 5870 \times 64 \times 10^{-6}} + \frac{0.2 \times 10^{-3}}{4\pi \times 10^{-7} \times 64 \times 10^{-6}} \right)} \approx 85 \text{ turns} \quad (4.16)$$

The number of turns on the 5 V and 15 V secondary windings are calculated in (4.17) as:

$$N_{s5} = \frac{N_p}{n} = \frac{85}{20.455} \approx 5 \text{ turns} \qquad N_{s15} = N_{s5} \times \frac{V_{o15} + V_d}{V_{o5} + V_d} = 5 \times \frac{15+1}{5+1} \approx 14 \text{ turns} \quad (4.17)$$

To obtain the maximum flux density, the reluctance is calculated in (4.18) as:

$$\begin{aligned}\Re &= \frac{l_e}{\mu_o \times \mu_r \times A_e} + \frac{l_g}{\mu_o \times A_e} \\ &= \frac{38\times10^{-3}}{4\pi\times10^{-7}\times5870\times64\times10^{-6}} + \frac{0.2\times10^{-3}}{4\pi\times10^{-7}\times64\times10^{-6}}\ \text{H}^{-1} \\ &= 2.567\times10^{6}\ \text{H}^{-1}\end{aligned} \tag{4.18}$$

and the flux density is calculated as:

$$\begin{aligned}B_{max} &= \frac{N_p \times I_{pr\_peak}}{\Re \times A_e} \\ &= \frac{85\times0.487}{2.567\times10^{6}\times64\times10^{-6}} \\ &= 0.252\ \text{T}\end{aligned} \tag{4.19}$$

The next step is to calculate the copper wire thickness needed for the coupled inductor. By choosing the current density (J) as 3 A/mm^2, the diameter and area of the copper wire for the primary, 5 V side and the 15 V side are calculated using (4.20), (4.21) and (4.22) respectively as:

$$\begin{aligned}d_p &= \sqrt{\frac{4}{\pi}\times\frac{I_{pr\_rms}}{J}} & A_p &= \frac{\pi}{4}\times d_p^2 \\ &= \sqrt{\frac{4}{\pi}\times\frac{0.198}{3}} & &= \frac{\pi}{4}\times0.290^2 \\ &= 0.290\ \text{mm} & &= 0.066\ \text{mm}^2\end{aligned} \tag{4.20}$$

$$\begin{aligned}d_{s5} &= \sqrt{\frac{4}{\pi}\times\frac{I_{s5\_rms}}{J}} & A_{s5} &= \frac{\pi}{4}\times d_{s5}^2 \\ &= \sqrt{\frac{4}{\pi}\times\frac{0.816}{3}} & &= \frac{\pi}{4}\times0.589^2 \\ &= 0.589\ \text{mm} & &= 0.272\ \text{mm}^2\end{aligned} \tag{4.21}$$

$$d_{s15} = \sqrt{\frac{4}{\pi} \times \frac{I_{s15\_rms}}{J}} \qquad A_{s15} = \frac{\pi}{4} \times d_{s15}^2$$
$$= \sqrt{\frac{4}{\pi} \times \frac{0.327}{3}} \qquad = \frac{\pi}{4} \times 0.372^2 \qquad (4.22)$$
$$= 0.372 \text{ mm} \qquad = 0.109 \text{ mm}^2$$

The final step in the design of the flyback converter is to determine the window area. The window area is calculated to determine whether the amount of turns will fit into the core window or not. The window area of the copper wire is calculated with (4.23) as:

$$\begin{aligned} A_{cu} &= N_p \times A_p + N_{s5} \times A_{s5} + 3 \times N_{s15} \times A_{s15} \\ &= 85 \times 0.066 + 5 \times 0.272 + 3 \times 14 \times 0.109 \\ &= 11.56 \text{ mm}^2 \end{aligned} \qquad (4.23)$$

and the required window area is calculated with (4.24) as:

$$\begin{aligned} A_w &= \frac{A_{cu}}{FF} \\ &= \frac{11.56}{0.4} \\ &= 28.9 \text{ mm}^2 \end{aligned} \qquad (4.24)$$

where *FF* is the filling factor chosen as 0.4. From the datasheet of the RM8 core, the window area was given as $A_w = 30$ mm^2, which is more than the area required for the windings to fit on the core.

4.3.2 Power electronics design

The final step in the design of the flyback converter is to design the power electronics. The components that must be specified are:

- MOSFET,
- Diode,
- Output filter capacitors.

The maximum current and voltage of the MOSFET is calculated using (4.25):

$$V_{max} = V_{in\_max} + n \times (V_o + V_d) \qquad I_{max} = \frac{I_{pr\_peak} \times D_{max}}{2}$$
$$= 350 + 20.455 \times (5 + 1) \qquad = \frac{0.487 \times 0.45}{2} \qquad (4.25)$$
$$= 472.73\ V \qquad = 110\ mA$$

where V_d is the forward voltage of the 5 V output diode. The specifications of the switching device are given in table 4-5.

Table 4-5 MOSFET specifications

Type	V_{DSS}	$R_{DS(on)}$	I_D
IRFBC30	600V	$< 2.2\Omega$	3.6A

The secondary diodes should be fast recovery diodes, or schottky diodes. For the 5 V output, the diode must withstand 23 V reverse voltage, 500 mA average current and peak currents of up to 2 A. The diode for the 15 V output must be able to withstand 76 V reverse voltage, 200 mA average current and peak currents of up to 800 mA. The diode on the 5 V output is an MBR1545CT schottky diode. The specifications of the diode are given in table 4-6.

Table 4-6 Schottky diode specifications

Type	V_R	t_{rr}	I
MBR1545CT	45 V	25ns	15 A

An ultra fast avalanche sinterglass diode was used for the 15 V output. The specifications of the diode are given in table 4-7.

Table 4-7 Diode specifications

Type	V_R	t_{rr}	I_{FAV}
BYV27-150	150 V	25 ns	2 A

Note that the components are adequately derated. This is to ensure that the components do not operate at their limits and it also increases the life cycle of the flyback converter. The output filter capacitances for the 5 V- and 15 V sides are calculated using (4.26) as:

$$\begin{aligned} C_5 &= \frac{(1-D_{min})\times I_5}{V_r \times f_s} & C_{15} &= \frac{(1-D_{min})\times I_{15}}{V_r \times f_s} \\ &= \frac{(1-0.193)\times 0.5}{5\times 0.02\times 50000} & &= \frac{(1-0.193)\times 0.2}{15\times 0.02\times 50000} \\ &= 80.7\ \mu F & &= 10.76\ \mu F \end{aligned} \tag{4.26}$$

Taking into consideration the values calculated above, the components were specified with a factor of safety. The capacitors on the 15 V outputs are 22 µF, 63 V electrolytic capacitors and on the 5 V output a 100 µF, 16 V electrolytic capacitor is used. Figure 4-5 shows the PCB layout of the flyback converter.

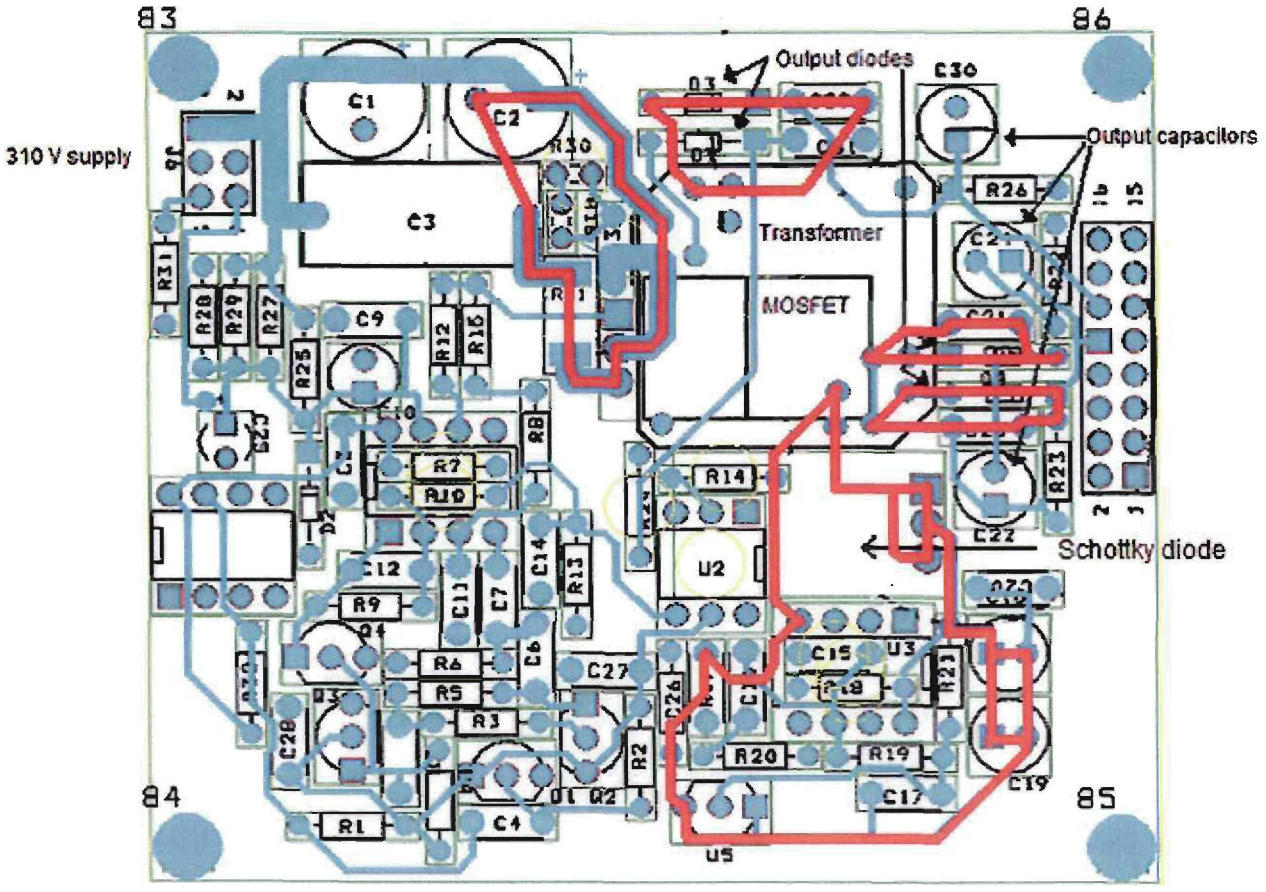

Figure 4-5 PCB layout of the flyback converter

All the critical components are named in figure 4-5. These are the coupled inductor, the MOSFET, the schottky diode and the output capacitors and diodes. The high switching frequency is a source of noise, therefore the high frequency loops (red lines) around the coupled inductor should be kept as small as possible. The primary current loop (loop to the left) is relatively small as is the current loops for the 15 V output (small loops to the right). However, the 5 V output current loop (bottom loop) is very big. This is not the most optimum design because most of the current will flow through this loop. Care was however taken not to place control electronics close to any of these loops.

4.4 Power amplifier design

4.4.1 Inverter design

The inverter is used to connect the supply and the load to each other. A three phase voltage is required (explained in section 2.3) to drive the motor. Figure 4-6 shows the configuration of the switches and the freewheeling diodes.

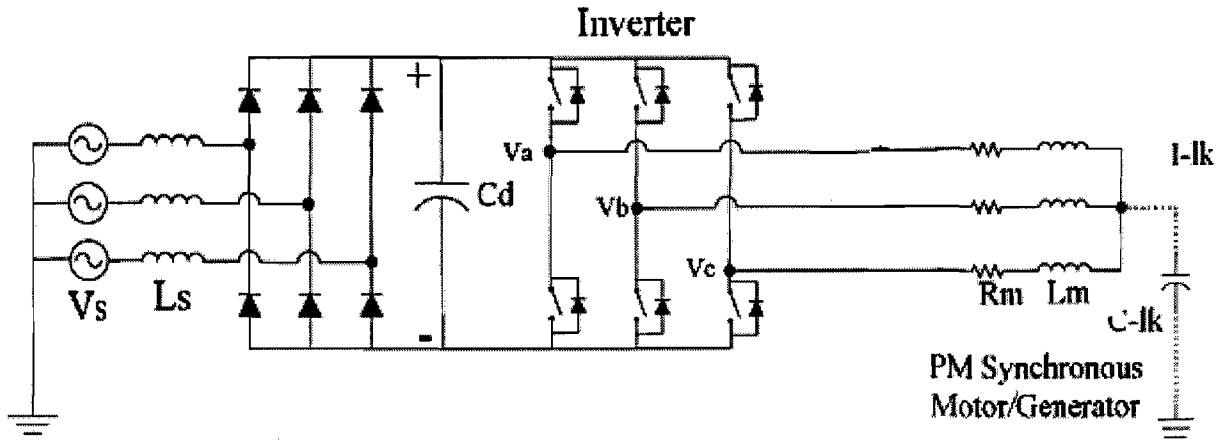

Figure 4-6 Switch configuration

Depending on the application, either a metal-oxide semiconductor field effect transistor (MOSFET) or an insulated gate bipolar transistor (IGBT) is used. The MOSFET experiences high losses at high switching frequencies and the on-state resistance also increases with higher temperatures [17].

An IGBT is basically a bipolar transistor with an isolated gate. The IGBT has less on-state losses than the MOSFET but has inferior switching speed in comparison to the MOSFET. The IGBT is more suited for high temperature applications since the voltage drop across the IGBT does not increase as drastically with higher temperatures as it would in MOSFET devices. IGBTs are thus preferred in higher voltage applications and the MOSFET in applications where high operating frequencies are required.

The high-end specifications of both switching devices are shown in table 4-8.

Table 4-8 Switching device specifications

	MOSFET	IGBT
Voltage	500 V	1.2 kV
Current	50 A	400 A
Frequency	1 MHz	50 kHz
Power	100 kW	100's of kW

From the drive specification in table 4-1 it is known that the device must be able to withstand a 310 V dc voltage and a current of 25 A. The switching frequency of the device is 50 kHz. Comparing the specifications in table 4-8 with the specifications from table 4-1, the IGBT was

chosen as the switching device. The chosen device is a warp-speed, 600V, 27 A IGBT (IRG4PC50W) in a TO-247 package.

The freewheeling diodes serve a very important purpose. Due to the inductive nature of the PMSM load, a power amplifier constructed with switches without freewheeling diodes will fail as the current through an inductor changes with time. The placement of freewheeling diodes guarantees continuity in the inductive load current. The diodes will provide a path for the coil current when all the switches are off for a while. This takes place when the two switching devices in the same leg of the bridge are turned-off for a short period of time to avoid cross conduction or short circuiting the bridge.

For the application the HFA25PB60 diode is used. This is a 600V, 25 A diode with a reverse recovery time of 23 ns.

4.4.2 Thermal design

The losses in the circuit are due to the switching devices and the current sensing resistors. The design specifications of the drive are given in table 4-9.

Table 4-9 Drive design specifications

	Parameter	Test Conditions	Application Conditions
T_j	Junction temperature	150 °C	150 °C
I_C	Collector current	27 A	20 A
V_{cc}	Collector voltage	480 V	310 V
V_{GE}	Gate – Emittor voltage	15 V	15 V
R_G	Gate resistor	5 Ω	10 Ω
Vce(on)	Collector to emitter saturation voltage	1.65 V	
Ets	Device switching loss	1.58 mJ	

An estimate of the total switching energy is calculated for the worst case as:

$$\begin{aligned} E_{ts-new} &= \frac{I_{C-new}}{I_{C-old}} \frac{V_{CC-new}}{V_{CC-old}} \frac{R_{G-new}}{R_{G-old}} E_{ts-old} \\ &= \frac{7.95}{27} \cdot \frac{310}{480} \cdot \frac{10}{5} \cdot 1.58 \times 10^{-3} \text{ J} \\ &= 0.601 \text{ mJ} \end{aligned} \tag{4.27}$$

where $I_{c\text{-}old}$, $V_{cc\text{-}old}$, $R_{g\text{-}old}$ and $E_{ts\text{-}old}$ are the rated current, voltage, gate resistance and total switching loss of the device respectively. $I_{c\text{-}new}$, $V_{cc\text{-}new}$ and $R_{g\text{-}new}$ are the operating current, voltage and gate resistance respectively. Since this is a three phase power amplifier, $I_{c\text{-}new}$ is specified as the average current that flows through a half cycle of a sine wave with maximum amplitude of 25 A. The switching power losses are now determined using the total switching energy together with the switching frequency:

$$\begin{aligned} P_{sw} &= E_{ts} f_s \\ &= 0.601 \times 10^{-3} \cdot 50 \times 10^{3} \\ &= 30.07 \text{ W} \end{aligned} \tag{4.28}$$

The IGBT also displays conductive losses due to the on-state voltage drop across the collector-emittor terminals. The conductive losses are obtained from

$$\begin{aligned} P_{on} &= V_{CE(on)} I_C d \\ &= 1.65 \cdot 7.95 \cdot 0.5 \text{ W} \\ &= 6.55 \text{ W} \end{aligned} \tag{4.29}$$

where d is the duty cycle and I_C the average collector current. The H-bridge is operated at a duty cycle close to 50 %.The total power losses for a single IGBT switch is determined using

$$\begin{aligned} P_{IGBT} &= P_{sw} + P_{on} \\ &= 30.07 + 6.55 \text{ W} \\ &= 36.63 \text{ W} \end{aligned} \tag{4.30}$$

A non-inductive power metal film resistor was identified from the CADDOCK MP915 series. The resistor losses are determined using the rms current and the resistor value:

$$\begin{aligned} P_{R_{sense}} &= I_{rms}{}^2 R_{sense} d \\ &= 17.677^2 \cdot 0.02 \cdot 0.5 \text{ W} \\ &= 3.125 \text{ W} \end{aligned} \tag{4.31}$$

Since there are three current sensing resistors, one in each IGBT half-bridge configuration, the losses in the sense resistor must be multiplied by 3 to obtain the total losses of the resistors as

$$\begin{aligned} P_{R_{sense}} &= P_{R_{sense}} x3 \\ &= 9.375 \text{ W} \end{aligned} \tag{4.32}$$

The total power losses in the H-bride are determined using (4.33)

$$\begin{aligned} P_{H-Bridge} &= 6\left(P_{IGBT}\right) + P_{R_{sense}} \\ &= 6\left(36.63\right) + 9.375 \text{ W} \\ &= 229.14 \text{ W} \end{aligned} \tag{4.33}$$

To ensure that these losses do not cause the switching devices to exceed their safe operating temperature, an appropriate heat sink is designed. To electrically isolate the components from the heat sink, thermal pads (ISOSTRATE 2000 K3) with a thermal impedance of 0.23 °C-in^2/W are used. The case to sink thermal resistance of the IGBTs are calculated with (4.34) as

$$\begin{aligned} R_{\theta CS} &= \frac{0.23}{0.8 \times 0.626} \\ &= 0.46 \text{ °C/W} \end{aligned} \tag{4.34}$$

The case to sink thermal resistance of the sense resistor is calculated with (4.35) as

$$\begin{aligned} R_{\theta CS} &= \frac{0.23}{0.32 \times 0.44} \\ &= 1.63 \text{ °C/W} \end{aligned} \tag{4.35}$$

By using the thermal resistance and the power dissipated by the IGBT, the maximum allowable temperature of the heat sink due to the IGBT can be calculated with (4.36) as

$$\begin{aligned} T_S &= T_j - Q_{IGBT}\left(R_{\theta JC} + R_{\theta CS}\right) \\ &= 150 - 36.63(0.64 + 0.24) \\ &= 117.7\ ^\circ\text{C} \end{aligned} \tag{4.36}$$

where T_s is the temperature of the heat sink, T_j the maximum allowable junction temperature, Q_{IGBT} the losses of the device, $R_{\theta JC}$ the junction to case resistance and $R_{\theta CS}$ the case to sink resistance. The maximum allowable temperature due to the diode is determined with (4.37) as

$$\begin{aligned} T_S &= T_j - Q_{DIODE}\left(R_{\theta JC} + R_{\theta CS}\right) \\ &= 150 - 20.6(0.83 + 0.25) \\ &= 127.75\,^\circ\text{C} \end{aligned} \tag{4.37}$$

The sense resistor heat sink temperature is calculated with (4.38). This is a 15 W resistor with thermal resistance of 0.12 W/°C with 3.125 W losses:

$$\begin{aligned} T_S &= \frac{125(18 - Q)}{15} - QR_{\theta CS} \\ &= \frac{125(18 - 3.125)}{15} - 3.125 \times 1.63 \\ &= 118.8\ ^\circ\text{C} \end{aligned} \tag{4.38}$$

The maximum temperature of the heat sink is chosen as 80 °C and the ambient temperature is chosen as 30 °C. The total losses of the power amplifier are 229.14 W. From these values the thermal resistance of the heat sink is obtained from (4.39):

$$\begin{aligned} R_{\theta SA} &= \frac{T_S - T_A}{Q_{H-Bridge}} \\ &= \frac{80 - 30}{229.14}\ ^\circ\text{C/W} \\ &= 0.218\ ^\circ\text{C/W} \end{aligned} \tag{4.39}$$

A finned aluminium heat sink is used. A cooling fan is integrated into the final heat sink configuration in order to lower the thermal resistance to well below 0.218 °C/W.

4.4.3 Optical isolation

Optical isolation is necessary to isolate the controller ground from the power electronic ground. A high speed HCPL-2631 opto-coupler is used for the isolation. Figure 4-7 shows a block diagram of optical isolation scheme.

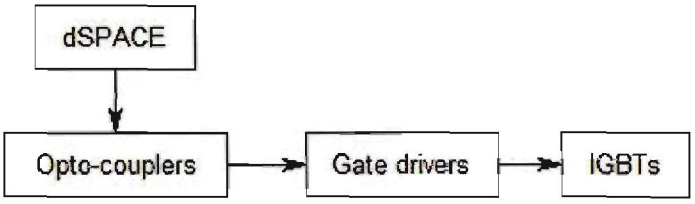

Figure 4-7 Opto-coupler connection block diagram

PWM signals are sent from dSPACE® to the inputs of the opto-coupler. The outputs of the opto-couplers are connected to the high- and low side inputs of the gate drivers (discussed in next section). A 100 nF decoupling capacitor connected between the 5 V supply and the ground. The two outputs (*VO1* and *VO2*) are connected through a 2.7 kΩ pull-up resistor to the 5 V supply. The diagram of the isolation circuit is shown in figure 4-8.

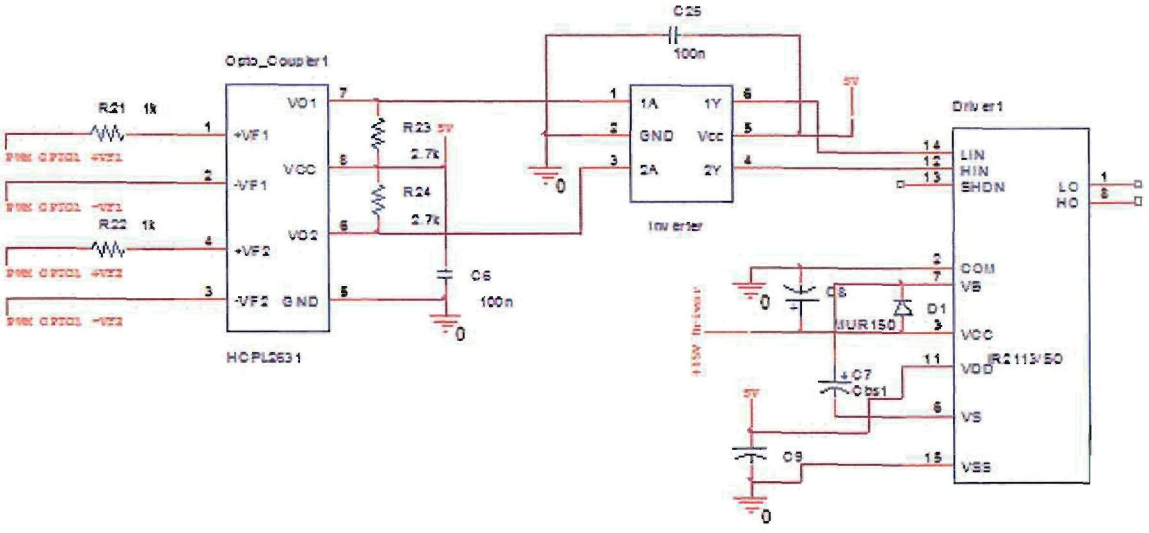

Figure 4-8 Isolation circuit diagram

The opto-coupler inverts the signal from the controller. This means that should the input to the device be low, the output of the device will be high. The result of this would be that all the switches will switch on simultaneously causing damage to the devices. This was problematic in previous designs. In the current design however, an inverter is placed between the output of

the opto-coupler and the input of the gate driver. The signal is thus inverted again to ensure that when the inputs are low, the switching components are switched off.

4.4.4 Gate drive circuit

Gate drivers are used to supply the gate of the IGBT with a PWM signal. For the device to switch, the gate voltage must be 10 – 15 V larger than the collector voltage. The capacitance between the gate of the IGBT and the drain and source of the IGBT are very large. If a PWM signal is applied directly to the gate the internal capacitor will cause the gate voltage to increase very slowly [18]. This will result in high turn on losses.

The device chosen for this application is an IR2113S, a surface mount gate driver from International Rectifier. In the high side configuration, the device can drive an IGBT that operates at 500 – 600 V. It is also a very fast switching device. One gate driver is sufficient to switch two IGBTs (high- and low-side). For this application, six switching devices are used which means that three gate drivers are needed. Figure 4-9 shows the gate driver circuit diagram.

The value of the gate resistor is chosen so that the maximum output current of the gate driver (2 A) is not exceeded. The value of R_g is calculated with (4.40) as

$$\begin{aligned} R_g &= \frac{V_{cc}}{I_{g\_max}} \\ &= \frac{15}{2} \\ &= 7.5\ \Omega \end{aligned} \tag{4.40}$$

where R_g is the gate resistance, V_{cc} is the supply voltage and I_{g_max} is the maximum peak gate current. To ensure that the gate driver does not operate at rated output current, the gate resistor is chosen as $10\,\Omega$.

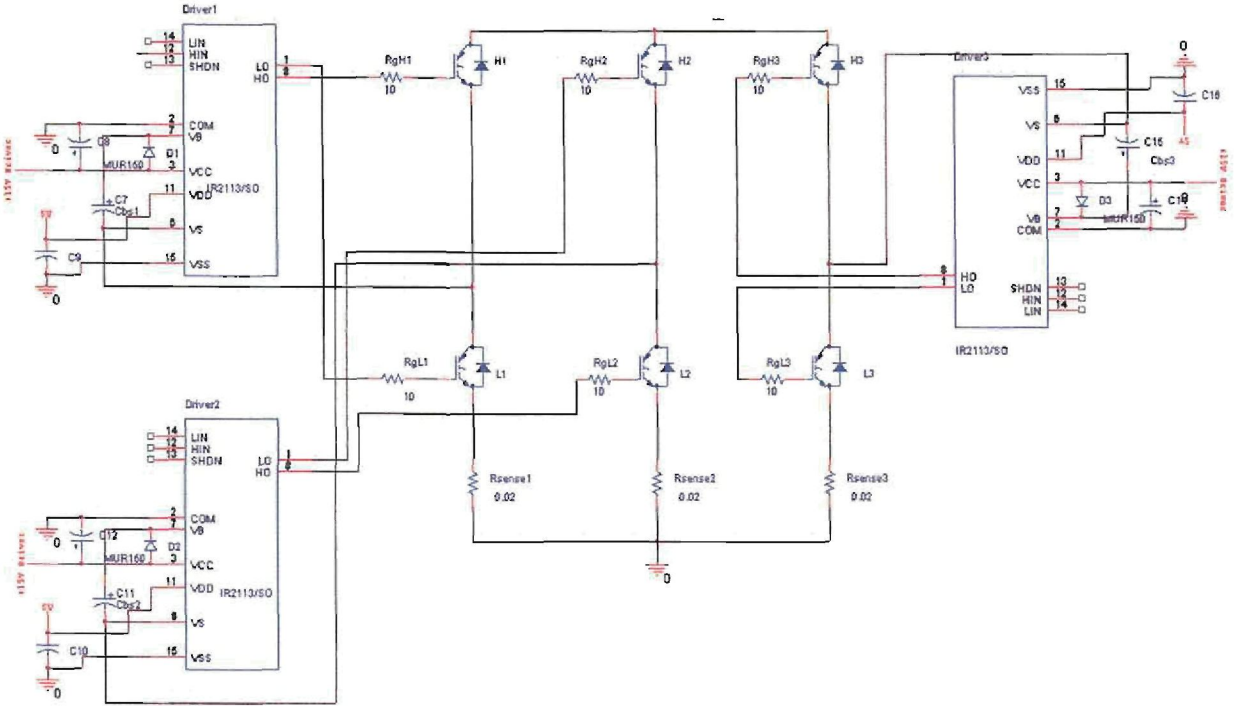

Figure 4-9 Gate driver circuit diagram

The low-side IGBT is connected to ground which means that the device is driven directly from the 15 V of the gate driver. The emitter of the high-side IGBT and the collector of the low-side are connected to each other. Due to this configuration, the high-side devices are driven from a floating supply. From figure 4-9 it can be seen that there are bootstrap capacitors as well as bootstrap diodes. When the high-side is not conducting, the bootstrap capacitor will charge through the bootstrap diode to 15 V and will discharge this energy to the high-side when the high-side IGBTs conduct.

The desired bootstrap component information is calculated with (4.41) – (4.43) [19]

$$\begin{aligned} Q_{bs} &= 2Q_g + \frac{I_{qbs}}{f_{sw}} + Q_{ls} \\ &= 2\times 180\times 10^{-9} + \frac{125\times 10^{-6}}{50\times 10^{3}} + 5\times 10^{-9} \\ &= 367.5\ \text{nC} \end{aligned} \tag{4.41}$$

where Q_{bs} is the minimum charge requirements of the bootstrap capacitor, Q_g is the total gate charge of the high-side IGBT, I_{qbs} is the quiescent supply current, f_{sw} is the operating frequency and Q_{ls} is the level shift charge per cycle [19]. Now that the minimum charge requirements are known, the minimum capacitance of the bootstrap capacitor is calculated as

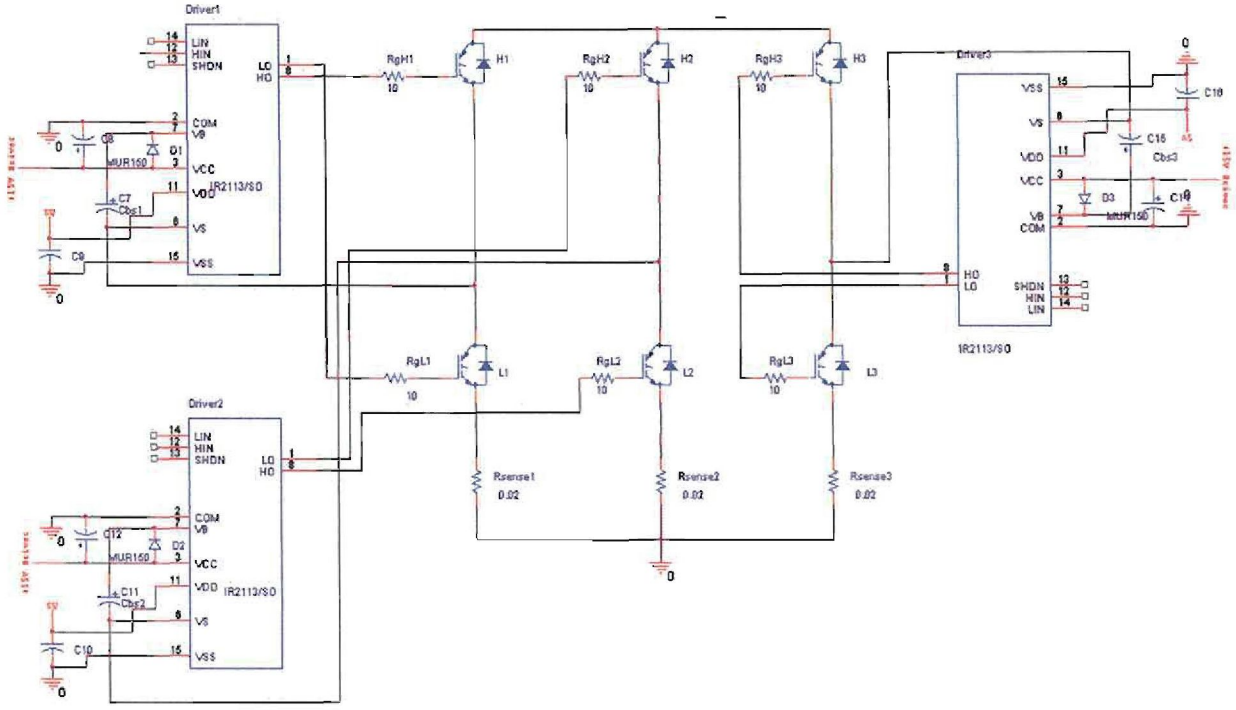

Figure 4-9 Gate driver circuit diagram

The low-side IGBT is connected to ground which means that the device is driven directly from the 15 V of the gate driver. The emitter of the high-side IGBT and the collector of the low-side are connected to each other. Due to this configuration, the high-side devices are driven from a floating supply. From figure 4-9 it can be seen that there are bootstrap capacitors as well as bootstrap diodes. When the high-side is not conducting, the bootstrap capacitor will charge through the bootstrap diode to 15 V and will discharge this energy to the high-side when the high-side IGBTs conduct.

The desired bootstrap component information is calculated with (4.41) – (4.43) [19]

$$\begin{aligned} Q_{bs} &= 2Q_g + \frac{I_{qbs}}{f_{sw}} + Q_{ls} \\ &= 2\times 180\times 10^{-9} + \frac{125\times 10^{-6}}{50\times 10^{3}} + 5\times 10^{-9} \\ &= 367.5\ \text{nC} \end{aligned} \tag{4.41}$$

where Q_{bs} is the minimum charge requirements of the bootstrap capacitor, Q_g is the total gate charge of the high-side IGBT, I_{qbs} is the quiescent supply current, f_{sw} is the operating frequency and Q_{ls} is the level shift charge per cycle [19]. Now that the minimum charge requirements are known, the minimum capacitance of the bootstrap capacitor is calculated as

$$\begin{aligned} C_{bs} &= \frac{2Q_{bs}}{V_{cc} - V_f - V_{LS} - V_{Min}} \\ &= \frac{367.5 \times 10^{-9}}{15 - 1.25 - 1.3 - 8.2} \\ &= 113.07 \text{ nF} \end{aligned} \tag{4.42}$$

where V_{cc} is the supply voltage, V_f is the forward voltage drop across the diode, V_{LS} is the voltage drop across the low-side IGBT and V_{Min} is the minimum voltage between V_S and V_B. A 4.7 μ tantalum capacitor was used for the bootstrap capacitor.

When the high-side is on, the dc supply voltage is seen over the bootstrap diode. The diode must have a high temperature reverse leakage current [17] and an ultra-fast recovery time to minimize the charge fed back to the supply due to the bootstrap capacitor. The current of the bootstrap diode is calculated as

$$\begin{aligned} I_F &= Q_{bs} f_{sw} \\ &= 366.3 \times 10^{-9} \cdot 50 \times 10^3 \\ &= 18.3 \text{ mA} \end{aligned} \tag{4.43}$$

The specifications of the bootstrap diode are shown in table 4-10.

Table 4-10 Bootstrap diode specifications

Type	V	t_{rr}	I_R
MUR150	500 V	50 ns	5 uA

4.4.5 Protection

There are three types of protection implemented on the power amplifier. The protection includes thermal protection, short circuit protection and soft start protection that are discussed in this section.

Thermal protection

An over-temperature resistor (thermal sensor) is used to protect the power amplifier of harmful operating temperatures. The device is mounted near the temperature sensitive devices (IGBTs) and the sensor protects the circuit from temperatures exceeding 75 °C. The sensor works the same as an NTC (negative temperature coefficient resistor) as the thermal protection system sends a low voltage signal to the DSP controller under normal operating conditions. The value of the NTC is 100 kΩ and will decrease to 100 Ω as the temperature increases. When the temperature surpasses 75 °C, a high voltage value will be sent to the DSP controller and all the PWM signals will be terminated.

Short circuit protection

The most important safety feature of the power amplifier is the short circuit or over current protection. The total current that flows through system are monitored or sensed via the sense resistor. These currents include the current through the switches as well as the current through the load. The short circuit protection diagram is shown in figure 4-10.

The current is sensed through a 0.02 Ω resistor and then filtered with an *RC* filter and the frequency of the filter is calculated with the use of (4-44) as 360 kHz. This value was chosen high enough to allow fast reaction and low enough to prevent noise from triggering the circuit.

$$f = \frac{1}{2\pi RC} \tag{4.44}$$

Should the current exceed 25 A, the output of the comparator will turn high, applying a high on the shutdown of the gate driver that will terminate the PWM signals to the IGBTs. Note that all the outputs are connected together. This is to ensure that should one output turn high, that the PWM signals to all the IGBTs are then terminated.

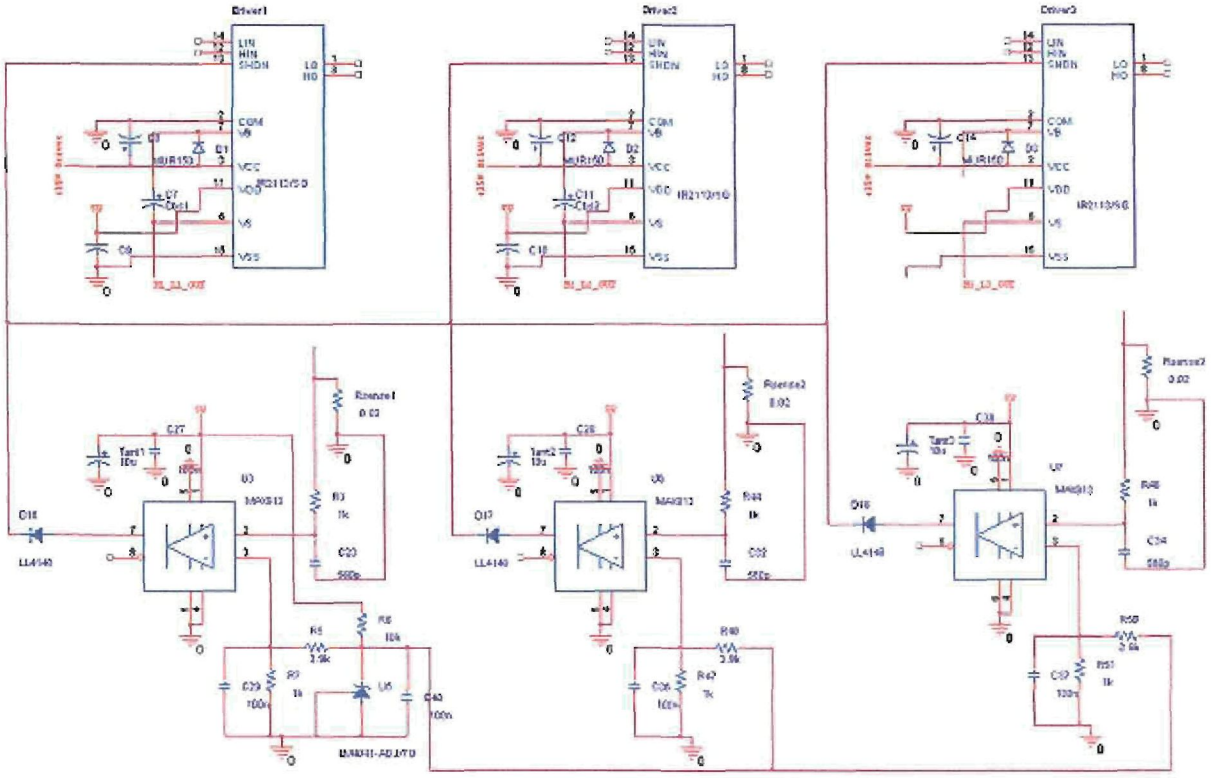

Figure 4-10 Short circuit protection diagram

Previous designs implemented only one sense resistor and one comparator for the short circuit protection. In the current layout there are three resistors and three comparators. In the layout of the power amplifier, the path length between the source of the low-side IGBT, the sense resistor and the feedback to the gate driver must be as short as possible. If this path is too long, a parasitic inductance is created that generates a negative voltage which causes the gate driver with the longest path to the sense resistor to overheat. Overheating increases the chance of gate driver failure. By placing a sense resistor and comparator near the source of every low-side IGBT, this loop is shortened eliminating the parasitic inductance and increasing the life of the gate driver.

A LL4148 diode is placed between the output of the comparator and the shutdown pin of the gate driver to ensure that the outputs of the three comparators do not affect one another.

External enable

The external enable is used to protect the IGBTs from switching on together when compiling the software. When using dSPACE® as DSP controller, the software must be compiled before execution. When compiling, all the outputs of dSPACE® are set high causing all the switching

devices to switch on simultaneously which can destroy the devices. The diagram of the external enable is shown in figure 4-11.

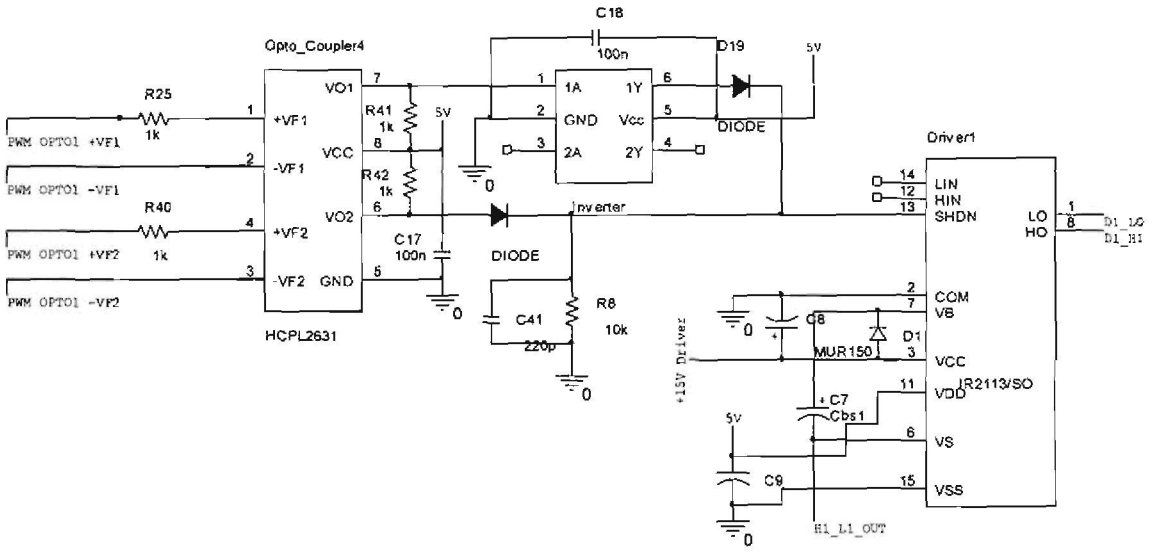

Figure 4-11 External activation diagram

The external enable works almost like an XOR-gate meaning that both conditions must be valid for execution. In figure 4-11 it can be seen that both digital signals are passed through opto-couplers to isolate the digital ground from the analogue ground. One of the opto-coupler's outputs is inverted and combined with the non-inverting signal in a logic OR operation through diodes. The output is then connected to the shutdown pin of the gate driver that will terminate the PWM signal on the gate of the IGBT.

If input 1 (+VF1) is high and input 2 (+VF2) is low then output 1 (V01) will be low and output 2 (V02) will be high. Output 1 is then inverted and becomes high. Both outputs are high and will activate the shutdown pin of the gate driver that disables the IGBTs. The IGBTs will be enabled only when input 1 is low and input 2 high.
The circuit diagram of the power amplifier is given in appendix A.

4.5 Analogue circuit design

To measure the speed of the motor, pick-up coils were built into the stator of the PMSM. It is a strand of wire that is wound with the stator windings. The pick-up coils will detect a change in magnetic field when the stator turns and will produce a sinusoidal output that can be used to calculate the speed of the motor. The analogue circuit is used for conditioning the signals of the pick-up coils. Figure 4-12 shows the diagram of the analogue circuit.

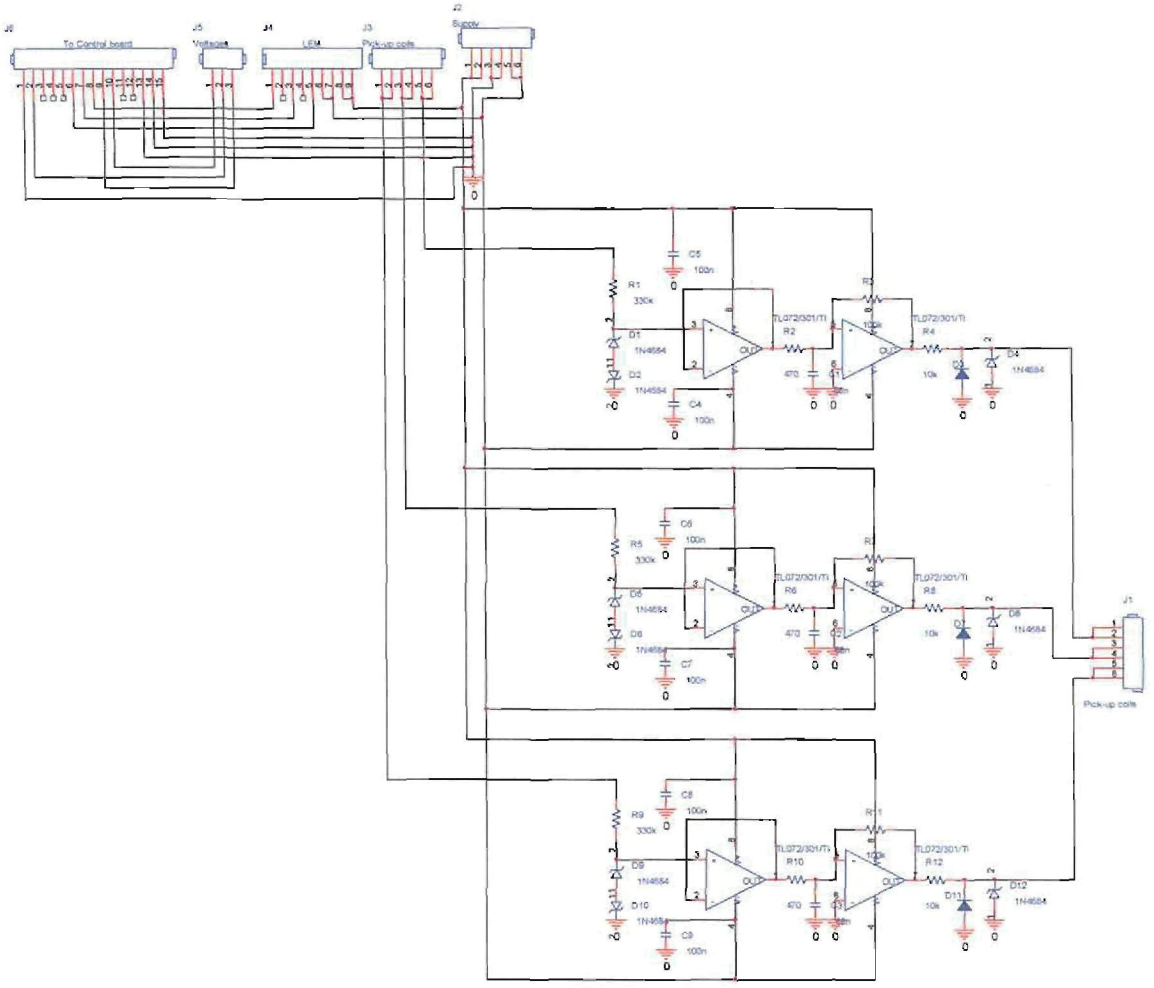

Figure 4-12 Analogue circuit diagram

To determine the speed of the motor, zero crossing detecting must be implemented. In figure 4-12 it can be seen that the input of the pick-up coil is clamped by two back-to-back zener diodes at 12 V. The signal goes through a voltage follower or buffer. The buffer has a very high impedance to ensure that no current is drawn from the actual signal [20]. The signal goes through a non-inverting operational amplifier that is set up as a comparator. The zero crossing detection is done here. The positive input will be compared to the negative input. Since the negative input is connected to 0 V, the positive input will be compared to ground. This means that every time the signal crosses the zero plane, a negative or positive pulse will be generated on the output of the comparator that is equal to the rail voltage of the comparator. The comparator is configured as a Schmitt trigger to reduce its sensitivity to noise. The output of the comparator is clamped to ensure that the output is never negative and never larger than 12 V. The TL072 package was used for the buffer and comparator because it has a $\pm$ 15 V supply and it is not sensitive to noise.

4.6 Drive layout

The PCB layout of drive is critical to the successful operation. The PCB layout of the drive is shown in figure 4-13.

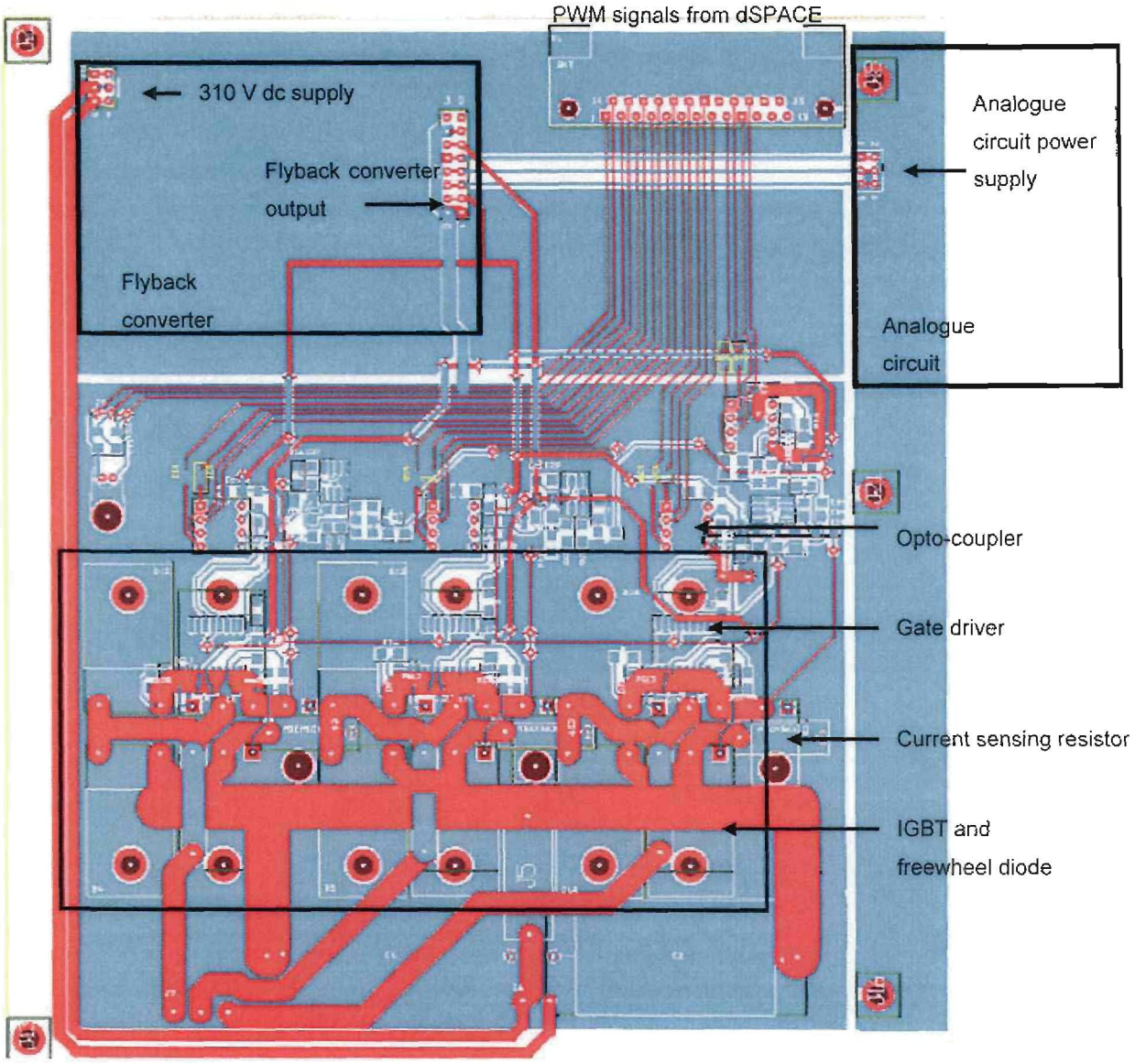

Figure 4-13 Drive PCB layout

The drive unit constitutes three sub-assemblies or PCBs; the flyback converter, analogue board and main power board. The flyback and analogue boards are piggybacked onto the main power board. The PWM signals from dSPACE® enters the drive from the top with the use of a DB25 connector. The 310 V dc supply for the power amplifier is also used as supply for the flyback converter. The outputs of the flyback converter are routed to the opto-couplers and gate drivers to supply these components with 5 V and 15 V respectively. The flyback also provides

± 15 V for the analogue circuit. The 310 V supply to the drain of the IGBTs is a very thick track. This will reduce the losses in these tracks.

The layout of the drive was optimized through optimal placement of the components. To minimize the effect of noise all high frequency current loops were kept as small as possible. High dv/dt surfaces were also kept as small as possible. The gate drivers were placed on top of the low-side of the IGBTs. This was is to ensure that the path lengths between the outputs of the gate drivers and the gates of the IGBTs are as short as possible. The sense resistor and the de-coupling capacitors of each half-bridge configuration were placed next to it. This ensures that the high frequency loops are kept very small. These are the most critical components. The rest of the components were placed close to each other to keep the board as small as possible. The use of a flyback converter also saved space. Normally, transformers would be used to generate the 5 V and 15 V required as supply for the small signal components.

To minimize the size even more, surface mount components were used for all the small signal components. The SMD1206 surface mount package was used for the components. For the inverter and the bootstrap capacitor, the SMD0806 package was used.

4.7 Filter design

The proposed filter design can be seen in figure 4-14. Two capacitors (*C3* and *C4*) are connected in series between the dc supply and ground. The mid-point (o) between the two capacitors is used as a "ground" for the filter [21]. On the output of the inverter, an inductor is connected in series with the line and a resistor and capacitor connected to ground. The negative ends of the capacitors are connected to the mid-point mentioned.

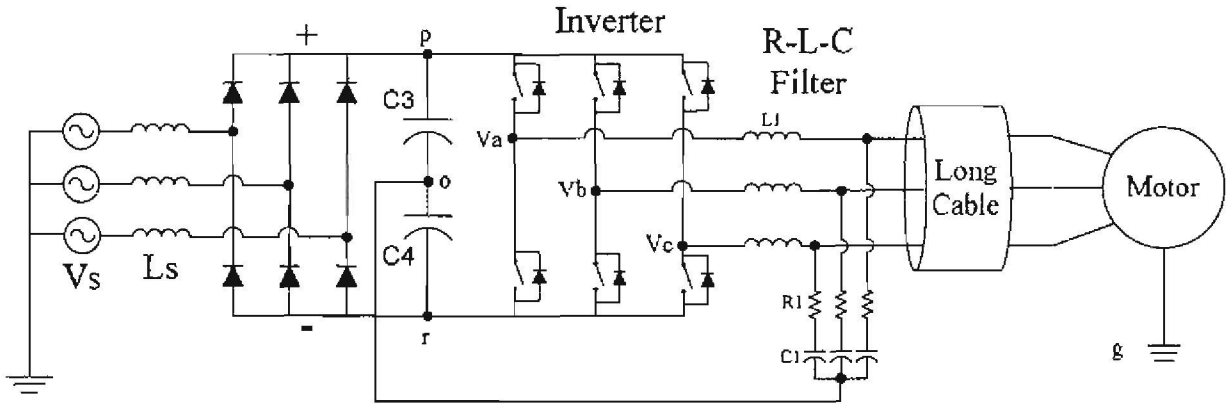

Figure 4-14 Proposed filter [21]

The inductor and capacitor values are calculated with the use of (4.45)

$$f_c = \frac{1}{2\pi\sqrt{LC}} \tag{4.45}$$

where f_c is the cut-off frequency of the filter, L is the inductor and C the capacitor. The cut-off frequency is chosen an order lower than the switching frequency at 5 kHz. The capacitor value is chosen as 3 µF motor-run capacitor. The required inductance is calculated with (4.46) as:

$$\begin{aligned} f_c &= \frac{1}{2\pi\sqrt{LC}} \\ L &= \frac{1}{(2\pi fc)^2 C} \\ &\cong 300\ \mu H \end{aligned} \tag{4.46}$$

The equation will be valid for any chosen inductor value or any chosen capacitor value as long as the frequency is kept the same.

The design process of the inductor includes the following steps:

- select an inductor core,
- calculate the amount of turns,
- calculate the rms current,
- determine the area of the copper wire,
- determine the diameter of the copper wire,
- calculate the window area,
- calculate the required area,
- determine whether the core will saturate.

The design of the inductor is an iterative process. The most difficult part of the design is to choose an inductor core that is available on the market. The inductor core chosen for the design was the TOR400-52 from MicroMetals. The specifications of the core are given in table 4-11.

Table 4-11 Inductor core specifications

ℓ (flux path length)	25 cm
A (area of the flux in)	3.46 cm^2
ID (core inside diameter)	57.2 mm
μ_r (permeability of material)	75
J (current denity)	3 A/mm^2

After selecting an appropriate core, the amount of turns of the inductor is calculated with (4.47) as:

$$\begin{aligned} N &= \sqrt{\frac{L.\ell}{\mu.\mu_r.A}} \\ &= \sqrt{\frac{300x10^{-6}.25x10^{-2}}{4\pi x10^{-7}.75.3.46x10^{-4}}} \\ &= 47.9576 \text{ turns} \end{aligned} \tag{4.47}$$

The number of turns was chosen as 48. The rms current is calculated with (4.48). The peak current was chosen 1.2 times bigger than the rated current of 25 A.

$$\begin{aligned} i_{rms} &= 0.707.i_{peak} \\ &= 0.707x30 \\ &= 21.21\,A \end{aligned} \tag{4.48}$$

The area of the copper wire is calculated with (4.49) as

$$\begin{aligned} A_{cu} &= \frac{i_{rms}}{J} \\ &= \frac{21.21}{3x10^{-6}} \\ &= 7.07 \text{ mm}^2 \end{aligned} \tag{4.49}$$

where A_{cu} is the area of the wire. With the area of the copper wire known the diameter of the wire can be calculated with (4.50) as

$$\begin{aligned} D &= \sqrt{\frac{4Acu}{\pi}} \\ &= \sqrt{\frac{4x7.07x10-6}{\pi}} \\ &= 3 \text{ mm} \end{aligned} \tag{4.50}$$

where D is the diameter of the copper wire. The next step is to calculate the window area. The window area is the area that can be used for the windings. The window is calculated with (4.51) as

$$\begin{aligned} A_w &= \frac{\pi d^2}{4} \\ &= \frac{\pi x57.2x10^{-3}}{4} \\ &= 26 \text{ mm}^2 \end{aligned} \tag{4.51}$$

The required area must also be calculated. This is the area that the windings will cover. The required area must be smaller than the window area or the windings will not fit onto the core. The required area is calculated with (4.52)

$$\begin{aligned} A_{req} &= \frac{N.A_{cu}}{FF} \\ &= \frac{48x7.07x10^{-6}}{0.4} \\ &= 8.4 \text{ mm}^2 \end{aligned} \tag{4.52}$$

where FF is the filling factor chosen as 0.4. The next step is to determine whether or not the core will saturate. This phenomenon is due to the magnetic flux that flows through the core. The flux density is calculated with (4.53):

$$\begin{aligned} B &= \frac{N.i_{peak}.\mu.\mu_r}{\ell} \\ &= \frac{48x30x4\pi x10^{-7}x75}{25x10^{-2}} \\ &= 0.5424 \text{ T} \end{aligned} \tag{4.53}$$

The chosen core saturates at 0.7 T which means that the calculated flux is well within limits. The losses due to the inductor are calculated with (4.54):

$$P = \left(\frac{f}{\left(\frac{a}{B_{ac}^{\ 3}}\right)+\left(\frac{b}{B_{ac}^{\ 2.3}}\right)+\left(\frac{c}{B_{ac}^{\ 1.65}}\right)} + d \cdot f^2 \cdot B_{ac}^{\ 2}\right) \cdot A_e \cdot 1x10^4 \cdot \ell \cdot 1x10^2 \qquad (4.54)$$

where B_{ac} is the ac flux density, P the losses of the inductor and a, b, c and d the magnetic core constants. The losses in each inductor were calculated as 20 W. The resistor of the filter circuit only has an effect on the damping (ζ) of the system. The damping is calculated with (4.55) as

$$\begin{aligned} \zeta &= \frac{R}{2}\sqrt{\frac{C}{L}} \\ &= \frac{1}{2}\sqrt{\frac{3.3x10^{-6}}{300x10^{-6}}} \\ &= 0.05 \end{aligned} \qquad (4.55)$$

The resistor value is determined from the simulation. Various values for the resistor were evaluated through simulation until the correct damping was obtained. The diagram of the filter is shown in figure 4.15.

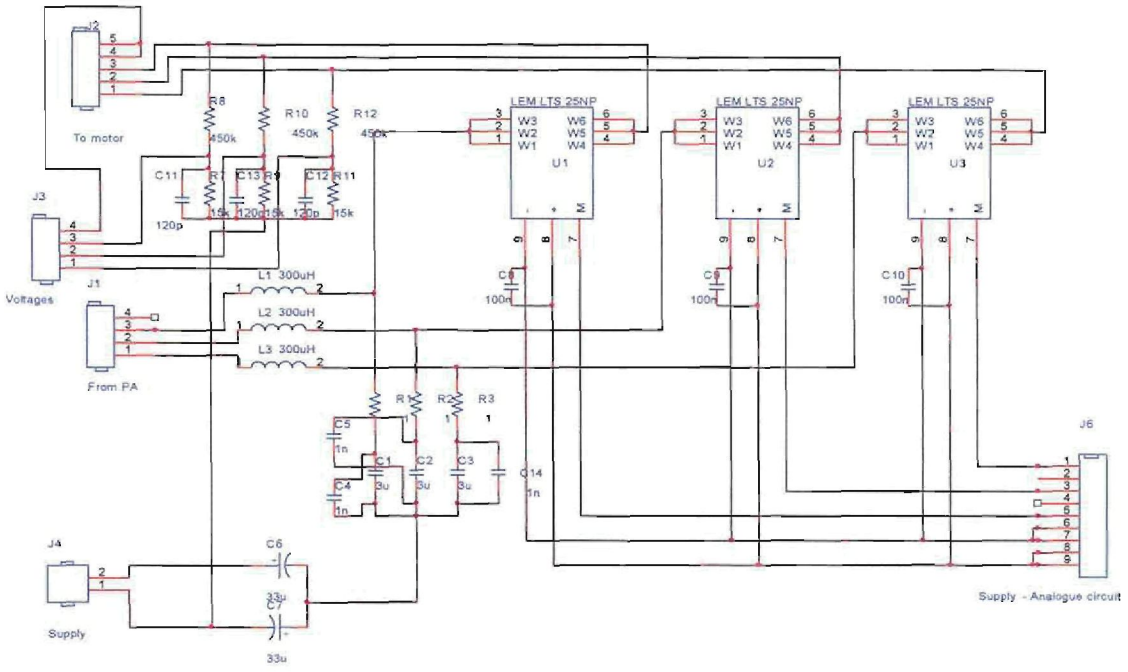

Figure 4-15 Filter diagram

4.7.1 RLC filter simulation

The simulation is done in SIMULINK® with the power systems blockset. The simulation block diagram is seen in figure 4-16. The simulation includes the power amplifier, the filter as well as the PMSM. PWM signals are fed to a universal bridge (set up as a six switch inverter). The output goes through the RLC filter to an RL load that represents the PMSM. The back-EMF is also added to the simulation.

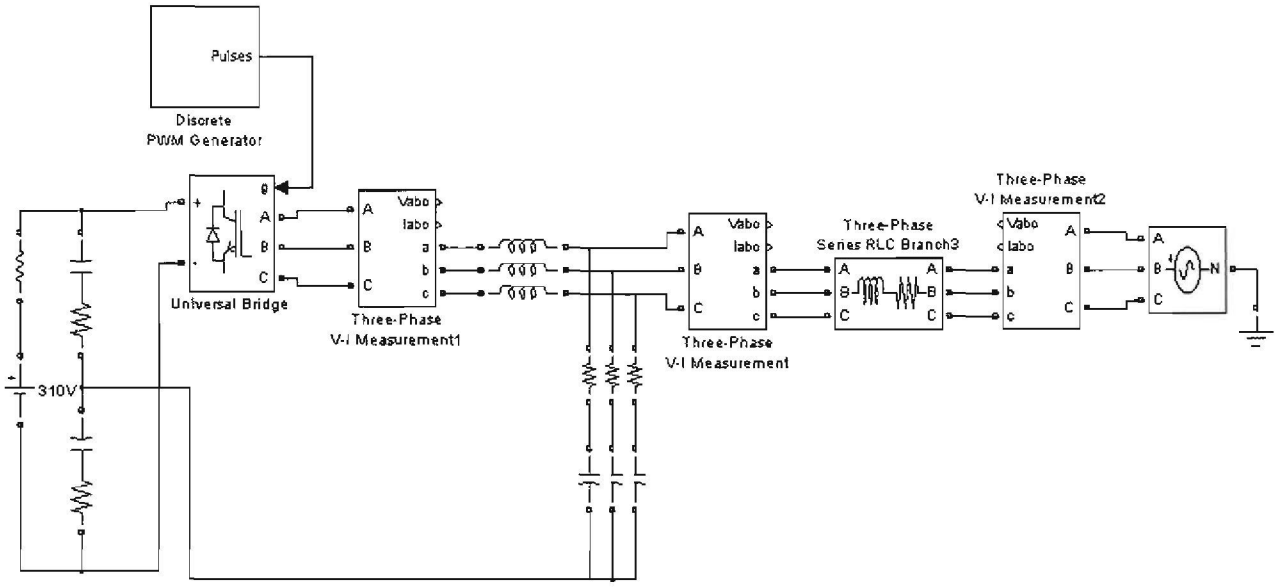

Figure 4-16 Simulation block diagram

The simulation was run for 12 ms with a variable step solver and a sampling time of 10 µs. Figure 4-17 shows the voltage output of the power amplifier.

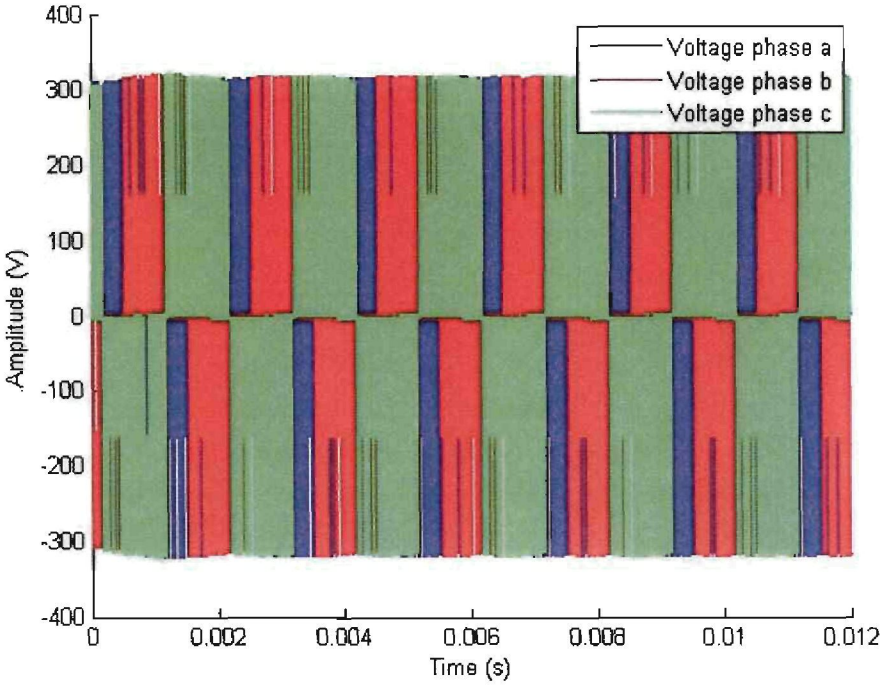

Figure 4-17 Voltage output of the power amplifier

The output is three PWM signals that are phase shifted by 120°. The voltage on the output of the filter can be seen in figure 4-18.

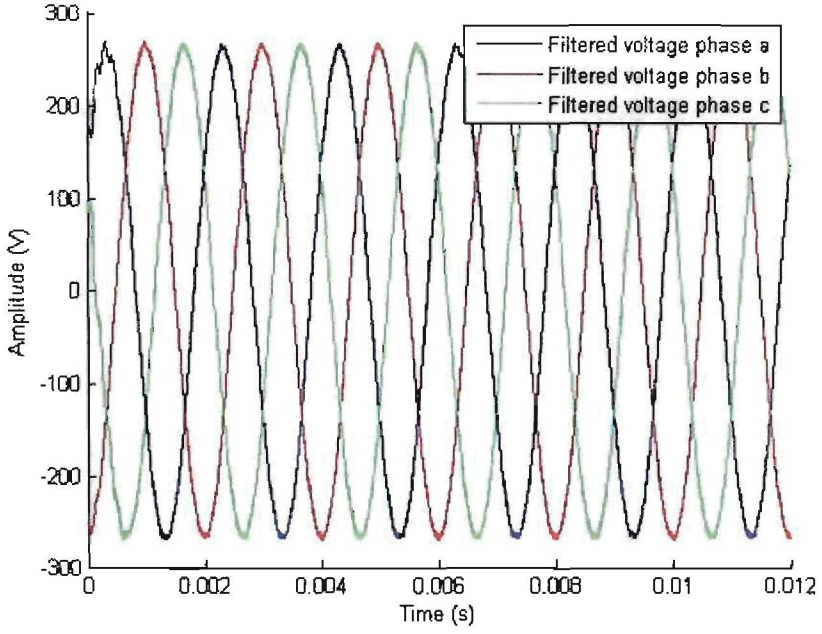

Figure 4-18 Filtered voltage

The PWM output of the power amplifier is filtered to obtain a sinusoidal signal that is applied to each phase of the motor. Figure 4-19 shows the current on the output of the power amplifier.

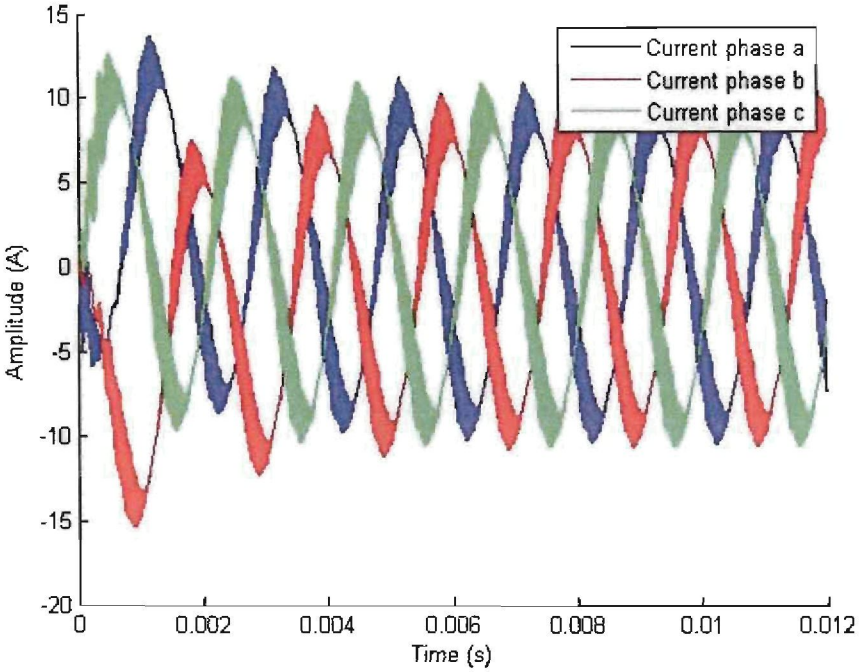

Figure 4-19 Current on the output of the power amplifier

Notice the ripple on the current. Current ripple will increase the losses of the system resulting in a less efficient motor. The ripple is almost completely removed with the filter. The filtered current can be seen in figure 4-22.

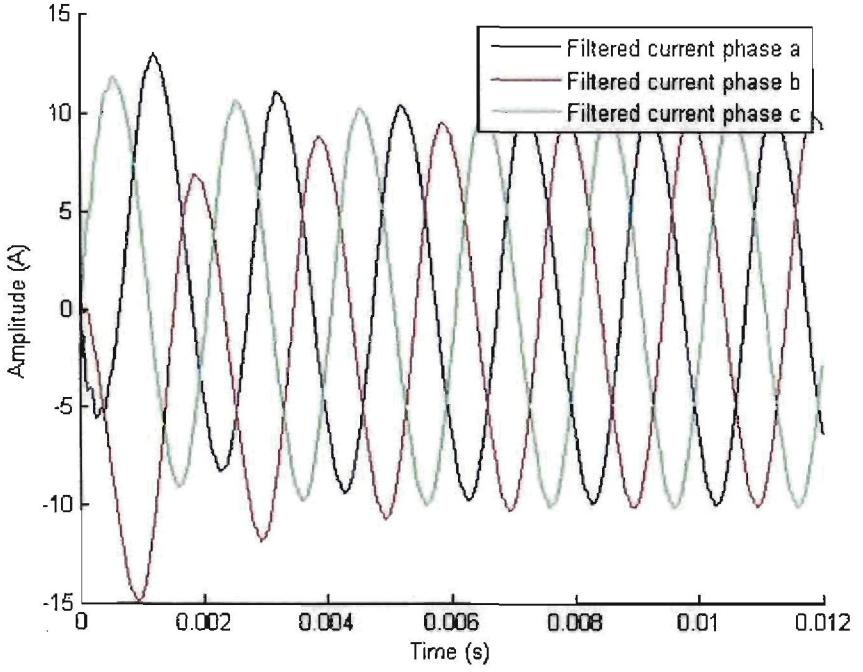

Figure 4-20 Filtered current

The filter board also includes three current sensors (LEM sensors) that measure the current in each phase of the motor. The sensors used are LAH25-NP sensors that can measure up to 25 A. The currents measured by the sensors are used as input to the V/f control (chapter 3).

In chapter 4 the power amplifier for the PMS was designed and simulated. The power amplifier design includes thermal protection and short circuit protection. The sub-components of the power amplifier (rectifier, analogue circuit and filter) were also designed and simulated. The system integration and testing is the next step and is discussed in chapter 5

5
Chapter
System evaluation

Chapter 5 contains a detailed discussion on system integration and implementation. Results are obtained from the test setup as well as the PMSM setup. The final product of the power amplifier, flyback converter, analogue circuit and the filter are shown as well.

5.1 Implementation results

After completion of the power amplifier design, the power amplifier was built and implemented. Measurements were done on the actual system to verify that the power amplifier operates correctly and to verify that the measured results correlate with the simulated results.

5.1.1 Flyback converter

The flyback converter is used as power supply to the analogue circuitry. The flyback converter supplies 5 V and 15 V to the gate drivers of the IGBTs and 5 V to the opto-couplers as well as 5 V to the comparators. It also supplies the analogue circuit with ± 15 V. The flyback will turn on when the supply exceeds 150 V and has an under voltage lock-out at 140 V.

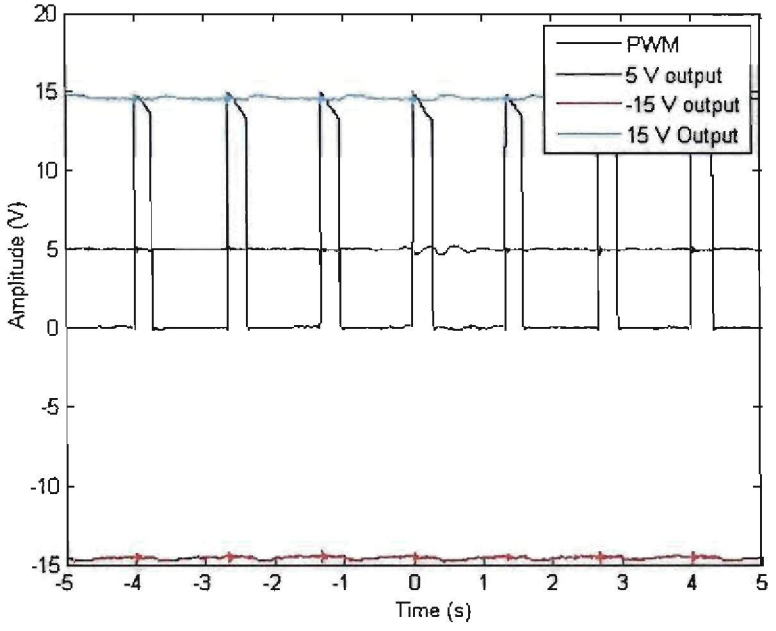

Figure 5-1 Voltage outputs of the flyback converter

The 5 V and 15 V outputs of the flyback converter is shown in figure 5-1. The 5 V and 15 V output of the flyback converter remained constant for an input voltage range of 150 V to 310 V. The supply was also tested under various load conditions and still operated within specification. The flyback converter is implemented on a PCB as shown in figure 5-2.

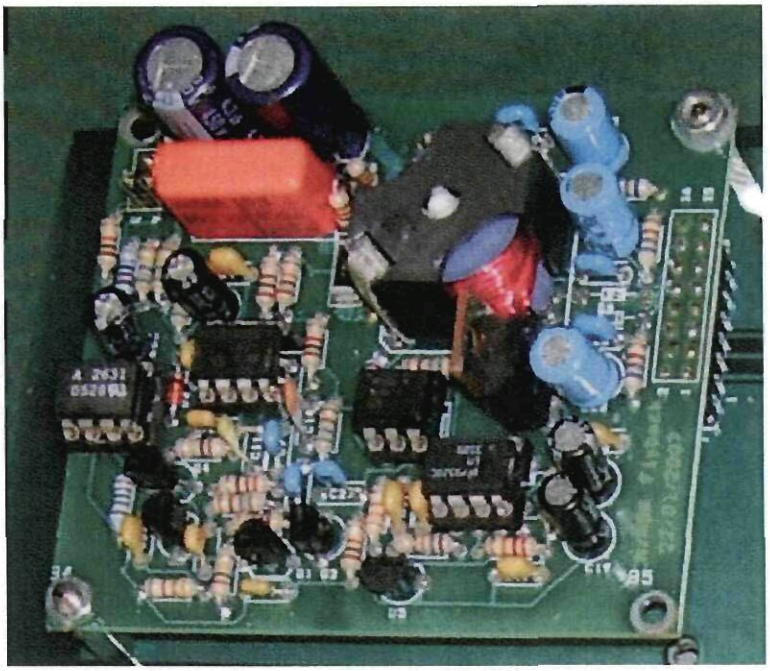

Figure 5-2 Flyback converter

5.1.2 Analogue Circuit

The purpose of the analogue circuit is to serve as interface between the high voltage pick-up coils and dSPACE® (figure 5-3). The circuit is operated from a ± 15 V supply that is generated by the flyback converter. The pick-up coil signals enter from the right. The maximum voltage of the pick-up coils is 310 V. The voltage is clipped with two zener diodes where the signal enters. The zero crossing of the input signals are detected and a digital signal is sent to dSPACE®.

The analogue circuit that is used for signal conditioning is shown in figure 5-3. The currents that are measured by the LEM sensors on the ac filter circuit also enter the circuit through the DB9 connector and are connected to dSPACE through the DB15 connector.

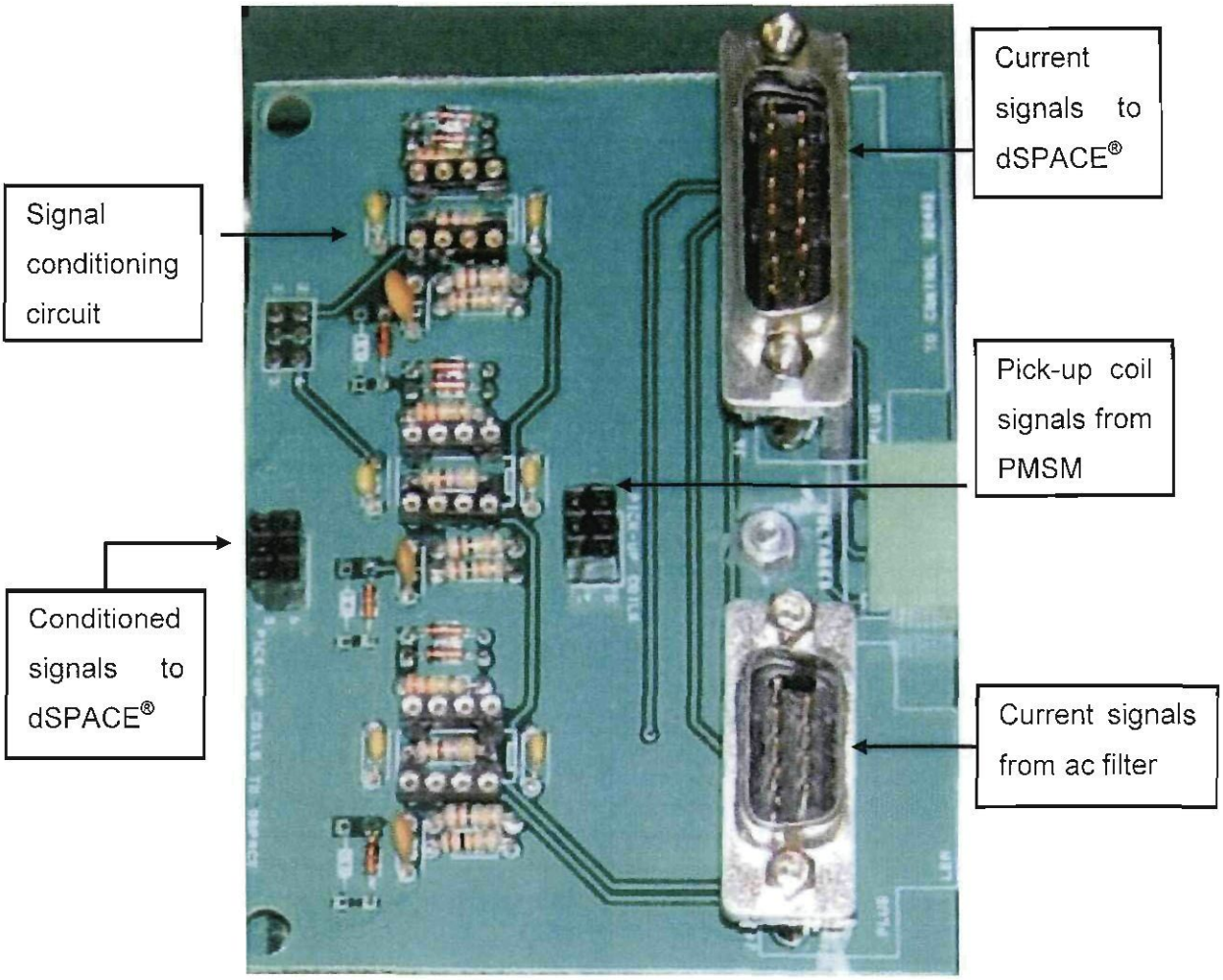

Figure 5-3 Analogue circuit

The pick-up coil signals could not be used. Since the pick-up coils are wound with the stator windings, the 50 kHz switching noise contaminated the pick-up signals. Even when the cut-off frequency of the RC filter on the comparator was reduced to 500 Hz, the signal still had too much interference. The analogue circuit on the other performed according to the simulated values.

5.1.3 Power Amplifier

The power amplifier was implemented as described in section 4.4 (figure 5-4). The flyback converter and the analogue circuit are piggybacked on the power amplifier to keep the path lengths between the circuits as short as possible in order to minimize parasitic inductance.

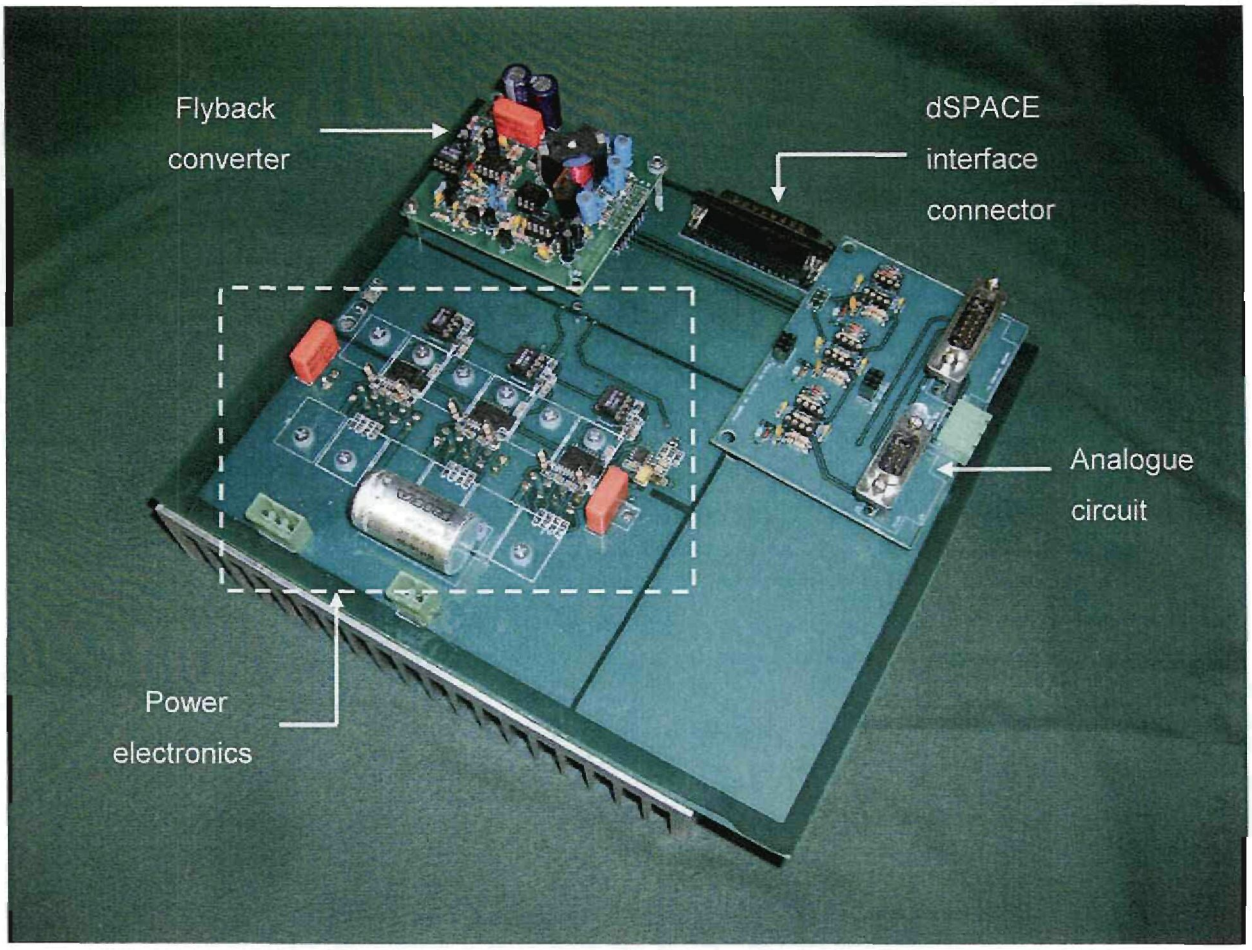

Figure 5-4 Power amplifier

A variety of tests were done to verify that the power amplifier operates correctly. A test setup was done to test the performance of the power amplifier. The V/f control was also confirmed on the actual model. This section discusses both these test methods.

Test setup

The power amplifier was connected to the stator of the PMSM to represent the correct load. The PWM controller was set up as an H-bridge with a dead-time of 1 µs. Various tests were done on the power amplifier to ensure correct operation. The small signal electronics were tested first. The flyback converter was powered up to test whether or not the PWM signals are correctly applied on the gate drivers. Figure 5-5 shows the PWM signals on the low-side of the first two IGBTs.

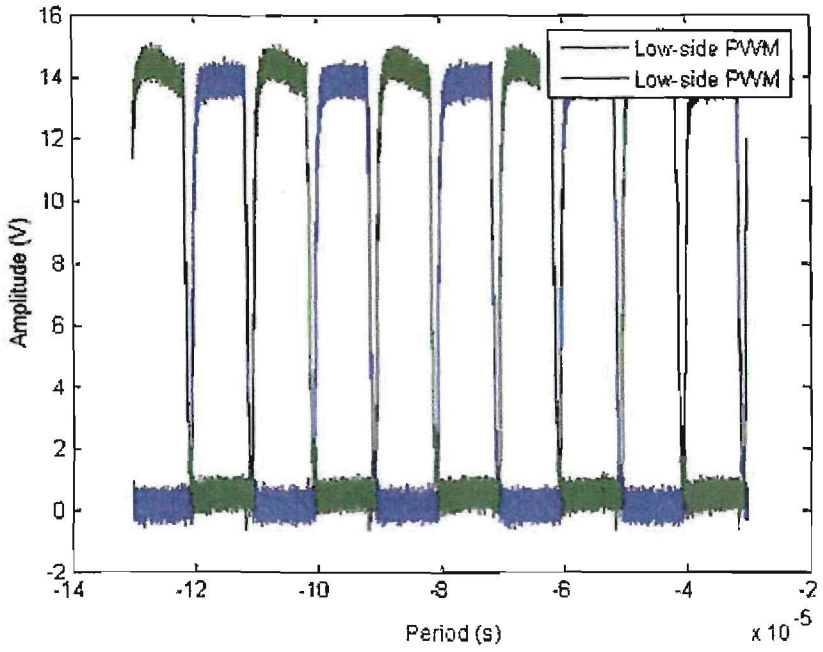

Figure 5-5 Low side PWM signals at driver output

The PWM signals on the two low sides of the IGBT configuration must be 180^0 out of phase because the IGBTs in the same half bridge can not switch together. From the figure it can be seen that the PWM signals are in fact 180^0 out of phase with a dead-time of 1µs.

Figure 5-6 shows the PWM signals of the high and low side of the same half bridge configuration with no supply voltage connected to the power electronics. The PWM signals are in phase which means that the high and low side of the IGBTs are switching correctly.

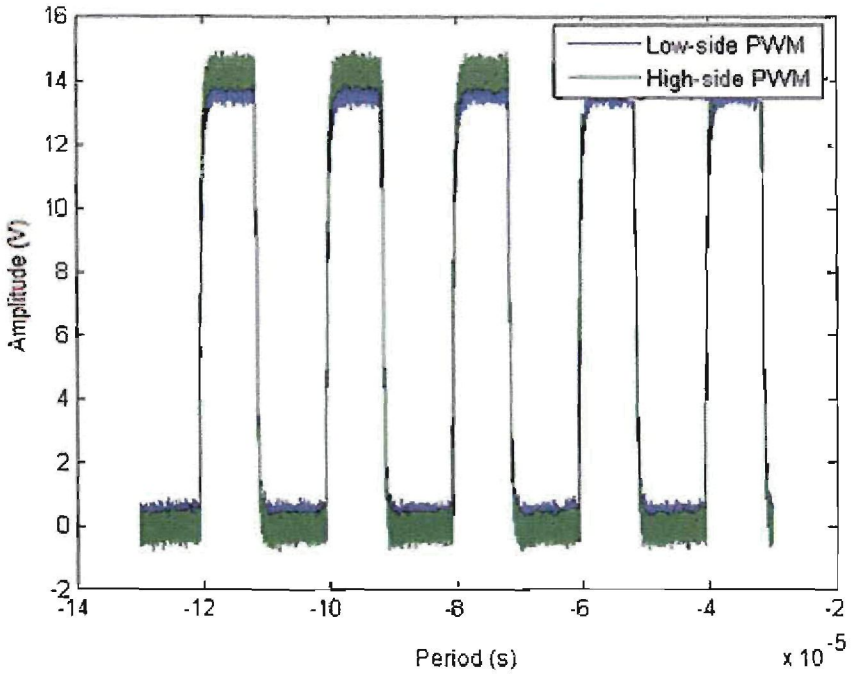

Figure 5-6 High and low side PWM signals at driver output

The high voltage side is powered up to test the switching devices as well as the other features of the power amplifier as discussed in section 4.4. Figure 5-7 shows the output voltage of the power amplifier with a sinusoidal reference.

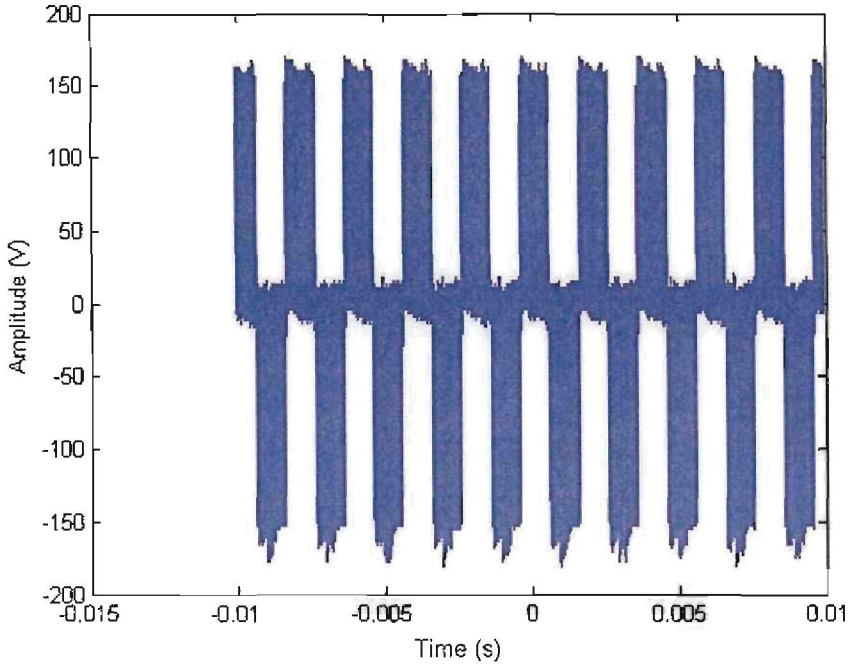

Figure 5-7 Differential voltage on output of PA

The voltage was measured with the use of a differential probe to eliminate any ground loops. From figure 5-8 it can be seen that the voltage is very noisy.

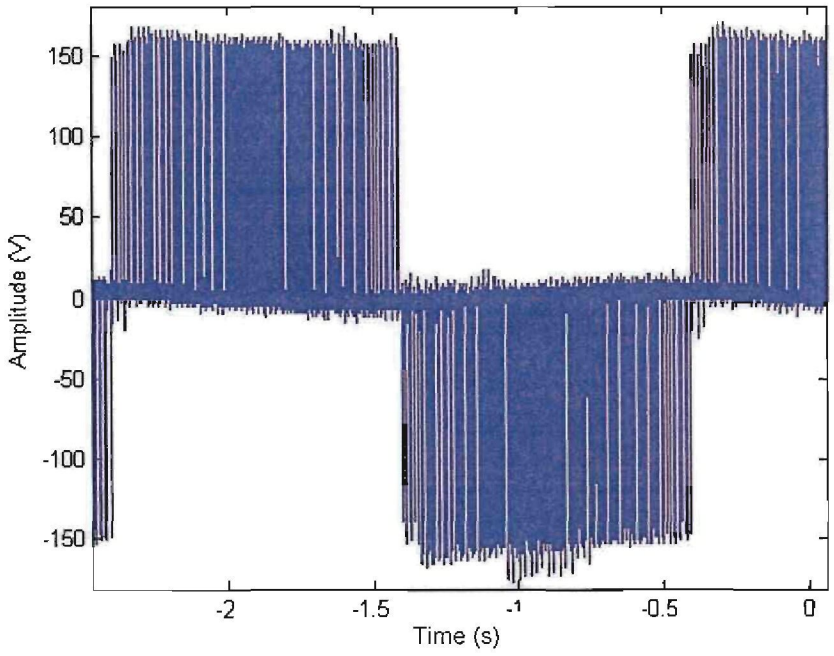

Figure 5-8 Differential voltage on output of PA (zoomed)

When looking at figure 5-8 the voltage consists of the 50 kHz PWM signals. When taking the average of the PWM signals, the output will be a sine wave. The filtered voltage output is discussed in the next section.

5.1.4 AC Filter

The filter was implemented as described in section 4-6. The capacitor for the filter was specified as a 3 μF, 600 V WIMA capacitor. However, a 3 μF motor-run capacitor was used. The motor-run capacitor is a 50 Hz capacitor where the WIMA is a high frequency device. Tests show that the capacitor was satisfactory for the filtering requirements.

The ac filter is mounted on a heat sink as shown in figure 5-9. The filter is placed in an aluminium enclosure with a 220 V ac cooling fan that is used to channel the heat away from the components because the filter is placed inside an enclosure.

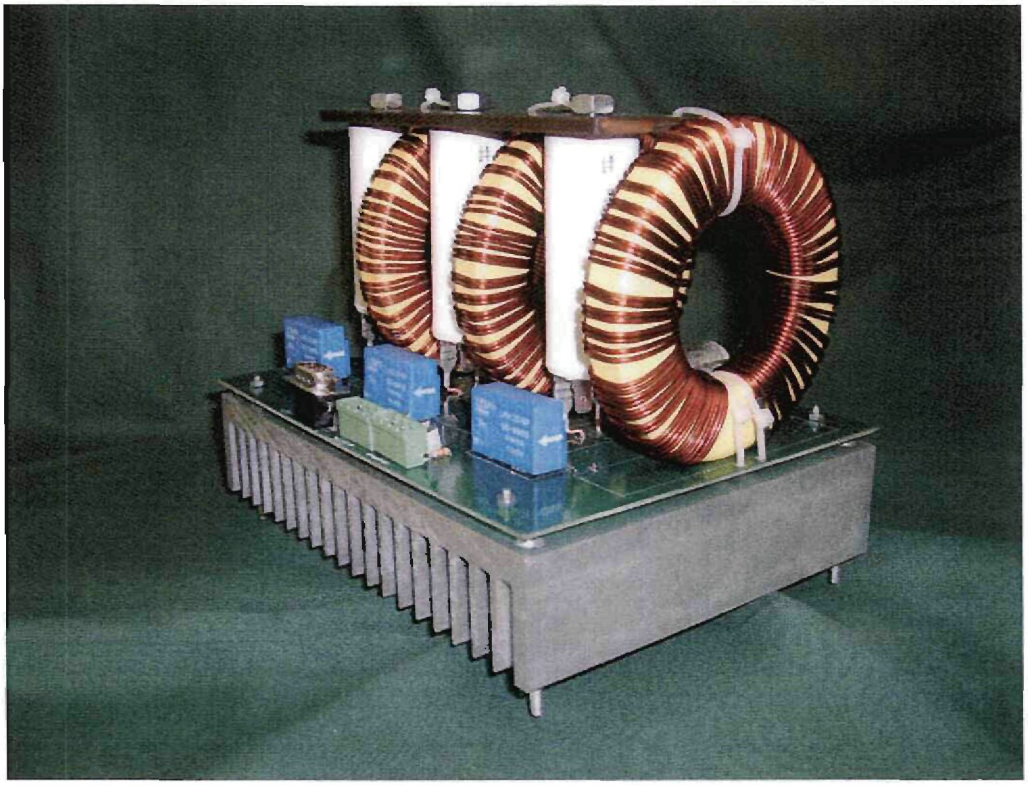

Figure 5-9 AC filter

The voltage in figure 5-7 is filtered to obtain the voltage in figure 5-10. The PWM signals are filtered to obtain a sinusoidal waveform.

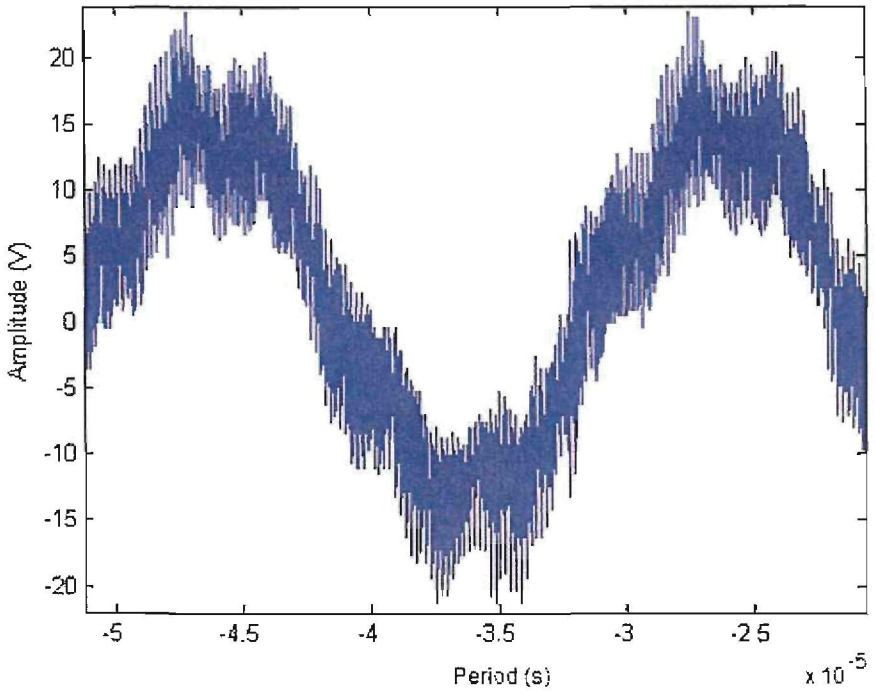

Figure 5-10 Differential voltage at output of filter

The ac filter was designed to minimise EMI as well as reduce the current ripple on the output of the power amplifier. The main purpose of the filter however, is to reduce the current ripple. The output current of the power amplifier before and after the filter can be seen in figure 5-11.

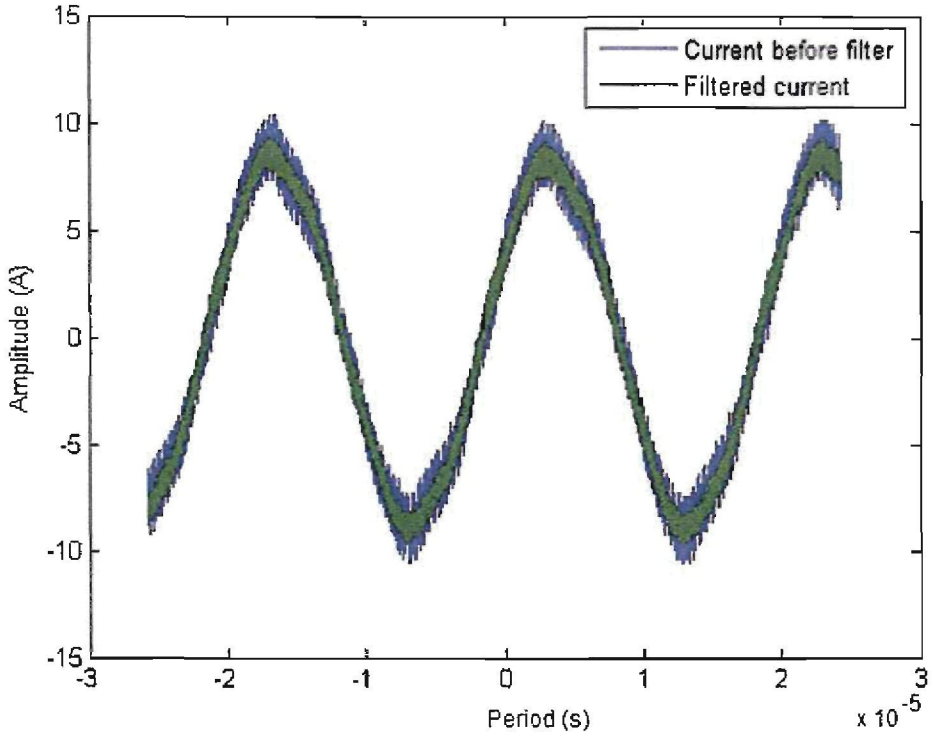

Figure 5-11 Current before and after the filter

Notice the reduction in ripple on the current. This will reduce losses in the system.

The tests done on the power amplifier show that the power electronics is designed and implemented correctly. The power amplifier will be able to supply the PMSM with sufficient power to reach the specified speed.

PMSM setup

The power amplifier, flyback converter, analogue circuit and ac filter were integrated into the control enclosure. The PMSM was spun up to 1400 rpm in a period of 500 s to verify the V/f speed control functions as simulated in chapter 3.

The voltage command reference as calculated in chapter 3 is shown in figure 5-12.

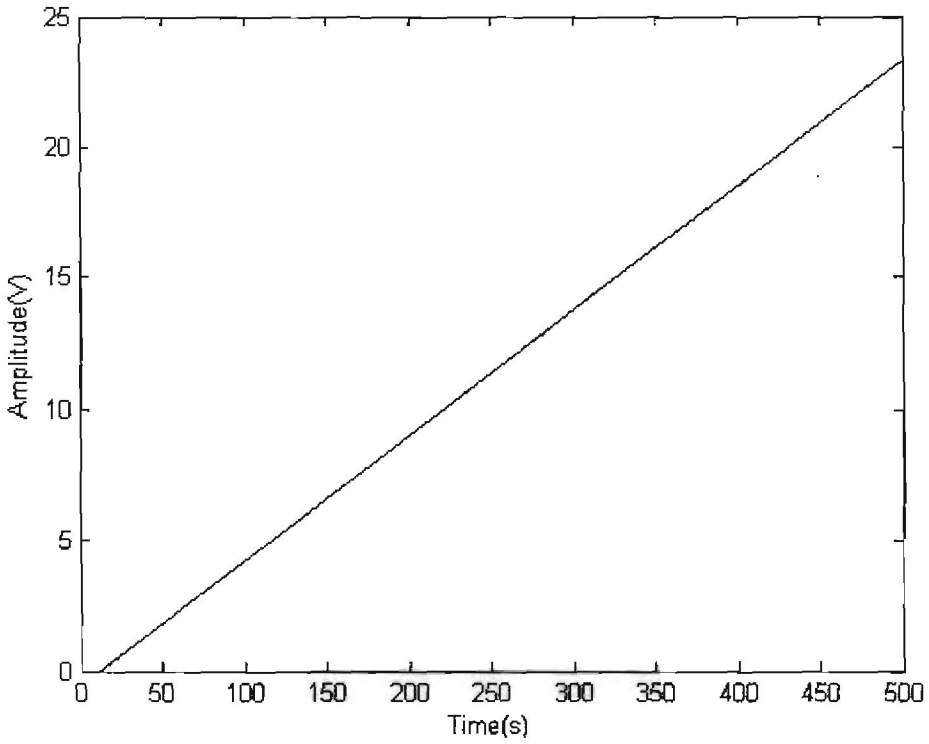

Figure 5-12 Voltage reference

The voltage reference from the control implemented on the PMSM correlates with the voltage command as shown in figure 3-10. The voltage applied to each phase of the motor is shown in figure 5-13.

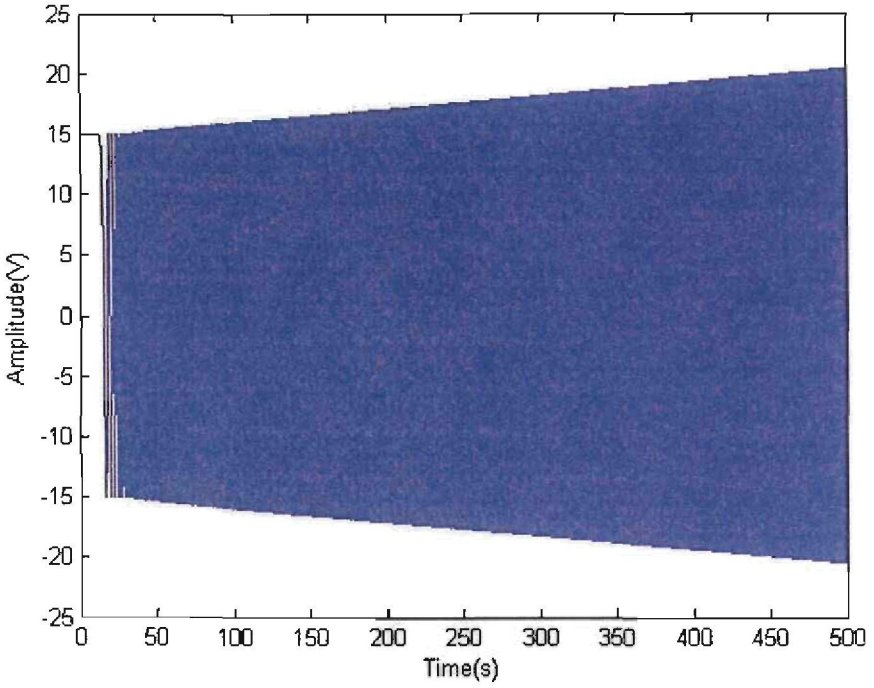

Figure 5-13 Voltage applied to each phase of the motor

The amplitude of the applied voltage increases over time and the initial value of the voltage is kept constant at 4 V in figure 3-11. The model was originally implemented with a constant voltage as simulated, but the start-up time was too long, so the initial value was increased to 15 V. For a larger value the power amplifier runs in current limit mode. 15 V is thus the optimum value to start the motor and avoid the aforementioned conditions.

Figure 5-14 shows how the frequency of the applied voltage increases over time. This is to keep the V/f ratio constant as indicated figure 3-12.

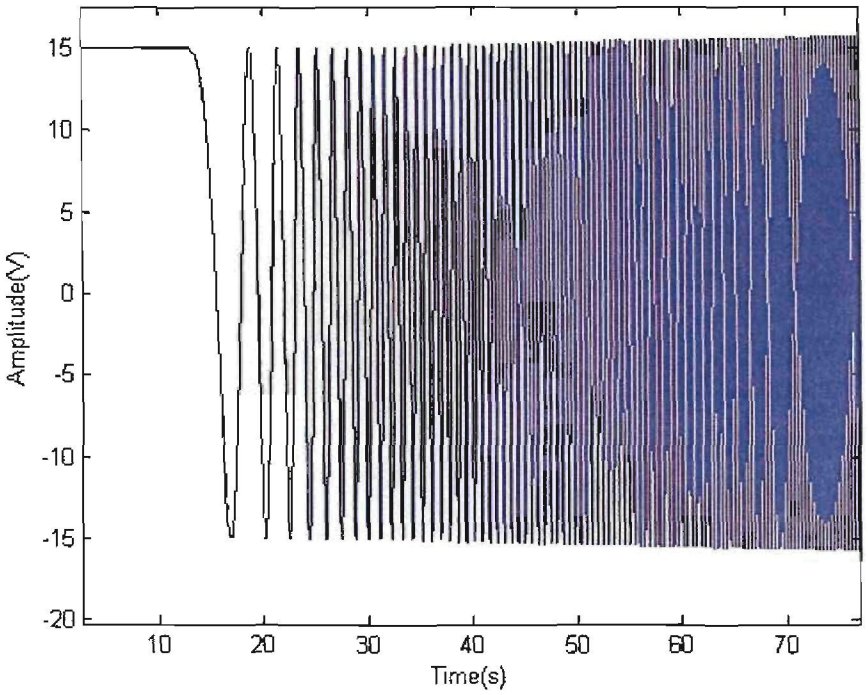

Figure 5-14 Frequency increase over time

The reference speed and the actual speed of the PMSM are shown in figure 5-15. The reference speed is calculated directly from the applied frequency with the use of (5.1)

$$f = \frac{pxN}{60} \tag{5.1}$$

where f is the applied frequency, p is the number of pole pairs and N is the speed of the motor in *rpm*. The speed of the PMSM was measured on the flywheel. The digital signal from the speed sensor was manipulated to obtain the actual speed of the PMSM. The results correlate very well with the simulated results.

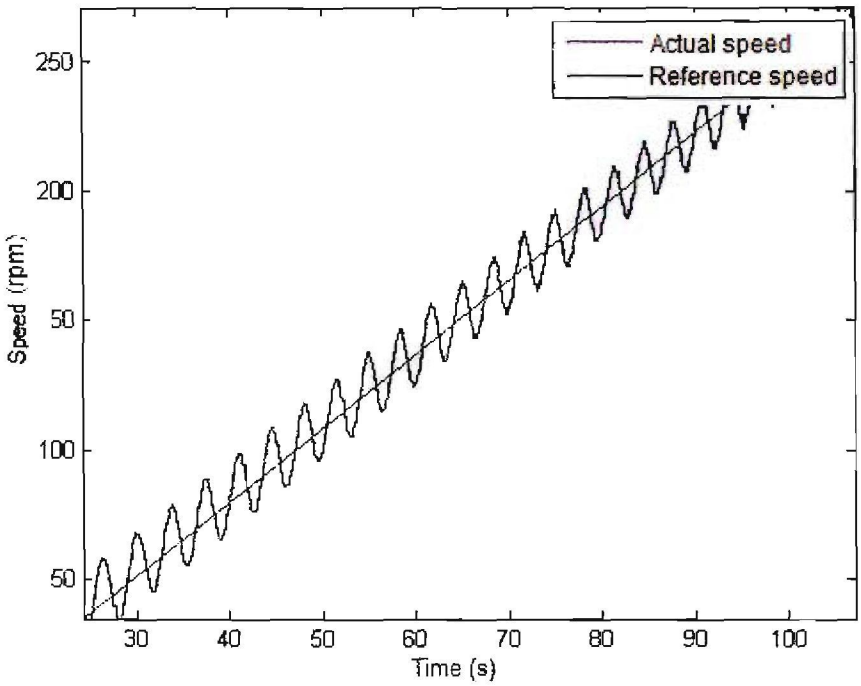

Figure 5-15 Speed and reference speed

The current that flows in each phase of the motor was also measured with the use of the LAH-25NP current sensors. The current is shown in figure 5-16. Note how the amplitude of the current increase as the speed increases. The amplitude of the current increases to ensure that the motor speeds up in synchronism. Figure 5-17 shows how the frequency of the current increase over time.

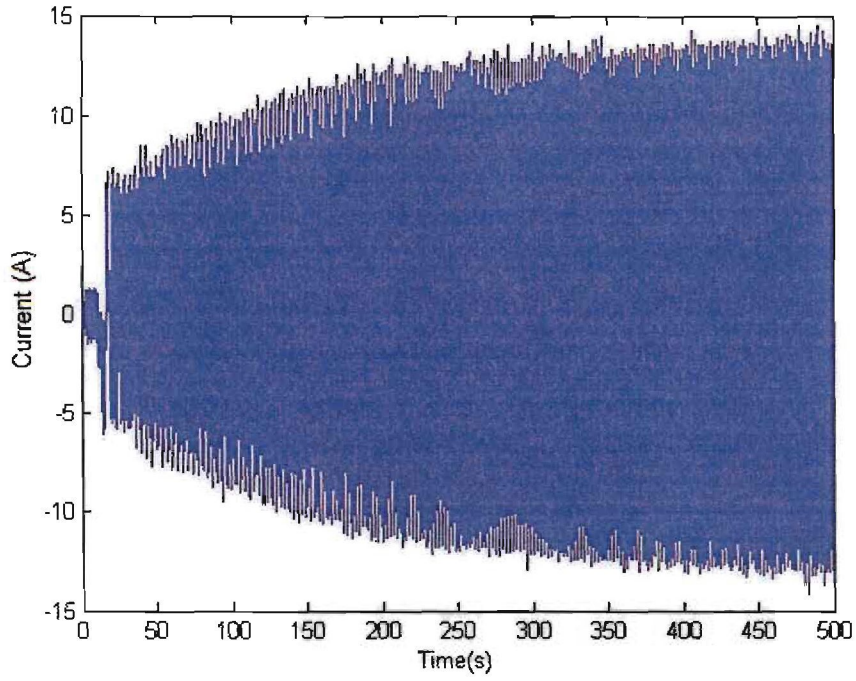

Figure 5-16 Current in each phase of the motor

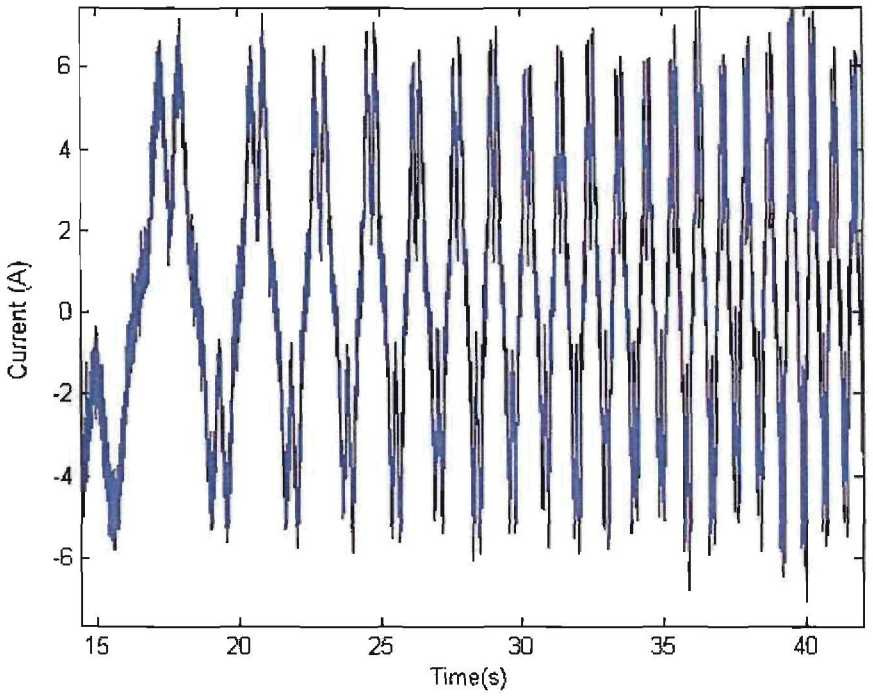

Figure 5-17 Frequency change over time

5.2 Final Assembly

The power amplifier with the flyback converter, analogue circuit and ac filter was incorporated into the final assembly. The final assembly can be seen in figure 5-18. The ac filter enclosure with the ac fan is on the left of the figure. On the other side of the filter enclosure (not shown in the figure) there is an outlet vent that ensures the cool air from the fan has a path to flow. The hot air is blown into the atmosphere. The power amplifier with the flyback converter and the analogue circuit is on the right of the figure. The dSPACE® connection is at the bottom of the power amplifier. The 310 V input and the output signals to the PMSM is on top of the power amplifier. The components are built into the control enclosure where all the control of the PMSM is located.

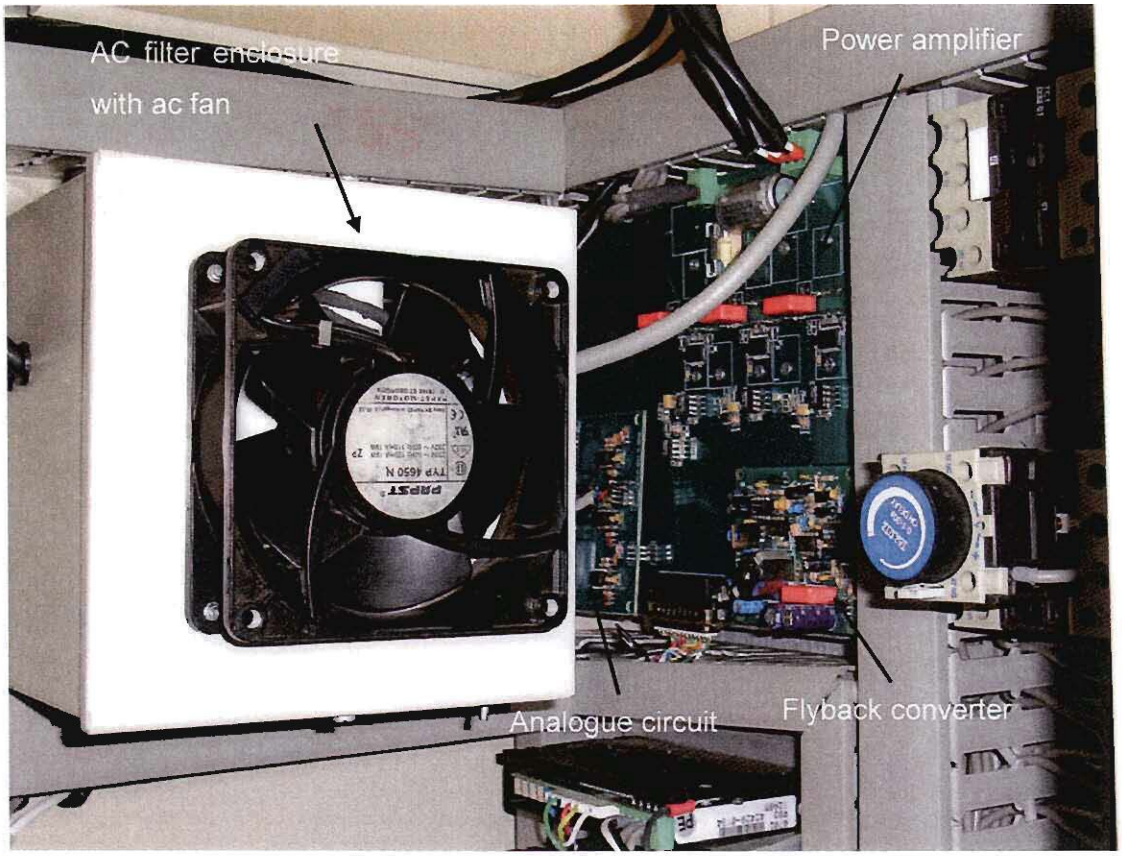

Figure 5-18 Final assembly

Chapter 5 gave a detailed discussion of system integration and implementation. The implementation results for the test setup and the PMSM setup were shown and discussed. The figures of the power amplifier, flyback converter, analogue circuit and the filter were also shown and explained. Then the final assembly was illustrated and discussed. In chapter 6 a conclusion is given and recommendations are made on how to improve the system.

6
Chapter
Conclusion and recommendations

Chapter 6 contains the conclusion and recommendations. An un-modelled phenomenon is discussed and explained and recommendations are made on how to improve the system in the future.

6.1 Conclusion

The power amplifier and its subcomponents were designed as specified. The designed components were simulated to determine the behaviour of the component. A control algorithm for speed control of the PMSM was also developed and simulated to verify its performance. Tests done on the hardware showed that the design was successful and that the simulated results were accurate. However, tests done on the performance of the system after the final implementation, showed a phenomenon that was not simulated. This phenomenon occurred when the reference speed of the motor was suddenly set to a fixed value. The power amplifier went into current limit mode for short time intervals. The speed and the reference speed of the motor were measured to determine the source of the current limit effect. It was found that when the reference speed of the motor is kept constant the actual speed will oscillate around the reference speed. This is because the damping of the system is very low. The measured speed and reference speed of the PMSM when setting the reference speed to a constant value is shown in figure 6-1. The PMSM was spun up normally and then the reference speed was clamped at 500 rpm.

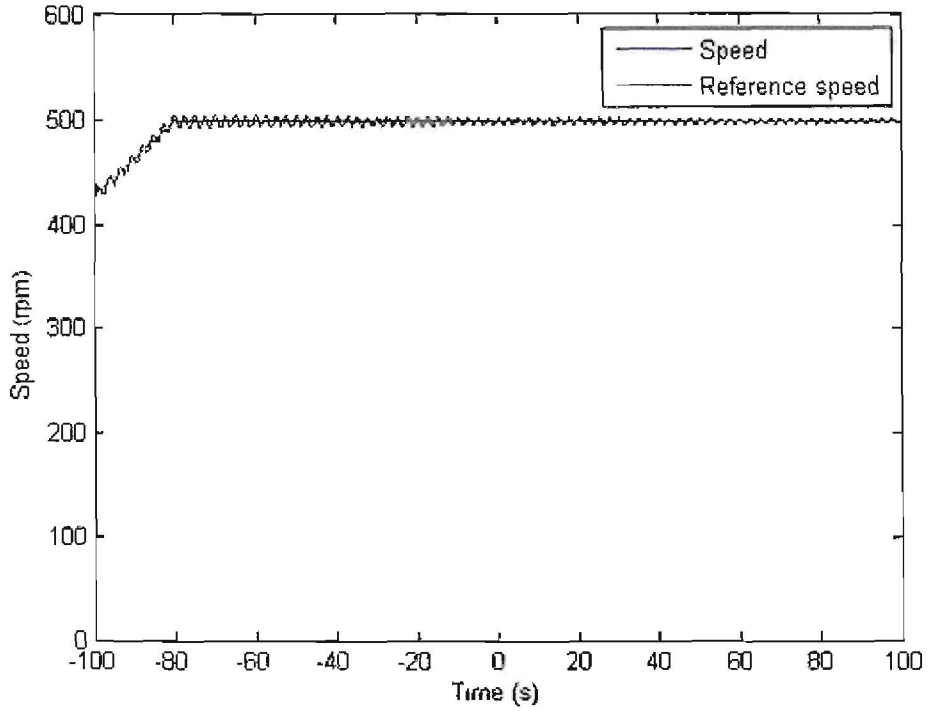

Figure 6-1 Speed and reference speed

The oscillating effect of the speed around the reference speed can be seen in the figure. To observe this effect better figure 6-2 zoomed in on the speed.

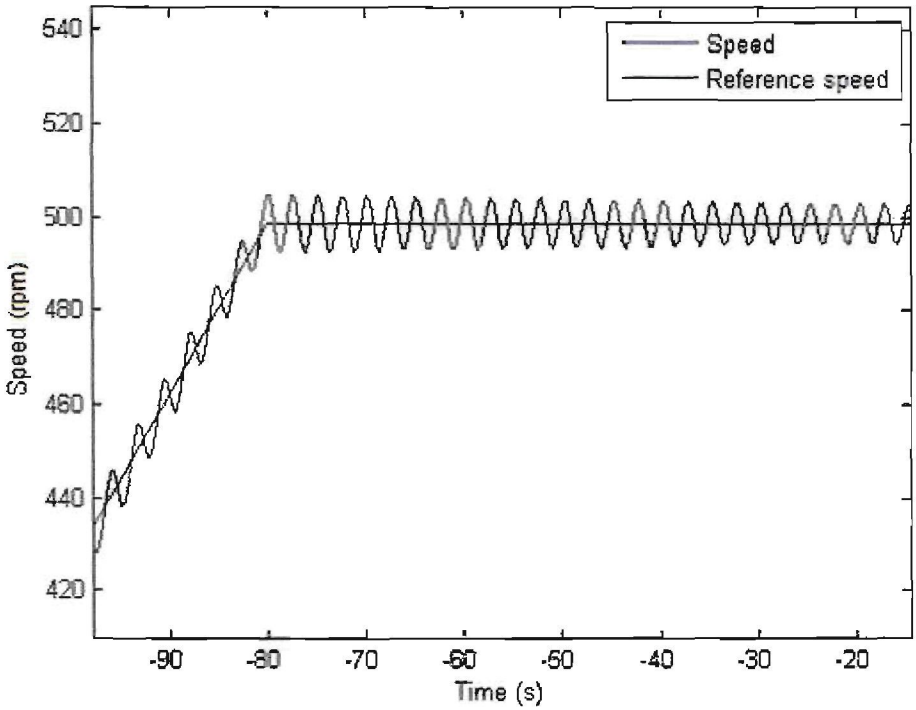

Figure 6-2 Speed and reference speed (zoomed)

In both figures it can be seen that the oscillating effect of the speed decreases over time and eventually stabilizes on the reference speed. To ensure that this behaviour was acceptable, the speed-up sequence of the PMSM had to be simulated to represent the abovementioned conditions. From the simulation was found that these conditions will occur when the damping of the system was very low. The simulated results are shown in figure 6-3.

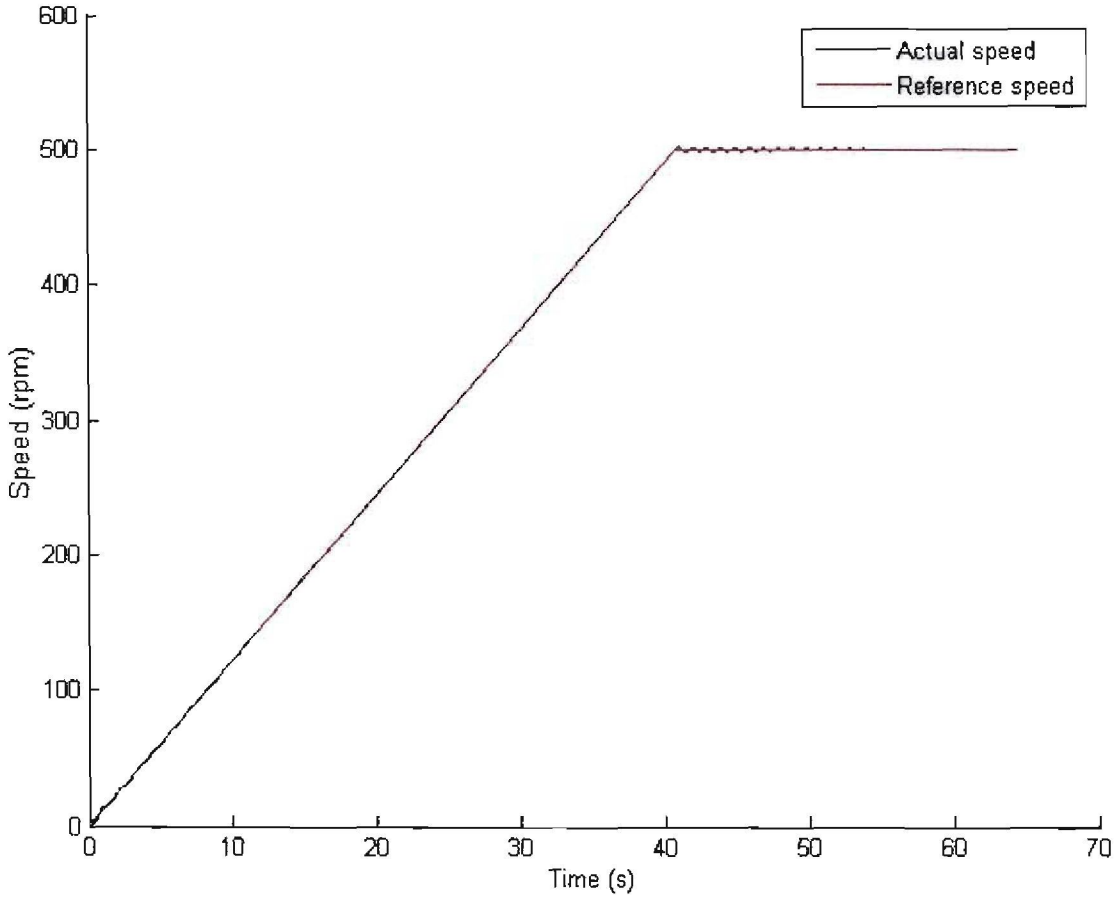

Figure 6-3 Simulated speed and reference speed

This figure shows that when the reference speed is kept constant at 500 rpm, the same oscillating effect of the speed of the PMSM occurs. Figure 6-4 indicates the speed when zoomed in.

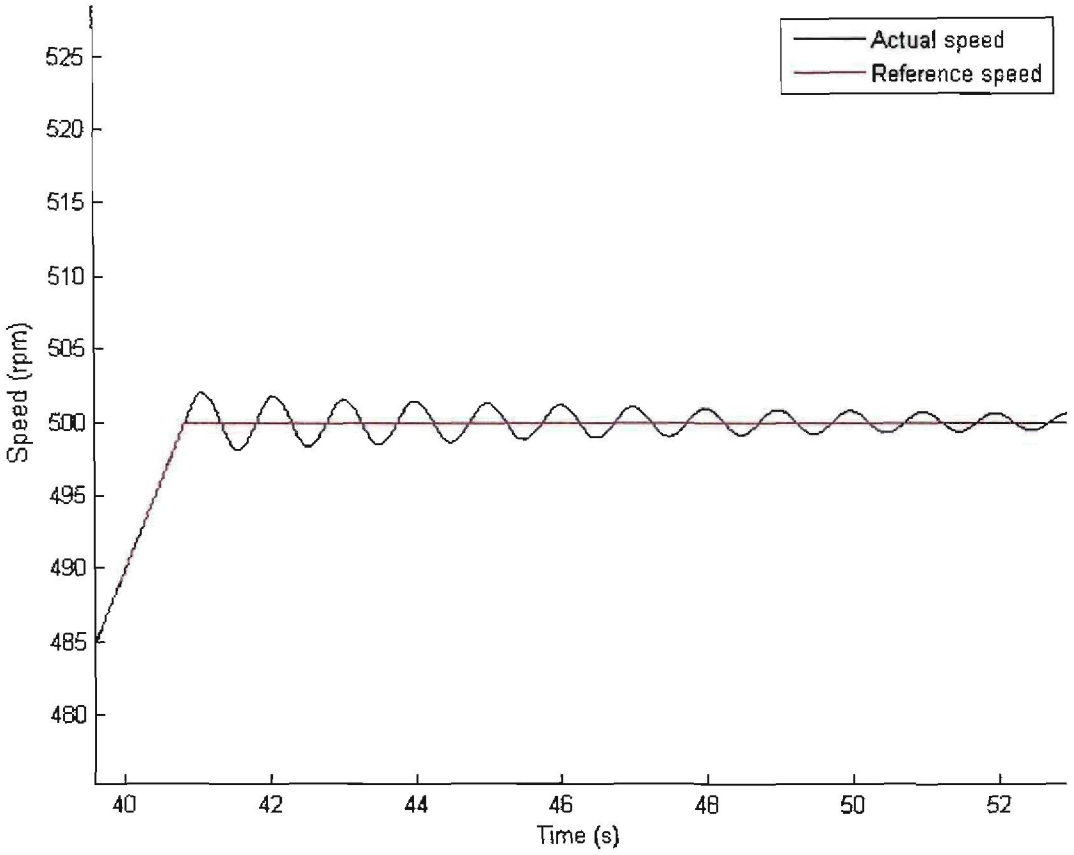

Figure 6-4 Simulated speed and reference speed (zoomed)

This oscillating effect will not appear at high speeds, because the stabilizing loop will compensate for the overshoot and counter the oscillation.

6.2 Recommendations

The power amplifier layout as discussed in chapter 4.6 is optimum and great amount of time was spent to achieve this. The protection systems of the power amplifier performed to specification except for the short circuit protection. Tests showed that for the short circuit test the current drawn from the load is proportional to the supply voltage. This is not a problem when working at low voltages, but the IGBTs are specified in the data sheet to withstand a peak repetitive current of 220 A. In this case the IGBTs will have to withstand 310 A peak repetitive current when the supply is 310 V. It is recommended that a shut down feature be implemented for short circuit conditions, rather than pulse for pulse current limiting.

The flyback converter was not synchronised. By adding a synchronising signal, equal to the switching frequency of the flyback, the performance of the flyback converter can also be improved.

Another improvement would be to implement a filter (chapter 4.7) for the pick-up coils as well. As mentioned, the noise on the pick-up coil signals made it impossible to record the data. Even when the cut-off frequency of the filter on the analogue circuit was increased to 500 Hz, the signals could still not be used.

The power amplifier was used to drive the PMSM as a motor in this application. Future work will require that the PMSM be operated as both a motor and a generator. The controller must be reconfigured to establish PMSM generation.

6.3 Closure

The purpose of this project was to design a three phase ac drive that must be able to drive a PMSM and control the speed of the machine from standstill to rated speed. The drive and all the sub-components was modelled and designed to specification. Tests showed that the performance of the drive were adequate for the control of the PMSM speed. However, the PMSM could not reach the rated speed of 30 000 rpm because the system is not yet safe enough to operate at this speed. The test done on the PMSM at 5000 rpm showed that the project was a success.

In this chapter conclusions were made regarding the project. The un-modelled phenomenon was discussed and explained and recommendations were made on how to improve the system.

APPENDIX

Appendix A: Power amplifier circuit diagram

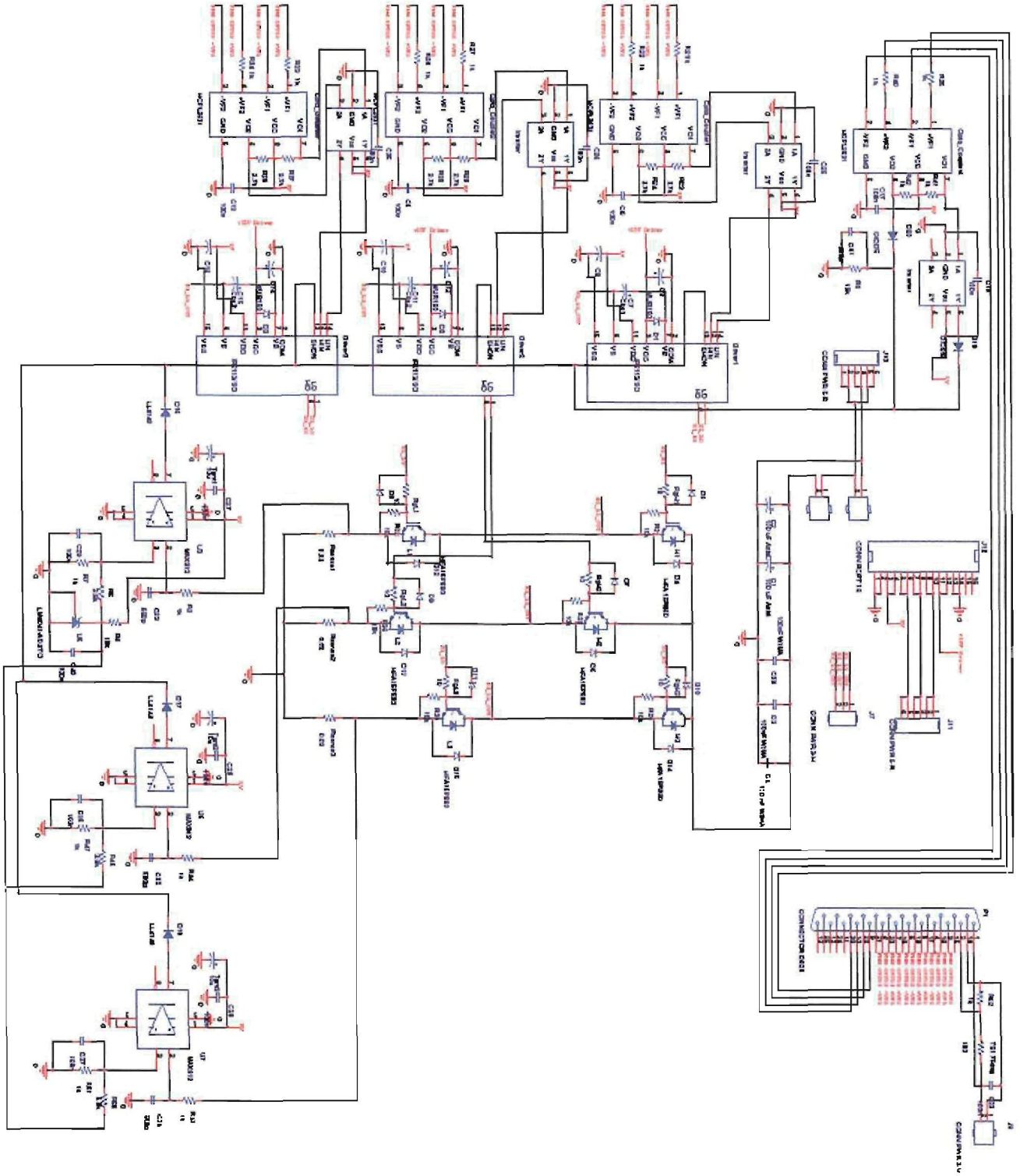

Appendix B: Data CD

B.1. Dissertation

B.2. SIMULINK® simulation models

B.3. ORCAD® designs

B.4. Photos

B.5. Papers

REFERENCES

[1] I. Boldea, S.A Nasar, "Electric Drives" 2nd edition, CRC Press, Taylor and Francis Group, 2006.

[2] N. Mohan, Electric Drives, An Integrative Approach. Minneapolis, MN: Minnesota Power Electron. Res. Edu., 2000.

[3] P. Pillay and R. Krishnan, "Control characteristic and speed controller design for a high performance permanent magnet synchronous motor drive," IEEE Trans. Power Electron., vol. 5, no. 2, pp. 151–159, Apr. 1990.

[4] Y. Zhang, "Load disturbance resistance speed controller design for PMSM," IEEE Transaction on industrial electronics, vol. 53, no. 4, August 2006.

[5] P. Pillay and R. Krishnan, "Modeling, simulation, and analysis permanentmagnet motor drives, Part I: The permanent-magnet synchronous motor drive," *IEEE Trans. Ind. Appl.*, vol. 25, no. 2, pp. 265–273, Mar./Apr. 1989.

[6] L. Xu, "Implementation and Experimental Investigation of Sensorless Control chemes for PMSM in Super-High Variable Speed Operation," IEEE 1998.

[7] J. Faiz, M. R. Azizian, and M. Aboulghasemian-Azami, "Simulation and analysis of brushless DC motor drives using hysteresis, ramp comparison and predictive current control techniques," *Simul. Pract. Theory*, vol. 3, no. 6, pp. 347–363, Jan. 1996.

[8] O. A. Mohammed, "Physical Modeling of PM Synchronous Motors for Integrated Coupling With Machine Drives," IEEE Transactions on magnetics, vol. 41, no. 5, May 2005.

[9] C. Mademlis, J. Xypteras and N. Margaris, "Loss Minimization in Surface Permanent-Magnet Synchronous Motor Drives," IEEE Transactions on industrial electronics, vol. 47, no. 1, February 2000.

[10] J. K. Gieras and M.Wing, "*Permanent Magnet Motor Technology: Design and Applications*," New York: Marcel Dekker, 1997.

[11] K. Lee, D. Jung and I. Ha, "An Online Identification Method for Both Stator Resistance and Back-EMF Coefficient of PMSMs Without Rotational Transducers," IEEE Transactions on industrial electronics, vol. 51, no. 2, April 2004.

[12] P. Vas, M. Zordan, M. Rashed and C.H. Ng, "Field-weakening in high-performance PMSM drives," COMPEL, August 2001.

[13] Song Chi, Student Member, Longya Xu, "Development of Sensorless Vector Control for a PMSM Running up to 60,000 rpm," IEEE 2005.

[14] M.H Rashid, "Power Electronics Handbook," ACADEMIC PRESS, 2001.

[15] M.J. Hoeijmakers, "Modelvorming Bij Draaistroommachines," TUDelft, November 1996.

[16] P.D Chandana Perera, Frede Blaabjeg, John K, Paul Thohersen, "A Sensorless, Stable V/f Control Method for Permanent Magnet Synchronous Motor Drives" January 2003

[17] J.P. Agrawal, "Power electronic systems: theory and design," Prentice Hall, New Jersey, 2001.

[18] International Rectifier. (2003, May). HV Floating MOS-Gate Driver ICs. International Rectifier Application Note. [Online]. AN978-b, pp. 1-10. Available: http://www.irf.com

[19] J. Adams. (2003, May). Bootstrap component selection for control IC's. International Rectifier Design Tip. [Online]. DT 98-2a, pp. 1-4. Available: http://www.irf.com

[20] D.A. Neamen, "Electronic Circuit Analysis and Design, Second Edition," McGraw-Hill, New York, 2001.

[21] W. Santiago, "Inverter Output Filter Effect on PWM Motor Drives of a Flywheel Energy Storage System," NASA/TM, 2004.